

UC Santa Cruz

UC Santa Cruz Electronic Theses and Dissertations

Title

Casein Kinase 1δ and PERIOD2 regulate circadian rhythms through a combination of substrate selectivity and feedback inhibition

Permalink

<https://escholarship.org/uc/item/8118s2b2>

Author

Philpott, Jonathan Michael

Publication Date

2022

Supplemental Material

<https://escholarship.org/uc/item/8118s2b2#supplemental>

Peer reviewed|Thesis/dissertation

University of California
Santa Cruz

**Casein Kinase 1 δ and PERIOD2 regulate circadian rhythms through a
combination of substrate selectivity and feedback inhibition**

A dissertation submitted in partial satisfaction
of the requirements for the degree of

DOCTOR OF PHILOSOPHY

in

Chemistry & Biochemistry

by

Jonathan M. Philpott

December 2022

The Dissertation of Jonathan M.
Philpott
is approved:

Professor Carrie L. Partch,
Advisor

Professor Ted Holman, Chair

Professor Seth M. Rubin

Peter F. Biehl
Vice Provost and Dean of Graduate Studies

Copyright © by
Jonathan M. Philpott
2022

TABLE OF CONTENTS

- 1.0 Biochemical mechanisms of period control within the mammalian circadian clock
 - 1.1 Abstract
 - 1.2 Introduction to the mammalian circadian clock
 - 1.3 Evidence and structural basis for the distinct roles of CRY1/2
 - 1.4 CRY and its autoregulatory tail
 - 1.5 Post-translational regulation of PER2 stability
 - 1.6 Structural organization of PER2
 - 1.7 Control of PER2 degradation by phosphodegrons
 - 1.8 The Casein Kinase-Binding Domain stabilizes PER2 through a phosphoswitch
 - 1.9 Other post-translational modifications influence PER2 stability
 - 1.10 A central role for CK1 in eukaryotic circadian period determination
 - 1.11 Anion-dependent regulation of a structural switch in CK1 δ
 - 1.12 Regulation of CK1 δ/ϵ activity by its disordered C-terminal tail
 - 1.13 Concluding remarks
- References
- 2.0 Casein Kinase 1 dynamics underlie substrate selectivity and the PER2 circadian phosphoswitch
 - 2.1 Abstract
 - 2.2 Introduction
 - 2.3 Results
 - 2.3.1 The *tau* mutant has decreased activity on the FASP region
 - 2.3.2 *tau* exhibits a gain of function on the Degron
 - 2.3.3 The *tau* mutation disrupts anion binding at Site 1 and Site 2 on CK1
 - 2.3.4 Eliminating anion binding at Site 2 differentially regulates CK1 activity on the FASP and Degron

- 2.3.5 The activation loop switch is intrinsic to the CK1 family of kinases
- 2.3.6 *tau* stabilizes the rare 'loop up' conformation of the CK1 activation loop
- 2.3.7 The activation loop allosterically controls the dynamics of loop L-EF in *tau*
- 2.3.8 *Tau* dynamically reshapes the substrate-binding cleft in CK1
- 2.3.9 *Tau* influences the global dynamics of CK1
- 2.3.10 Circadian alleles from *Drosophila* to humans occur throughout CK1
- 2.3.11 Other short period mutants exhibit differential activity on the FASP and Degron
- 2.3.12 The ratio of FASP/Degron enzyme efficiency correlates with PER2 stability
- 2.4 Discussion
- 2.5 Materials and methods
- References
- 3.0 Chapter 3: PERIOD phosphorylation leads to feedback inhibition of CK1 activity to control circadian period
- 3.1 Summary
- 3.2 Introduction
- 3.3 Results
 - 3.3.1 CK1 phosphorylates the serine cluster in the PER2 FASP region in a sequential manner
 - 3.3.2 CK1 follows an ordered distributive mechanism gated by slow non-consensus priming
 - 3.3.3 Sequential phosphorylation of FASP leads to feedback inhibition of CK1
 - 3.3.4 pFASP binds to CK1 via conserved anion binding sites to occlude the substrate binding cleft
 - 3.3.5 Molecular dynamics simulations support stable binding mode of pFASP:CK1 crystal structures

- 3.3.6 Circadian rhythms are shortened by small deletions in the conserved FASP region of PER
- 3.3.7 The phosphorylated *Drosophila* PER-Short region binds CK1 to inhibit kinase activity
- 3.4 Discussion
- 3.5 Materials and methods
- References
- 4.0 Future directions
- 4.1 Dissecting the molecular level details of CK1 dynamics and substrate selectivity
 - 4.1.1 Summary
 - 4.1.2 Molecular dynamics and biochemistry support a model for priming of the FASP region
 - 4.1.3 The free energy landscape of the activation loop is governed by an allosteric network
 - 4.1.4 Targeting the allosteric network interactions disrupts kinase activity on the Degron
- 4.2 The molecular determinants of CK1 activity and β -TrCP recruitment at the PER2 PAS-degron
 - 4.2.1 Summary
 - 4.2.2 Molecular features of the β -TrCP recognition motif in the context of the PER2 PAS-Degron
 - 4.2.3 Phosphorylation of S480 is a key determinant of β -TrCP recruitment
 - 4.2.4 Determining the phosphorylation profile of a minimal hPER2 Degron substrate
 - 4.2.5 Phosphorylation of the hPER2 Degron in the context of the PAS domains
- 4.3 Targeting CK1 to modulate kinase activity on PER2 substrates
- 4.4 Materials and methods
- References
- 5.0 Conclusions

- 5.1 The core molecular clock is highly interconnected
- 5.2 Protein dynamics are key determinants of protein function and circadian timing
- 5.3 CK1 feedback regulation is a hallmark of the mammalian circadian clock
- 5.4 Molecular level details of PER2 turnover are critical for understanding circadian period
- 5.5 CK1 and PER2 form a critical regulatory nexus within the core molecular clock

LIST OF FIGURES

- 1.1 Changes to the core molecular clock control mammalian circadian period
- 1.2 Structural features of CRY period control within the mammalian clock
- 1.3 PER2 stability is tightly regulated by post-translational modifications
- 1.4 Regulatory mechanisms control CK1 δ activity in the mammalian clock
- 2.1 *tau* alters CK1 substrate selectivity on PER2 to enhance Degron phosphorylation
 - 2.1.1 Supplemental figure (relates to figure 2.1)
- 2.2 *tau* disrupts anion binding on CK1 δ
 - 2.2.1 Supplemental figure (relates to figure 2.2)
- 2.3 *tau* alters an intrinsic molecular switch in the activation loop of CK1 δ
 - 2.3.1 Supplemental figure (relates to figure 2.3)
- 2.4 Probing the dynamics of CK1 δ with GaMD simulations
 - 2.4.1 Supplemental figure (relates to figure 2.4)
- 2.5 *tau* influences the principal modes of motion in CK1 δ
 - 2.5.1 Supplemental figure (relates to figure 2.5)
- 2.6 Proximity of CK1 alleles map to catalytic and substrate binding sites
 - 2.6.1 Supplemental figure (relates to figure 2.6)

- 2.7 Substrate discrimination on the PER2 phosphoswitch is regulated by the CK1 activation loop switch
 - 2.7.1 Supplemental figure (relates to figure 2.7)
- 3.1 CK1 phosphorylates the human PER2 FASP region sequentially.
 - 3.1.1 Supplemental figure (relates to figure 3.1)
- 3.2 CK1 follows an ordered distributive mechanism on the human PER2 FASP region
- 3.3 Phosphorylation of the human PER2 FASP region inhibits CK1 activity
 - 3.3.1 Supplemental figure (relates to figure 3.3)
- 3.4 The human PER2 pFASP binds to the active site of CK1
 - 3.4.1 Supplemental figure (relates to figure 3.4)
- 3.5 Molecular dynamics simulations of CK1:5pFASP
- 3.6 Circadian rhythms are shortened by small deletions in the conserved FASP domain of human PER2
 - 3.6.1 Supplemental figure (relates to figure 3.6)
 - 3.6.2 Supplemental figure (relates to figure 3.6)
- 3.7 The phosphorylated PER-Short domain of *Drosophila* PER binds CK1 Site 1 to inhibit kinase activity
- 4.1 Biochemistry and molecular dynamics of modeled CK1:FASP complex suggest priming mechanism
- 4.2 The *tau* mutation allosterically reshapes the free energy landscape of the CK1 substrate binding region
- 4.3 Mutation of interacting residues identified within allosteric network disrupt kinase activity on Degron peptide
- 4.4 The hPER2 β -TrCP recognition motif has unique molecular features
- 4.5 Phosphorylation of S480 in hPER2 is a key determinant of β -TrCP recruitment
- 4.6 The altered mPER2 substrate selectivity of CK1 *tau* is recapitulated with hPER2 substrates
- 4.7 NMR spectra of the emerging phosphorylation profile of the minimal Degron peptide

- 4.8 NMR kinase assay can monitor site-specific Degron activity in the context of the tandem PAS domains
- 4.9 CK1 contains targetable pockets that are positions to effect substrate selectivity

LIST OF TABLES

- 2.1 X-ray crystallography data collection and refinement statistics
- 2.2 Enzymatic efficiency of CK1 δ Δ C (WT and mutants)
- 2.3 Survey of anion binding and activation loop conformation in CK1 family member structures
- 2.4 Details of simulated systems
- 3.1 X-ray crystallography data collection and refinement statistics

ACKNOWLEDGMENTS

I would like to acknowledge Seth Rubin and the members of the Rubin lab for their continued engagement and feedback on my projects throughout my dissertation. Our shared lab meetings and resources have been instrumental to my time here.

I would like to give special acknowledgement to Clarisse Ricci for her amazing work contributing to projects throughout this dissertation. Her molecular level insights from molecular dynamics experiments and general aesthetic have been instrumental in guiding me towards a deeper understanding of CK1 function.

I would like to give special acknowledgement to my advisor, Carrie Partch. Her dedication to scientific rigor and the circadian field has been truly inspiring. I am extremely grateful for the opportunity to develop a wide range of skills in a lab with such a collaborative ethos and hard work ethic. Carrie's mentorship has cultivated a collegial environment where working with other lab members is a pleasure and I will be sad to leave.

I would like to acknowledge the members of my lab, current and past. They have made coming to work fun and they have provided support, encouragement, and friendship throughout my time here. Late nights and conversations in the lab are among the best memories I have made during my graduate studies.

I would like to acknowledge all the members of my cohort and my girlfriend Kaitlyn. We have created such strong ties and friendships and I don't know how I could have accomplished the last 5 years without you! We've had so much fun and I'm so excited for what the future has in store for us.

I would finally like to acknowledge my family for their love and support on my journey. Without you I would have never had the opportunity to follow my dreams. I never imagined I'd be where I am today, but you have supported me through all of my decisions, and I am so thankful!

Abstract

Title: Casein Kinase 1 δ and PERIOD2 intrinsically regulate circadian timing through a combination of substrate selectivity and feedback inhibition

Author: Jonathan M. Philpott

Biological clocks such as circadian rhythms are perhaps among the most fundamentally conserved adaptations of organisms that have evolved under the light/dark cycle of earth. These rhythms confer an advantage to organisms by allowing them to anticipate daily environmental changes. While the genetic networks that govern circadian rhythms in mammals are now fairly well-established, a picture of the molecular mechanisms that regulate the intrinsic timing of circadian rhythms is only recently beginning to emerge. In this dissertation, I discuss the molecular level details of the mammalian clock and provide new insights that shed light on the biochemical mechanisms of period control within.

Chapter 2 describes how Casein Kinase 1 δ and ϵ (CK1) post-translationally control PERIOD (PER) stability. CK1 is a deeply conserved circadian protein, yet little is known about its regulation of functionally antagonistic sites in PER that control circadian timing. The balance of CK1 activity within these two regions defines a model of PER2 stability known as the phosphoswitch. In this chapter, we discover an allosteric conformational

switch in the CK1 activation loop segment that influences substrate specificity on PER2 to directly regulate its stability. We further show that period-altering mutations of the kinase across organisms differentially modulate the activation loop switch and provide a framework to understand and manipulate CK1 regulation of circadian period.

PER proteins are fundamental in defining the phase and timing of circadian rhythms, likely due to their role as stoichiometrically limiting factors in the assembly of repressive complexes that provide feedback inhibition of transcription within the clock. CK1-dependent changes in PER abundance are therefore central to circadian timing. CK1 phosphorylation of PER2 is mediated by the stable anchoring of CK1 to PER2 via the Casein Kinase 1 Binding Domain (CK1BD). This stable interaction is also required for CK1-mediated displacement of CLOCK from DNA. Chapter 3 describes the role of CK1 phosphorylation of the PER2 FASP region in the regulation of PER2 stability and repressive activity. We show that the phosphorylated FASP region (pFASP) directly interacts with and inhibits CK1 δ , and that stable anchoring to the CK1BD increases the kinetics of FASP phosphorylation and product inhibition. We solve multiple crystal structures of CK1 δ bound to pFASP and conduct accelerated molecular dynamics simulations to reveal a mechanism of inhibition where phosphoserines in pFASP anchor into conserved anion binding sites along the substrate binding cleft and active site of the kinase. We further show how limiting phosphorylation within the FASP region reduces

product inhibition and find that feedback inhibition is a conserved mechanism within *Drosophila* PER.

Much of the work in this dissertation focuses on the molecular determinants that regulate the stabilizing arm of the PER2 phosphoswitch. Chapter 4 discusses the molecular features of PER2 degradation and provides a survey of the current state of my contributions to this area. I provide a framework for extending previous studies using reagents from mPER2 into hPER2, and further discuss future directions to shed light on mechanisms of regulation for CK1 activity within the PER2 Degron and the recruitment of β -TrCP.

In summary, throughout this dissertation I have used an integrative approach of utilizing biochemistry, biophysics, molecular dynamics, and tissue culture to describe how CK1 and PER2 form a critical regulatory nexus within the mammalian circadian clock. In addition to the findings discussed herein, this work has provided a framework for targeted mutations to further develop a molecular level understanding of circadian timekeeping, as well as an avenue to develop novel therapeutics to target the clock and modulate circadian period.

CHAPTER 1

Biochemical mechanisms of period control within the mammalian circadian clock

Acknowledgments

Philpott JM, Torgrimson MR, Harold RL, Partch CL. Biochemical mechanisms of period control within the mammalian circadian clock. *Semin Cell Dev Biol.* 2022 Jun;126:71-78

The following co-authors are acknowledged for their contributions to the published work: JMP, MRT, RLH wrote the manuscript and CLP reviewed and provided edits.

We would like to thank our collaborators Rajesh Narasimamurthy, David Virshup (Duke-NUS Medical School) and Clarisse Ricci (UC San Diego) for fruitful conversations that have helped to frame our understanding of this system.

1.1 Abstract

Genetically encoded biological clocks are found broadly throughout life on Earth, where they generate circadian (*about a day*) rhythms that synchronize physiology and behavior with the daily light/dark cycle. Although the genetic networks that give rise to circadian timing are now fairly well-established, our understanding of how the proteins that constitute the molecular ‘cogs’ of this biological clock regulate the intrinsic timing, or period, of circadian rhythms has lagged behind. New studies probing the biochemical and structural basis of clock protein function are beginning to reveal how assemblies of dedicated clock proteins form and evolve through post-translational regulation to generate circadian rhythms. This review will highlight some recent advances, with an emphasis on structural analyses related to CK1 dependent stability of PER proteins, providing important insight into the molecular mechanisms of period control in mammalian clocks.

1.2 Introduction to the mammalian circadian clock

Circadian rhythms arise from genetically encoded molecular clocks that originate at the cellular level and operate with an intrinsic period of about a day (*circa diem*). The timekeeping encoded by these self-sustained biological clocks persists in constant darkness but responds acutely to changes in daily environmental cues, like light, to keep internal clocks aligned with the external environment [1]. Therefore, circadian rhythms are used to help organisms predict changes in their environment and temporally program regular changes in their behavior and physiology [2].

The circadian clock in mammals is driven by several interlocked transcription-translation feedback loops (TTFLs) [3]. The integration of these interlocked loops is a complicated process that is orchestrated by a core feedback loop in which the heterodimeric transcription factor complex, CLOCK:BMAL1, promotes the transcription of its own repressors, Cryptochrome and Period (CRY and PER) as well as other clock-controlled genes (**Figure 1A**). Notably, there is some redundancy in this system as paralogs of both PER (PER1-3) and CRY (CRY1-2) proteins participate in the core TTFL. In general, these proteins accumulate in the cytoplasm, interact with one another, and recruit a kinase that is essential for the clock, Casein Kinase 1 δ/ϵ (CK1 δ/ϵ), eventually making their way into the nucleus as a large complex to repress CLOCK:BMAL1 transcriptional activity [4, 5].

Despite this relatively simple model for the core circadian feedback loop, there is growing evidence that different repressor complexes that exist throughout the evening may regulate CLOCK:BMAL1 in distinct ways [6, 7]. PER proteins are essential for the nucleation of large protein complexes that form early in the repressive phase [4] by acting as stoichiometrically-limiting factors that are temporally regulated through oscillations in expression [8, 9]. As a consequence, circadian rhythms can be disrupted by constitutively overexpressing PER proteins [8] or established *de novo* with tunable periods through inducible regulation of PER oscillations [10]. CK1 δ/ϵ regulates PER abundance by controlling its degradation post-translationally [11-13]; accordingly, mutations in the kinase [14, 15] or its phosphorylation sites on PER2 [16, 17] can induce large (~4 hr) changes in circadian period, firmly establishing this regulatory mechanism as a central regulator of the mammalian circadian clock. CRY proteins bind directly to CLOCK:BMAL1 [18] and mediate the interaction of PER-CK1 δ/ϵ complexes with CLOCK:BMAL1 leading to phosphorylation of the transcription factor and its release from DNA [6, 19] as well as acting as direct repressors of CLOCK:BMAL1 activity by sequestering the transcriptional activation domain (TAD) of BMAL1 from coactivators like CBP/p300 [20, 21].

Much remains to be elucidated about the assembly and activity of these core clock proteins, but insight into the molecular basis of circadian period determination is growing thanks to the integration of genetic studies from model

organisms and humans with biochemical, structural, and cell-based studies. High-resolution structures have now been determined for most of the globular domains of core clock proteins and some of their complexes [22], with a growing appreciation for the important role that flexible linkers and intrinsically disordered regions play in tuning clock protein function and clock timing (**Figure 1B**) [23]. We will focus here on recent advances in our understanding of the mechanisms of period control by some of the negative elements of the core feedback loop (**Figure 1C**), highlighting the nanoscale structural and dynamic properties of clock proteins that influence their functional roles as repressors within the core TTFL. For a review of mutations in human CRY1 [24, 25] and CRY2 [26] that influence circadian timing, please refer to [27].

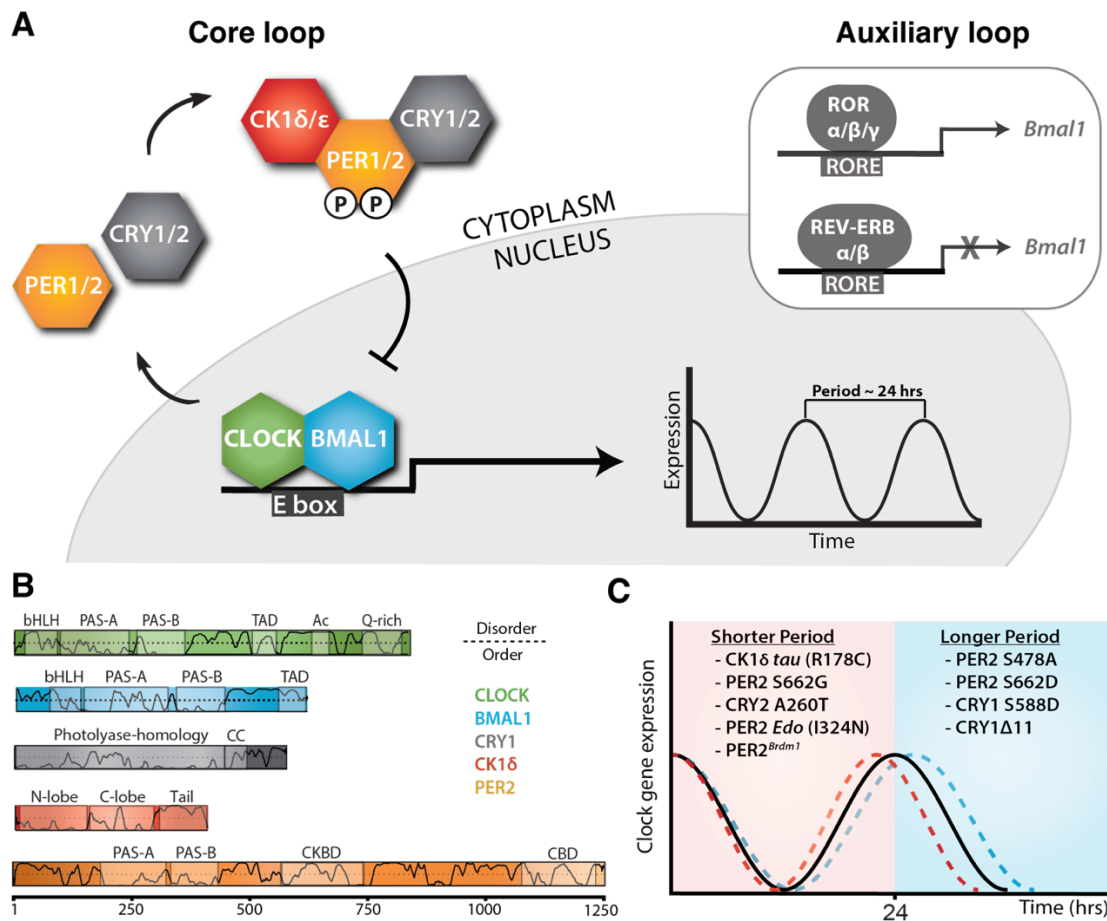


Figure 1.1 Changes to the core molecular clock control mammalian circadian period

(A) Simplified schematic of the core mammalian feedback loop mediated by CLOCK:BMAL1 expression of CRY and PER genes with an auxiliary loop that consists of the retinoic acid receptor-related orphan receptor α (ROR α) and the nuclear receptors REV-ERB α/β . (B) Functional domain architecture of core clock proteins with structured domains (boxes) and traces indicating the propensity for intrinsic disorder [28]: bHLH, basic helix-loop-helix; PAS, PER-ARNT-SIM; TAD, transactivation domain; Ac, acetyl-CoA binding, Q-rich, polyglutamine; CC, coiled-coil; CKBD, Casein Kinase 1-binding domain; and CBD, CRY-binding domain with residue numbering underneath. (C) Period effects from select mammalian clock alleles of core clock proteins.

1.3 Evidence and structural basis for the distinct roles of CRY1/2

Cryptochromes are crucial components of the core molecular clock and normal circadian rhythmicity [29]. For example, the locomotor activity of *Cry*-double-knockout mice is completely arrhythmic [30]. CRY1 and CRY2 are very similar in sequence and structure, but they appear to have distinct functions within the core molecular clock—*Cry1*-double-knockout mice have a shorter circadian period, while the converse is true for *Cry2*-double-knockout mice [29-31]. Apart from their apparent functional differences, CRY1 and CRY2 are differentially expressed, with CRY1 expression delayed relative to the other negative elements of the core clock [5, 32]. Yet the relatively delayed expression of CRY1 cannot account for the differential regulation between CRY1/2, as expression of CRY2 from a minimal CRY1 promoter recapitulates the shorter, CRY2-like period [33, 34]. Therefore, the alternate function of each CRY protein lies within the structurally encoded differences between the two. In line with this, CRY1 has been shown to bind more tightly to CLOCK:BMAL1, facilitating stronger repression than CRY2 [35], and increasing CRY1 affinity for CLOCK:BMAL1 leads to a longer period [20, 21]. Further, CRY1 is able to form a repressive complex with CLOCK:BMAL1 in the late repressive phase, around CT0-4, independent of CRY2 and PER proteins [7]. CRY2 on the other hand, is only found in the early repressive complexes that contain PERs and CRY1 [4, 5] (**Fig 2D**).

CRY1 and CRY2 proteins share a highly conserved photolyase homology region (PHR) domain and a non-conserved, intrinsically disordered C-terminal tail [36] (**Fig 2A**). Of these two functional domains, the PHR domain is required to generate normal circadian rhythms [37], whereas the tail can be deleted or modified to affect the amplitude and period of circadian rhythms [25, 38-40]. As a crucial negative element within the TTFL, CRY1 has been shown to bind directly to the transactivation domain (TAD) of BMAL1, via the CC helix domain (**Fig 2A**), to facilitate a direct mechanism of repression by sequestration of the TAD from coactivators [21, 41]. Outside of this direct mechanism of repression, CRY1 repression also depends on the interaction between the CRY PHR domain and the PAS domains of CLOCK:BMAL1, mediated through docking of the HI loop region of the CLOCK PAS-B domain into the conserved secondary pocket of the CRY PHR [42] (**Fig 2A, C**).

The secondary pocket of CRY1 and CRY2 are subtly divergent, leading to their differential effects on circadian period [34, 43]. A serine loop region that lies adjacent to the secondary pocket (**Fig 2B**) has been shown to be important for the overall structural dynamics in this region of the PHR domain [43]. The differential dynamics between CRY1 and CRY2 at the secondary pocket leads to their altered affinity for the HI loop of CLOCK PAS-B, and substitution of residues in either the secondary pocket or the serine loop can modulate the affinity of this interaction [34]. Moreover, the PER2 CRY-binding domain (CBD)

adds a layer of functional regulation to the CRY PHR:CLOCK PAS-B interaction by differentially remodeling the structure of the serine loop that is adjacent to the CRY secondary pocket (**Fig 2B**). PER2 therefore helps to equalize the affinity between the PHR and CLOCK PAS-B for CRY1 and CRY2, increasing CRY2 affinity and decreasing CRY1 affinity [43]. Since CRY2 is unable to form a repressive complex with CLOCK:BMAL1 independent of the PER and CRY1 proteins, it seems likely that PER at least partially facilitates CRY2 association and repression of CLOCK:BMAL1 within the early repressive complex through this mechanism.

1.4 CRY and its autoregulatory tail

The intrinsically disordered C-terminal tail of CRY1 and CRY2 also plays a role in modulating the interaction of CRY PHR:CLOCK PAS-B. The tail, particularly the region of exon 11, competes with the HI loop of CLOCK PAS-B for binding to the secondary pocket of the PHR (**Fig 2A**). This interaction is reduced in the presence of PER2, therefore it largely plays a role in the late repressive complex where CRY1 alone is bound to CLOCK:BMAL1 [24]. The importance of this interaction can be seen in familial Delayed Sleep Phase Syndrome (DSPS) caused by deletion of exon 11 in CRY1 [25]. Moreover, the tail also plays a role in regulating the stability of CRY1 through phosphorylation of S588 which prevents degradation by FBXL3. Mutation of this residue to a

phospho-mimetic or inhibition/deletion of the kinase that regulates its phosphorylation results in lengthened period [40, 44].

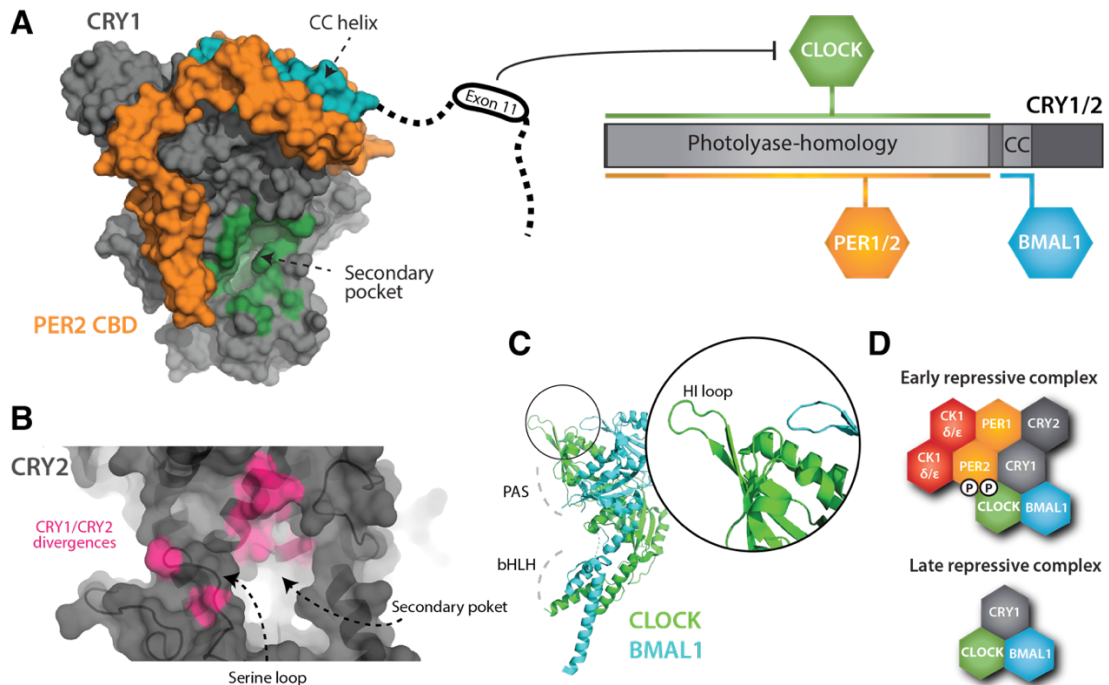


Figure 1.2 Structural features of CRY period control within the mammalian clock

(A) Structural surface representation of CRY photolyase-homology region (PHR, grey) in complex with PER2 CRY binding domain (CBD, orange), with CC-helix (blue) and secondary pocket (green) shown. Domain map indicates regions of CRY that bind to core clock proteins. (B) Zoom of the CRY PHR with key features highlighted. Pink coloring indicates divergence in residue composition between CRY1 and CRY2. (C) Cartoon representation of CLOCK:BMAL1 bHLH PAS-AB heterodimer. Zoom shows the HI loop of CLOCK PAS-B that binds to the secondary pocket of CRY. (D) Simplified depiction of core clock components involved in distinct repressive complexes throughout the circadian cycle.

1.5 Post-translational regulation of PER2 stability

Although transcriptional regulation by CLOCK:BMAL1 and downstream transcription factors is essential for generation of robust circadian rhythms, it is becoming increasingly clear that post-transcriptional and post-translational modifications of core clock components play an important role in both the generation of circadian rhythms and determination of its intrinsic period [45]. While many studies have identified roles for post-translational modification of CRY and PER proteins in clock timing, we will focus here on an in-depth analysis of the regulation of PER2 by CK1 δ/ϵ , as it relies on an elaborate integration of post-translational modifications that ultimately determine the relative abundance of PER2 needed to maintain a ~24-hour period [46].

1.6 Structural organization of PER2

PER1 and PER2 serve as interaction hubs for both CK1 δ/ϵ and cryptochromes with dedicated binding sites that maintain stable complexes with these core clock proteins throughout most of the repressive phase of the clock each day [4, 5] (**Figure 2A**), a feature that is notably absent in PER3 [47]. The flexibility of PER proteins likely contributes to their role as labile scaffolds for transcriptional regulators of the clock; PER1-3 are all predominantly intrinsically disordered, conferring a susceptibility to regulation by post-translational modifications and promiscuity for interaction partners [48-52] that is common among other intrinsically disordered proteins (IDPs) [53]. Two

tandem PER-ARNT-SIM (PAS) domains present in the N-terminus of all three PER isoforms allow them to form homodimers and heterodimers (**Figure 2A**) [54-56] mediated by the β -sheet surface of the PAS-B domain (**Figure 2B**). Deletion of the core PAS-B motif in the *Per2^{Brdm1}* mutant leads to a loss of circadian rhythms, demonstrating that protein-protein interactions facilitated by this region are essential for clock function [57]. Notably, mutation of just a single residue, W419E, at the dimer interface in the mouse PER2 PAS-B domain potently disrupts formation of homodimers [54] and was recently shown to reduce phosphorylation by CK1 δ [58]. Moreover, the PER2 *earlydoors* (*Edo*) mouse possesses a point mutation (I324N) in the interdomain linker connecting the PAS-A and B domains that reduces PER2 stability to shorten the circadian period [59]. Collectively, these findings demonstrate that dimerization via the PER PAS domains is critical for protein stability and clock timing, although more work is needed to understand the exact role that PAS domains play in orchestrating clock protein complexes and PER turnover.

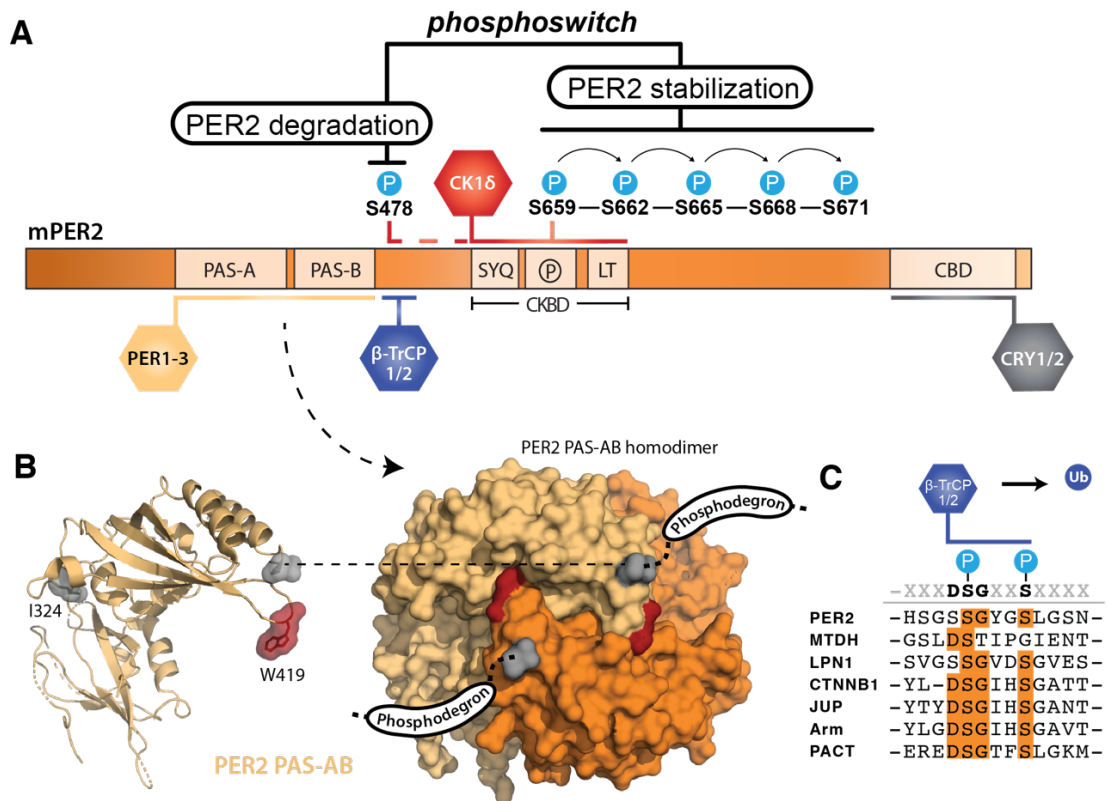


Figure 1.3 PER2 stability is tightly regulated by post-translational modifications

(A) Domain map of mouse PER2 depicting clock protein binding sites and the CK1 δ -dependent phosphoswitch model. CK1 δ dependent phosphorylation of the FASP region (P) within the CKBD antagonizes activity at the upstream phosphodegron, which is used to recruit the E3 ubiquitin ligases, β -TrCP1/2 for subsequent proteasomal degradation of PER2. (B) Left, cartoon representation of the mouse PER2 PAS-AB domain monomer with the location of the *Edo* mutation (I324N) and Trp residue required for dimerization (W419) highlighted, PDB: 3GDI. Right, surface representation of the PER2 PAS-AB homodimer. The phosphodegron is located in a disordered region immediately downstream of the PAS-B domain; the C-terminal residue is depicted in surface mode (gray) to show how each respective phosphodegron is poised to protrude from the same face of the dimer. (C) Alignment of phosphodegrons within human proteins that are targeted by β -TrCP1/2.

1.7 Control of PER2 degradation by phosphodegrons

The turnover of PER2 is primarily mediated by CK1 δ/ϵ -dependent phosphodegrons to intimately link kinase activity with PER2 stability. One well-studied phosphodegrogen site of mouse PER2 (S478) is located immediately downstream of the PAS-B domain. Dimerization of the PER2 PAS-AB domains positions the phosphodegrogen site (S478) of each monomer to protrude from the same face of the PAS-AB domain homodimer (**Figure 2B**) [54]. This phosphodegrogen largely conforms to the canonical β -TrCP recognition motif, DSG ϕ XS, where ϕ is a hydrophobic residue and the two conserved serines become phosphorylated to make the substrate competent for β -TrCP recognition (**Figure 2C**) [60]. CK1 δ/ϵ phosphorylation of S478 in mouse PER2, the first of the two serines in the motif, is required for interaction with the E3 ubiquitin ligases β -TrCP1/2, leading to ubiquitination of PER2 and its proteasomal degradation [12, 61, 62]. However, this PAS-B phosphodegrogen is unique to PER2; PER1 utilizes a different CK1 δ/ϵ -dependent phosphodegrogen N-terminal to the tandem PAS domains [13]. This N-terminal phosphodegrogen is also conserved in PER2 [61] and may play an auxiliary role in its turnover, as clock timing was only modestly impacted in the PER2 S478A transgenic mouse [63]. An interaction with the E3 ubiquitin ligase MDM2 also influences PER2 stability independently of CK1 δ/ϵ activity [64], opening the door for a complex integration of signals to mediate PER2 degradation.

1.8 The Casein Kinase-Binding Domain stabilizes PER2 through a phosphoswitch

Although other kinases such as CK1 α [65], CK2 [66], SIK3 [67] and Cdk5 [68] phosphorylate PER2, CK1 δ/ϵ is the only one that stably associates with PER2 throughout the night, moving from the cytoplasm into the nucleus with the other core clock proteins [4, 5]. CK1 δ and the related isoform CK1 ϵ bind to the Casein Kinase-Binding Domain (CKBD) in PER2 via two conserved motifs that flank a serine-rich region [12, 47]. Notably, mutation of the first residue (S662G) in a series of five consecutive serines that are phosphorylated in human PER2 markedly decreases its stability and shortens circadian period by ~4 hours to manifest as Familial Advanced Sleep Phase Syndrome (FASPS) [16, 17]. Because CK1 δ/ϵ dependent phosphorylation of PER2 in this region links circadian timekeeping to this human sleep disorder, the serine-rich cluster in the CKBD has been named the FASP region.

Recent studies have begun to elucidate the molecular basis for CK1 δ/ϵ activity in the FASP region of PER2 to understand how it exerts such powerful control over circadian period. Phosphorylation of the first serine in this cluster (S659 in mouse, S662 in humans) by CK1 δ leads to the obligately sequential phosphorylation of downstream serines (**Figure 2A**) [69]. Therefore, the human S662G FASPS allele eliminates the ability of CK1 δ to prime its activity downstream, disrupting all phosphorylation in the FASP region. There is strong evidence that FASP phosphorylation plays a critical role in stabilizing PER2

protein [16], as the S662G mutation in human PER2 (or the analogous S659A mutation in mouse PER2) [70] leads to premature turnover of the protein and a dramatically shorter circadian period of ~20 hours in a transgenic mouse model, while use of a phosphomimetic mutation (S662D) in human PER2 that presumably leads to constitutive priming of sequential FASP phosphorylation confers a long period of ~25 hours *in vivo* [17]. Although it is not yet known how FASP phosphorylation contributes to regulation of PER2 stability, mutation of the priming serine that blocks phosphorylation of FASP downstream serines increases CK1 δ/ϵ activity at the phosphodegron site S478 [71] to suggest that the phospho-FASP region could antagonize CK1 δ/ϵ activity at the phosphodegron site S478. The opposing effects of FASP and phosphodegron phosphorylation likely involves cellular phosphatases like PP1 that contribute to CK1 δ/ϵ -dependent regulation of circadian period through PER2 [72], although there could also be a direct mechanistic link between FASP phosphorylation and regulation of CK1 δ/ϵ activity. In fact, the functional linkage of phosphorylation at the FASP region and phosphodegron by CK1 δ/ϵ has been described as a phosphoswitch that introduces a phase-specific delay to PER2 degradation necessary for proper circadian timekeeping (**Figure 2A**) [73]. Interestingly, while introduction of the analogous priming site mutation in mouse PER1 (S714G) destabilized PER1 and led to a shorter circadian period, it also caused an advance in feeding rhythms not seen in the PER2 mutant [74], suggesting that further study of the regulation of PER turnover could help

uncouple distinct functions of PER1 and PER2 in control of circadian period and clock outputs.

1.9 Other Post-translational modifications influence PER2 stability

PER proteins are also subjected to a number of other post-translational modifications aside from phosphorylation. PER2 is O-GlcNAcylated within the FASP region [75], modifying the priming serine along with two sites downstream. Both O-GlcNAc transferase (OGT) and O-GlcNAcase (OGA), the enzymes responsible for adding or hydrolyzing O-GlcNAc, respectively, are expressed or activated in a circadian manner, and factors that increase O-GlcNAcylation also lead to a concomitant decrease in FASP phosphorylation that reduces PER2 protein levels [75, 76]. These results support a model for competition between O-GlcNAcylation and phosphorylation at this key regulatory region, suggesting a mechanism by which glucose metabolism could modulate the circadian clock by antagonizing phosphorylation of PER2 in the stabilizing FASP region to represent a direct link between the circadian clock and metabolism as a “nutrition switch” [46, 75].

Acetylation also plays an important yet enigmatic role in PER2 regulation of the clock, first observed through manipulation of SIRT1, the nicotinamide adenine dinucleotide (NAD⁺)-dependent deacetylase. Although PER2 becomes acetylated as it accumulates throughout the repressive phase of the circadian clock [77], the identity of the acetyltransferase(s) that modify PER2 is

currently not known, nor is it known where PER2 is acetylated throughout the protein. Nonetheless, loss of SIRT1 results in elevated levels of acetylated PER2 in mouse liver to attenuate the robustness of circadian rhythms, while overexpression of SIRT1 facilitates PER2 degradation [77, 78]. Because acetylation and ubiquitination both target lysine residues, it is possible that these modifications compete for the same residues to directly control PER2 stability. However, there is some evidence that regulation of PER2 by acetylation could be more complicated, as acetylation at K680 on mouse PER2, located downstream of the serine cluster in the FASP region, is hyperacetylated following inhibition of SIRT1 and leads to a decrease in FASP phosphorylation [79], suggesting that an interplay between acetylation and phosphorylation of the FASP region could also control CK1 δ/ϵ activity on PER2 to regulate the balance of the phosphoswitch.

1.10 A central role for CK1 in eukaryotic circadian period determination

The timing of eukaryotic circadian rhythms from green algae to humans is heavily influenced by CK1 δ/ϵ and its related orthologs [15, 80]. Like other Ser/Thr kinases, CK1 δ/ϵ has a typical two-lobed structure (**Figure 3A**), but little is known about the molecular mechanisms by which activity of the CK1 family is regulated. The activation loop is one key feature that distinguishes the CK1 family from other Ser/Thr kinases (**Figure 3B**) [81]. Unlike many other kinases, the kinase domain of CK1 family members is not regulated by activation loop

phosphorylation; therefore, they are considered to be constitutively active [82]. The CK1 family acts as phosphate-directed kinases that preferentially recognize a D/E/pSxxS consensus motif, where a phosphorylated serine or a similar negative charge within the substrate templates activity at a serine located 3 or 4 residues downstream (**Figure 3A**) [83]. Interestingly, at least two functionally important CK1 δ/ϵ dependent phosphorylation sites on PER2, the phosphodegron and the FASP priming site, do not conform to this consensus motif and likely serve as slow, rate-limiting steps for PER2 regulation [69, 71, 84]. Therefore, understanding the molecular basis for kinase activity and substrate selectivity by CK1 δ/ϵ has the potential to yield important insights into circadian timekeeping. In particular, a better understanding of the molecular mechanisms underpinning CK1 δ/ϵ dependent phosphorylation of PER will provide a framework for treating circadian disorders by targeting CK1 δ/ϵ to modulate the clock [85].

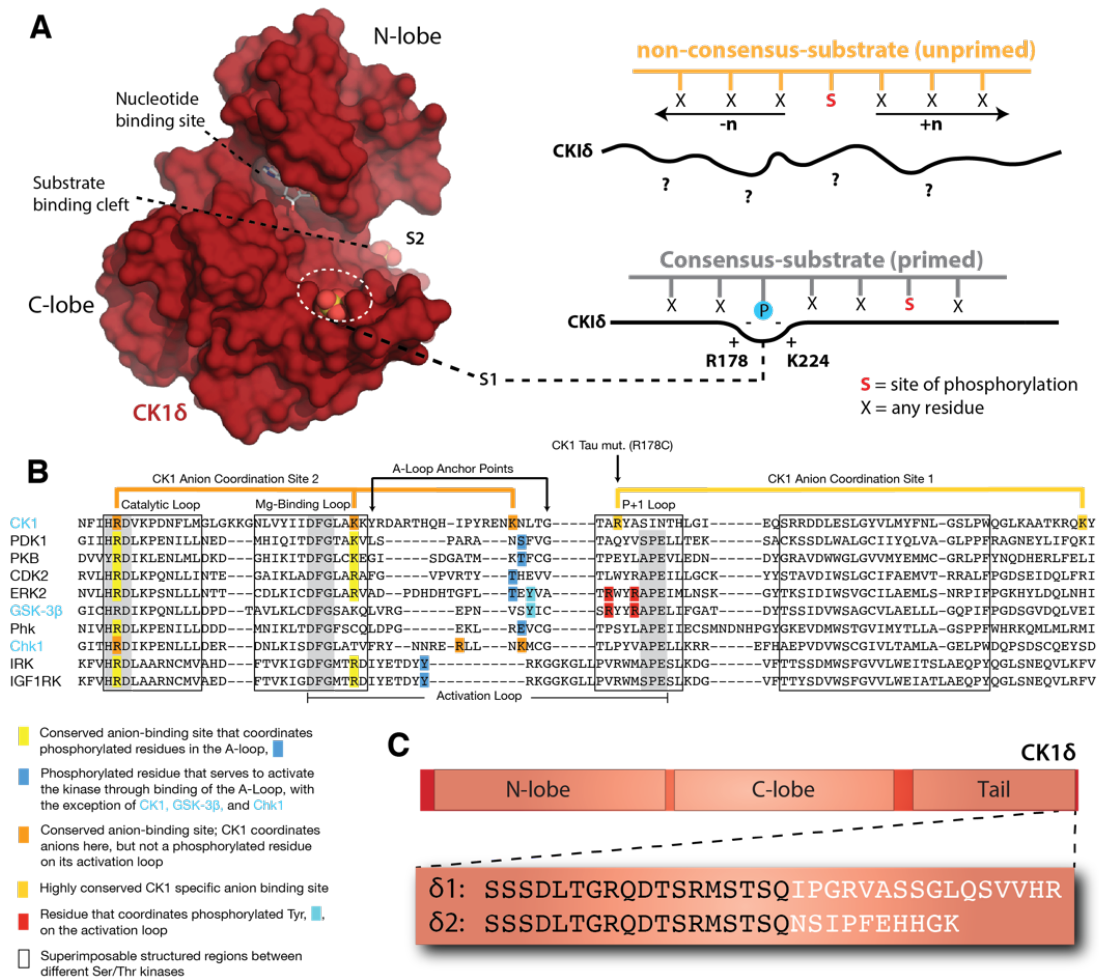


Figure 1.4 Regulatory mechanisms control CK1δ activity in the mammalian clock

(A) Left, Surface representation of the CK1δ kinase domain, PDB: 5X17. The substrate binding cleft is flanked by two highly conserved anion binding sites, S1 and S2. Right, CK1 is thought to use S1 to bind phosphorylated (or 'primed') substrates, leading to phosphorylation of the CK1 consensus motif, pSxxS. CK1 also exhibits non-consensus activity on unprimed sites. (B) Alignment of the activation loop and nearby regions in representative Ser/Thr kinases. CK1 lacks the conserved APE motif in the P+1 loop involved in substrate recognition. (C) Differences between the alternatively spliced variants CK1δ1 and CK1δ2 at the C-terminus of the kinase.

1.11 Anion-dependent regulation of a structural switch in CK1 δ

CK1 δ/ϵ contains several highly conserved anion binding sites located around the C-terminal lobe of the kinase domain, including two that flank either side of the substrate binding cleft (**Figure 3A, B**) [86-88]. We recently showed that these anion binding sites regulate the overall kinase activity of CK1 δ/ϵ , as well as influence the substrate specificity of the kinase at both consensus and non-consensus sites [71]. The significance of these highly conserved anion binding sites was initially suggested by the discovery of the first period-altering allele in mammals, the CK1 ϵ *tau* allele that causes a dramatically shortened circadian period of ~20 hours [89]. The R178C substitution in the *tau* kinase was predicted to disrupt an anion-binding pocket near the substrate binding region to decrease CK1 δ/ϵ activity [14]. While the *tau* mutant kinase did exhibit reduced activity on some generic kinase substrates (e.g., casein and phosvitin) as well as the FASP region of PER2, it led to a paradoxical gain of function at the PER2 phosphodegron that decreased stability of the protein [71, 90].

Crystal structures of the *tau* kinase domain recently revealed that disruption of the anion binding pocket at S1 in the mutant is linked to an allosteric structural switch in the activation loop that encodes a preference for the PER2 PAS-B phosphodegron site S478 [71]. Allostery is a common regulatory feature of protein kinases that allows for a switch-like, ultrasensitive regulation of their biological activity [91]. The activation loop and flanking regions distinguish CK1 from all other Ser/Thr kinases (**Figure 3B**) [92],

containing residues involved in the coordination of anions at three conserved sites, S1-S3. Therefore, these sites likely play a role in the CK1 family-specific regulation of kinase activity, perhaps through binding of anionic, phosphorylated residues. Interestingly, the entire substrate binding cleft that allosterically links anion binding to substrate selectivity is 95% identical from humans to green algae [71], suggesting that the mechanisms discovered in mammalian CK1 δ/ϵ may also regulate kinase activity and circadian period across other eukaryotic clocks.

1.12 Regulation of CK1 δ/ϵ activity by its C-terminal tail

The kinase activity of both CK1 δ and CK1 ϵ is inhibited by autophosphorylation of an intrinsically disordered inhibitory tail that follows the kinase domain to set these isoforms apart from other members of the CK1 family [93-96]. Because the full-length kinase autophosphorylates and slowly inactivates itself *in vitro*, most biochemical studies exploring the activity of CK1 δ/ϵ on clock proteins utilize the truncated, constitutively active protein (CK1 δ/ϵ Δ C) [69, 71, 87, 97], although new studies are finally beginning to explore the consequences of autophosphorylation in more detail [98, 99]. However, not much is known yet about how the phosphorylated tail interacts with the kinase domain to inhibit its activity; several autophosphorylation sites were previously identified on CK1 ϵ at S323, T325, T334, T337, S368, S405, S407 and S408 using limited proteolysis and phosphatase treatment [95] or

through Ser/Thr to Ala substitutions *in vitro* [96], although it is currently not known which (if any) of these sites are important for kinase regulation of the clock. One potential interface has been mapped between the kinase domain and autoinhibitory tail through crosslinking and mass spectrometry to suggest that the tail might dock some phosphorylated Ser/Thr residues close to the anion binding sites near the active site [100]. This study also provided evidence that the tail may be able to regulate substrate binding, and therefore control specificity of the kinase, by comparing the activity of CK1 α , a tailless kinase, with CK1 ϵ on two substrates, PER2 and Disheveled [100]. Understanding the role of tail autophosphorylation and its regulation of kinase activity is sure to shed light on control of circadian rhythms by CK1 δ/ϵ .

Some sites within the C-terminal tail of CK1 δ and/or CK1 ϵ are known to be phosphorylated by other kinases, such as AMPK [101], PKA [102], Chk1 [103], PKC α [104], and cyclin-dependent kinases [105, 106]. PKA phosphorylates S370 in CK1 δ to reduce its kinase activity; consistent with this, mutation of S370 to alanine increases CK1-dependent ectopic dorsal axis formation in *Xenopus laevis* [102]. Chk1 and PKC α also reduce CK1 δ kinase activity through phosphorylation of overlapping sites at S328, T329, S331, S370, and T397 in the tail of rat CK1 δ [103, 104]. Phosphorylation of CK1 δ T347 influences its activity on PER2 in cells, and was found to be phosphorylated by proline-directed cyclin-dependent kinases rather than autophosphorylation [105]. CDK2 was also found to reduce the activity of rat

CK1 δ *in vitro* through phosphorylation of additional sites at T329, S331, T344, S356, S361, and T397 [106]. Unlike the other kinases listed here, phosphorylation of S389 on CK1 ϵ by AMPK increases the apparent kinase activity on the PER2 phosphodegron in cells; consequently, activation of AMPK with metformin increased the degradation of PER2 [101]. Therefore, the phosphorylation of CK1 δ and/or CK1 ϵ tails by these other kinases therefore has the potential to link its regulation of PER2 and the circadian clock to metabolism, DNA damage response, and the cell cycle.

There is now strong evidence that the C-terminus of CK1 δ plays a direct role in regulation of circadian period. Recently, tissue-specific methylation of CK1 δ was shown to regulate alternative splicing of the kinase into two unique isoforms, δ 1 and δ 2, that differ only by the extreme C-terminal 15 residues (**Figure 3C**) [107]. Remarkably, expression of the canonical δ 1 isoform decreases PER2 half-life and circadian period, while the slightly shorter δ 2 isoform increases PER2 half-life and circadian period [107]. Further biochemical studies revealed that these two variants exhibit differential activity on the stabilizing priming site of the PER2 FASP region—the δ 1 isoform has a lower activity than δ 2, which also closely resembles the C-terminus of the ϵ isoform [69]. These data suggest that a very short region at the C-terminal end of the tail could play a major role in regulation of CK1 δ and the PER2 phosphoswitch to control circadian period. This is bolstered by the discovery of a missense mutation in the same region of the CK1 ϵ tail at S408N in humans

that has been associated with protection from Delayed Sleep Phase Syndrome (DSPS) and Non-24-hr Sleep-Wake Syndrome (N-24) [108]. Further studies will help to reveal biochemical mechanisms behind regulation of kinase activity and substrate selectivity by the C-terminal tail of CK1 δ and CK1 ϵ to determine how they play into regulation of circadian rhythms.

1.13 Concluding remarks

While there is much more to be learned, data from human genetics and mammalian model systems are finally being integrated with biochemical and structural studies of the core clock components to provide clues to the molecular basis of the circadian clock. Recent advances in biophysical techniques, such as cryo-EM, will help to further enhance our understanding of how the molecular ‘cogs’ of the core clock come together to affect circadian period and influence human behavior and physiology.

References

1. Aschoff, J., *Circadian Rhythms in Man*. Science, 1965. **148**(3676): p. 1427-32.
2. Bass, J. and M.A. Lazar, *Circadian time signatures of fitness and disease*. Science, 2016. **354**(6315): p. 994-999.
3. Takahashi, J.S., *Transcriptional architecture of the mammalian circadian clock*. Nat Rev Genet, 2017. **18**(3): p. 164-179.

4. Aryal, R.P., et al., *Macromolecular Assemblies of the Mammalian Circadian Clock*. Mol Cell, 2017. **67**(5): p. 770-782 e6.
5. Lee, C., et al., *Posttranslational mechanisms regulate the mammalian circadian clock*. Cell, 2001. **107**(7): p. 855-67.
6. Chiou, Y.Y., et al., *Mammalian Period represses and de-represses transcription by displacing CLOCK-BMAL1 from promoters in a Cryptochrome-dependent manner*. Proc Natl Acad Sci U S A, 2016. **113**(41): p. E6072-E6079.
7. Koike, N., et al., *Transcriptional architecture and chromatin landscape of the core circadian clock in mammals*. Science, 2012. **338**(6105): p. 349-54.
8. Chen, R., et al., *Rhythmic PER abundance defines a critical nodal point for negative feedback within the circadian clock mechanism*. Mol Cell, 2009. **36**(3): p. 417-30.
9. Lee, Y., et al., *Stoichiometric relationship among clock proteins determines robustness of circadian rhythms*. J Biol Chem, 2011. **286**(9): p. 7033-42.
10. D'Alessandro, M., et al., *A tunable artificial circadian clock in clock-defective mice*. Nat Commun, 2015. **6**: p. 8587.
11. Akashi, M., et al., *Control of intracellular dynamics of mammalian period proteins by casein kinase I epsilon (CKIepsilon) and CKIdelta in cultured cells*. Mol Cell Biol, 2002. **22**(6): p. 1693-703.
12. Eide, E.J., et al., *Control of mammalian circadian rhythm by CKIepsilon-regulated proteasome-mediated PER2 degradation*. Mol Cell Biol, 2005. **25**(7): p. 2795-807.
13. Shirogane, T., et al., *SCFbeta-TRCP controls clock-dependent transcription via casein kinase 1-dependent degradation of the mammalian period-1 (Per1) protein*. J Biol Chem, 2005. **280**(29): p. 26863-72.

14. Lowrey, P.L., et al., *Positional syntenic cloning and functional characterization of the mammalian circadian mutation tau*. Science, 2000. **288**(5465): p. 483-92.
15. Xu, Y., et al., *Functional consequences of a CK1delta mutation causing familial advanced sleep phase syndrome*. Nature, 2005. **434**(7033): p. 640-4.
16. Toh, K.L., et al., *An hPer2 phosphorylation site mutation in familial advanced sleep phase syndrome*. Science, 2001. **291**(5506): p. 1040-3.
17. Xu, Y., et al., *Modeling of a human circadian mutation yields insights into clock regulation by PER2*. Cell, 2007. **128**(1): p. 59-70.
18. Ye, R., et al., *Biochemical analysis of the canonical model for the mammalian circadian clock*. J Biol Chem, 2011. **286**(29): p. 25891-902.
19. Cao, X., et al., *Molecular mechanism of the repressive phase of the mammalian circadian clock*. Proc Natl Acad Sci U S A, 2021.
20. Gustafson, C.L., et al., *A Slow Conformational Switch in the BMAL1 Transactivation Domain Modulates Circadian Rhythms*. Mol Cell, 2017. **66**(4): p. 447-457 e7.
21. Xu, H., et al., *Cryptochrome 1 regulates the circadian clock through dynamic interactions with the BMAL1 C terminus*. Nat Struct Mol Biol, 2015. **22**(6): p. 476-484.
22. Partch, C.L., *Orchestration of Circadian Timing by Macromolecular Protein Assemblies*. J Mol Biol, 2020. **432**(12): p. 3426-3448.
23. Dunlap, J.C. and J.J. Loros, *Just-So Stories and Origin Myths: Phosphorylation and Structural Disorder in Circadian Clock Proteins*. Mol Cell, 2018. **69**(2): p. 165-168.
24. Parico, G.C.G., et al., *The human CRY1 tail controls circadian timing by regulating its association with CLOCK:BMAL1*. Proc Natl Acad Sci U S A, 2020. **117**(45): p. 27971-27979.

25. Patke, A., et al., *Mutation of the Human Circadian Clock Gene CRY1 in Familial Delayed Sleep Phase Disorder*. Cell, 2017. **169**(2): p. 203-215 e13.
26. Hirano, A., et al., *A Cryptochrome 2 mutation yields advanced sleep phase in humans*. Elife, 2016. **5**.
27. Parico, G.C.G. and C.L. Partch, *The tail of cryptochromes: an intrinsically disordered cog within the mammalian circadian clock*. Cell Commun Signal, 2020. **18**(1): p. 182.
28. Xue, B., et al., *PONDR-FIT: a meta-predictor of intrinsically disordered amino acids*. Biochim Biophys Acta, 2010. **1804**(4): p. 996-1010.
29. Vitaterna, M.H., et al., *Differential regulation of mammalian period genes and circadian rhythmicity by cryptochromes 1 and 2*. Proc Natl Acad Sci U S A, 1999. **96**(21): p. 12114-9.
30. van der Horst, G.T., et al., *Mammalian Cry1 and Cry2 are essential for maintenance of circadian rhythms*. Nature, 1999. **398**(6728): p. 627-30.
31. Michael, A.K., et al., *Animal Cryptochromes: Divergent Roles in Light Perception, Circadian Timekeeping and Beyond*. Photochem Photobiol, 2017. **93**(1): p. 128-140.
32. Ukai-Tadenuma, M., et al., *Delay in feedback repression by cryptochrome 1 is required for circadian clock function*. Cell, 2011. **144**(2): p. 268-81.
33. Edwards, M.D., et al., *Rhythmic expression of cryptochrome induces the circadian clock of arrhythmic suprachiasmatic nuclei through arginine vasopressin signaling*. Proc Natl Acad Sci U S A, 2016. **113**(10): p. 2732-7.
34. Rosensweig, C., et al., *An evolutionary hotspot defines functional differences between CRYPTOCHROMES*. Nat Commun, 2018. **9**(1): p. 1138.

35. Griffin, E.A., Jr., D. Staknis, and C.J. Weitz, *Light-independent role of CRY1 and CRY2 in the mammalian circadian clock*. Science, 1999. **286**(5440): p. 768-71.
36. Partch, C.L., et al., *Role of structural plasticity in signal transduction by the cryptochrome blue-light photoreceptor*. Biochemistry, 2005. **44**(10): p. 3795-805.
37. Khan, S.K., et al., *Identification of a novel cryptochrome differentiating domain required for feedback repression in circadian clock function*. J Biol Chem, 2012. **287**(31): p. 25917-26.
38. Gao, P., et al., *Phosphorylation of the cryptochrome 1 C-terminal tail regulates circadian period length*. J Biol Chem, 2013. **288**(49): p. 35277-86.
39. Li, Y., W. Xiong, and E.E. Zhang, *The ratio of intracellular CRY proteins determines the clock period length*. Biochem Biophys Res Commun, 2016. **472**(3): p. 531-8.
40. Liu, N. and E.E. Zhang, *Phosphorylation Regulating the Ratio of Intracellular CRY1 Protein Determines the Circadian Period*. Front Neurol, 2016. **7**: p. 159.
41. Czarna, A., et al., *Quantitative analyses of cryptochrome-mBMAL1 interactions: mechanistic insights into the transcriptional regulation of the mammalian circadian clock*. J Biol Chem, 2011. **286**(25): p. 22414-25.
42. Michael, A.K., et al., *Formation of a repressive complex in the mammalian circadian clock is mediated by the secondary pocket of CRY1*. Proc Natl Acad Sci U S A, 2017. **114**(7): p. 1560-1565.
43. Fribourgh, J.L., et al., *Dynamics at the serine loop underlie differential affinity of cryptochromes for CLOCK:BMAL1 to control circadian timing*. Elife, 2020. **9**.

44. Gao, P., et al., *Phosphorylation of the Cryptochrome 1 C-terminal Tail Regulates Circadian Period Length*. The Journal of Biological Chemistry, 2013. **288**(49): p. 35277-35286.
45. Crosby, P. and C.L. Partch, *New insights into non-transcriptional regulation of mammalian core clock proteins*. J Cell Sci, 2020. **133**(18).
46. Hirano, A., Y.H. Fu, and L.J. Ptacek, *The intricate dance of post-translational modifications in the rhythm of life*. Nat Struct Mol Biol, 2016. **23**(12): p. 1053-1060.
47. Lee, C., D.R. Weaver, and S.M. Reppert, *Direct association between mouse PERIOD and CKepsilon is critical for a functioning circadian clock*. Mol Cell Biol, 2004. **24**(2): p. 584-94.
48. Brown, S.A., et al., *PERIOD1-associated proteins modulate the negative limb of the mammalian circadian oscillator*. Science, 2005. **308**(5722): p. 693-6.
49. Duong, H.A., et al., *A molecular mechanism for circadian clock negative feedback*. Science, 2011. **332**(6036): p. 1436-9.
50. Duong, H.A. and C.J. Weitz, *Temporal orchestration of repressive chromatin modifiers by circadian clock Period complexes*. Nat Struct Mol Biol, 2014. **21**(2): p. 126-32.
51. Padmanabhan, K., et al., *Feedback regulation of transcriptional termination by the mammalian circadian clock PERIOD complex*. Science, 2012. **337**(6094): p. 599-602.
52. Robles, M.S., et al., *Identification of RACK1 and protein kinase Calpha as integral components of the mammalian circadian clock*. Science, 2010. **327**(5964): p. 463-6.
53. Oldfield, C.J. and A.K. Dunker, *Intrinsically disordered proteins and intrinsically disordered protein regions*. Annu Rev Biochem, 2014. **83**: p. 553-84.

54. Hennig, S., et al., *Structural and functional analyses of PAS domain interactions of the clock proteins Drosophila PERIOD and mouse PERIOD2*. PLoS Biol, 2009. **7**(4): p. e94.
55. Kucera, N., et al., *Unwinding the differences of the mammalian PERIOD clock proteins from crystal structure to cellular function*. Proc Natl Acad Sci U S A, 2012. **109**(9): p. 3311-6.
56. Yagita, K., et al., *Dimerization and nuclear entry of mPER proteins in mammalian cells*. Genes Dev, 2000. **14**(11): p. 1353-63.
57. Zheng, B., et al., *The mPer2 gene encodes a functional component of the mammalian circadian clock*. Nature, 1999. **400**(6740): p. 169-73.
58. Beesley, S., et al., *Wake-sleep cycles are severely disrupted by diseases affecting cytoplasmic homeostasis*. Proc Natl Acad Sci U S A, 2020. **117**(45): p. 28402-28411.
59. Militi, S., et al., *Early doors (Edo) mutant mouse reveals the importance of period 2 (PER2) PAS domain structure for circadian pacemaking*. Proc Natl Acad Sci U S A, 2016. **113**(10): p. 2756-61.
60. Wu, G., et al., *Structure of a beta-TrCP1-Skp1-beta-catenin complex: destruction motif binding and lysine specificity of the SCF(beta-TrCP1) ubiquitin ligase*. Mol Cell, 2003. **11**(6): p. 1445-56.
61. Ohsaki, K., et al., *The role of {beta}-TrCP1 and {beta}-TrCP2 in circadian rhythm generation by mediating degradation of clock protein PER2*. J Biochem, 2008. **144**(5): p. 609-18.
62. Reischl, S., et al., *Beta-TrCP1-mediated degradation of PERIOD2 is essential for circadian dynamics*. J Biol Rhythms, 2007. **22**(5): p. 375-86.
63. Masuda, S., et al., *Mutation of a PER2 phosphodegron perturbs the circadian phosphoswitch*. bioRxiv, 2019.

64. Liu, J., et al., *Distinct control of PERIOD2 degradation and circadian rhythms by the oncoprotein and ubiquitin ligase MDM2*. *Sci Signal*, 2018. **11**(556).
65. Hirota, T., et al., *High-throughput chemical screen identifies a novel potent modulator of cellular circadian rhythms and reveals CKIalpha as a clock regulatory kinase*. *PLoS Biol*, 2010. **8**(12): p. e1000559.
66. Oshima, T., et al., *Cell-based screen identifies a new potent and highly selective CK2 inhibitor for modulation of circadian rhythms and cancer cell growth*. *Sci Adv*, 2019. **5**(1): p. eaau9060.
67. Hayasaka, N., et al., *Salt-inducible kinase 3 regulates the mammalian circadian clock by destabilizing PER2 protein*. *Elife*, 2017. **6**.
68. Brenna, A., et al., *Cyclin-dependent kinase 5 (CDK5) regulates the circadian clock*. *Elife*, 2019. **8**.
69. Narasimamurthy, R., et al., *CK1delta/epsilon protein kinase primes the PER2 circadian phosphoswitch*. *Proc Natl Acad Sci U S A*, 2018. **115**(23): p. 5986-5991.
70. Vanselow, K., et al., *Differential effects of PER2 phosphorylation: molecular basis for the human familial advanced sleep phase syndrome (FASPS)*. *Genes Dev*, 2006. **20**(19): p. 2660-72.
71. Philpott, J.M., et al., *Casein kinase 1 dynamics underlie substrate selectivity and the PER2 circadian phosphoswitch*. *Elife*, 2020. **9**.
72. Lee, H.M., et al., *The period of the circadian oscillator is primarily determined by the balance between casein kinase 1 and protein phosphatase 1*. *Proc Natl Acad Sci U S A*, 2011. **108**(39): p. 16451-6.
73. Zhou, M., et al., *A Period2 Phosphoswitch Regulates and Temperature Compensates Circadian Period*. *Mol Cell*, 2015. **60**(1): p. 77-88.
74. Liu, Z., et al., *PER1 phosphorylation specifies feeding rhythm in mice*. *Cell Rep*, 2014. **7**(5): p. 1509-1520.

75. Kaasik, K., et al., *Glucose sensor O-GlcNAcylation coordinates with phosphorylation to regulate circadian clock*. Cell Metab, 2013. **17**(2): p. 291-302.
76. Durgan, D.J., et al., *O-GlcNAcylation, novel post-translational modification linking myocardial metabolism and cardiomyocyte circadian clock*. J Biol Chem, 2011. **286**(52): p. 44606-19.
77. Asher, G., et al., *SIRT1 regulates circadian clock gene expression through PER2 deacetylation*. Cell, 2008. **134**(2): p. 317-28.
78. Foteinou, P.T., et al., *Computational and experimental insights into the circadian effects of SIRT1*. Proc Natl Acad Sci U S A, 2018. **115**(45): p. 11643-11648.
79. Levine, D.C., et al., *NAD(+) Controls Circadian Reprogramming through PER2 Nuclear Translocation to Counter Aging*. Mol Cell, 2020. **78**(5): p. 835-849 e7.
80. van Ooijen, G., et al., *Functional analysis of Casein Kinase 1 in a minimal circadian system*. PLoS One, 2013. **8**(7): p. e70021.
81. Goldsmith, E.J., et al., *Substrate and docking interactions in serine/threonine protein kinases*. Chem Rev, 2007. **107**(11): p. 5065-81.
82. Johnson, L.N., M.E. Noble, and D.J. Owen, *Active and inactive protein kinases: structural basis for regulation*. Cell, 1996. **85**(2): p. 149-58.
83. Flotow, H., et al., *Phosphate groups as substrate determinants for casein kinase I action*. J Biol Chem, 1990. **265**(24): p. 14264-9.
84. Narasimamurthy, R. and D.M. Virshup, *The phosphorylation switch that regulates ticking of the circadian clock*. Mol Cell, 2021. **81**(6): p. 1133-1146.
85. Kim, D.W., et al., *Systems approach reveals photosensitivity and PER2 level as determinants of clock-modulator efficacy*. Mol Syst Biol, 2019. **15**(7): p. e8838.

86. Longenecker, K.L., P.J. Roach, and T.D. Hurley, *Three-dimensional structure of mammalian casein kinase I: molecular basis for phosphate recognition*. J Mol Biol, 1996. **257**(3): p. 618-31.
87. Shinohara, Y., et al., *Temperature-Sensitive Substrate and Product Binding Underlie Temperature-Compensated Phosphorylation in the Clock*. Mol Cell, 2017. **67**(5): p. 783-798 e20.
88. Zeringo, N.A., et al., *A monoclinic crystal form of casein kinase 1 delta*. Acta Crystallogr Sect F Struct Biol Cryst Commun, 2013. **69**(Pt 10): p. 1077-83.
89. Ralph, M.R. and M. Menaker, *A mutation of the circadian system in golden hamsters*. Science, 1988. **241**(4870): p. 1225-7.
90. Gallego, M., et al., *An opposite role for tau in circadian rhythms revealed by mathematical modeling*. Proc Natl Acad Sci U S A, 2006. **103**(28): p. 10618-23.
91. Kornev, A.P. and S.S. Taylor, *Dynamics-Driven Allostery in Protein Kinases*. Trends Biochem Sci, 2015. **40**(11): p. 628-647.
92. Nolen, B., S. Taylor, and G. Ghosh, *Regulation of protein kinases; controlling activity through activation segment conformation*. Mol Cell, 2004. **15**(5): p. 661-75.
93. Graves, P.R. and P.J. Roach, *Role of COOH-terminal phosphorylation in the regulation of casein kinase I delta*. J Biol Chem, 1995. **270**(37): p. 21689-94.
94. Rivers, A., et al., *Regulation of casein kinase I epsilon and casein kinase I delta by an in vivo futile phosphorylation cycle*. J Biol Chem, 1998. **273**(26): p. 15980-4.
95. Cegielska, A., et al., *Autoinhibition of casein kinase I epsilon (CKI epsilon) is relieved by protein phosphatases and limited proteolysis*. J Biol Chem, 1998. **273**(3): p. 1357-64.

96. Gietzen, K.F. and D.M. Virshup, *Identification of inhibitory autophosphorylation sites in casein kinase I epsilon*. J Biol Chem, 1999. **274**(45): p. 32063-70.
97. Isojima, Y., et al., *CKIepsilon/delta-dependent phosphorylation is a temperature-insensitive, period-determining process in the mammalian circadian clock*. Proc Natl Acad Sci U S A, 2009. **106**(37): p. 15744-9.
98. Guo, G., et al., *Autokinase Activity of Casein Kinase 1 delta/epsilon Governs the Period of Mammalian Circadian Rhythms*. J Biol Rhythms, 2019. **34**(5): p. 482-496.
99. Qin, X., et al., *PER2 Differentially Regulates Clock Phosphorylation versus Transcription by Reciprocal Switching of CKIepsilon Activity*. J Biol Rhythms, 2015. **30**(3): p. 206-16.
100. Dahlberg, C.L., et al., *Interactions between Casein kinase Iepsilon (CKIepsilon) and two substrates from disparate signaling pathways reveal mechanisms for substrate-kinase specificity*. PLoS One, 2009. **4**(3): p. e4766.
101. Um, J.H., et al., *Activation of 5'-AMP-activated kinase with diabetes drug metformin induces casein kinase Iepsilon (CKIepsilon)-dependent degradation of clock protein mPer2*. J Biol Chem, 2007. **282**(29): p. 20794-8.
102. Giamas, G., et al., *Phosphorylation of CKIdelta: identification of Ser370 as the major phosphorylation site targeted by PKA in vitro and in vivo*. Biochem J, 2007. **406**(3): p. 389-98.
103. Bischof, J., et al., *CKIdelta kinase activity is modulated by Chk1-mediated phosphorylation*. PLoS One, 2013. **8**(7): p. e68803.
104. Meng, Z., et al., *CKIdelta kinase activity is modulated by protein kinase C alpha (PKCalpha)-mediated site-specific phosphorylation*. Amino Acids, 2016. **48**(5): p. 1185-97.

105. Eng, G.W.L., Edison, and D.M. Virshup, *Site-specific phosphorylation of casein kinase 1 delta (CK1delta) regulates its activity towards the circadian regulator PER2*. PLoS One, 2017. **12**(5): p. e0177834.
106. Ianes, C., et al., *CK1delta activity is modulated by CDK2/E- and CDK5/p35-mediated phosphorylation*. Amino Acids, 2016. **48**(2): p. 579-92.
107. Fustin, J.M., et al., *Two Ck1delta transcripts regulated by m6A methylation code for two antagonistic kinases in the control of the circadian clock*. Proc Natl Acad Sci U S A, 2018. **115**(23): p. 5980-5985.
108. Takano, A., et al., *A missense variation in human casein kinase I epsilon gene that induces functional alteration and shows an inverse association with circadian rhythm sleep disorders*. Neuropsychopharmacology, 2004. **29**(10): p. 1901-9.

CHAPTER 2

Casein Kinase 1 dynamics underlie substrate selectivity and the PER2 circadian phosphoswitch

Acknowledgments

Philpott JM, Narasimamurthy R, Ricci CG, Freeberg AM, Hunt SR, Yee LE, Pelofsky RS, Tripathi S, Virshup DM, Partch CL. Casein kinase 1 dynamics underlie substrate selectivity and the PER2 circadian phosphoswitch. *Elife*. 2020 Feb 11;9:e52343

The following co-authors are acknowledged for their contributions to the published work: JMP, RN, and CGR provided conceptualization, formal analysis, and investigation. AMF, SRH, LEY, and RSP provided additional investigation. JMP, RN, and ST provided validation. JMP, CGR, DMV and CLP provided visualization. DMV and CLP provided conceptualization, supervision, funding acquisition and project administration.

We would like to thank Danny Forger, Jae Kyoung Kim, Yinglong Miao, and J Andrew McCammon for useful discussions and Sivakumar Parthiban for technical assistance. We also thank the beamline staff for their assistance at the Advanced Photon Source beamline 23-ID-D and Advanced Light Source beamline 8.3.1, as well as the San Diego Supercomputer Center (SDSC) for technical support. This work was funded by the National Medical Research

Council of Singapore Grant NMRC/CIRG/1465/2017 (to DMV) and National Institutes of Health Grants R01 GM031749 (to CGR), GM107069 and R01 GM121507 (to CLP), as well as funds from the NIH Office of the Director under Award S10 OD018455 for the 800 MHz NMR spectrometer used here. S Hunt was supported by NRSA F32 GM133149.

2.1 Abstract

Post-translational control of PERIOD stability by Casein Kinase δ and ϵ (CK1) plays a key regulatory role in metazoan circadian rhythms. Despite the deep evolutionary conservation of CK1 in eukaryotes, little is known about its regulation and the factors that influence substrate selectivity on functionally antagonistic sites in PERIOD that directly control circadian period. Here we describe a molecular switch involving a highly conserved anion binding site in CK1. This switch controls conformation of the kinase activation loop and determines which sites on mammalian PER2 are preferentially phosphorylated, thereby directly regulating PER2 stability. Integrated experimental and computational studies shed light on the allosteric linkage between two anion binding sites that dynamically regulate kinase activity. We show that period-altering kinase mutations from humans to *Drosophila* differentially modulate this activation loop switch to elicit predictable changes in PER2 stability, providing a foundation to understand and further manipulate CK1 regulation of circadian rhythms.

2.2 Introduction

Circadian rhythms are generated by a set of interlocked transcription/translation feedback loops that elicit daily oscillations in gene expression to confer temporal regulation to behavior, metabolism, DNA repair and more [1]. The PERIOD proteins (PER1 and PER2) nucleate assembly of

large, multimeric complexes with the circadian repressors CRY1 and CRY2 that directly bind to and inhibit the core circadian transcription factor, CLOCK:BMAL1, on a daily basis [2-4]. PERs are stoichiometrically limiting for the assembly of these essential repressive complexes [5]. In this way, their abundance and post-translational modification state relay important biochemical information on the relative timing of the clock to other core clock proteins. Therefore, the expression, modification, and protein stability of PER1 and PER2 is under particularly tight regulation.

While both transcriptional and post-transcriptional mechanisms feature importantly in the rhythmic generation of PER proteins [6, 7], much attention has been focused on the post-translational control of PER orchestrated by its cognate kinases, CK1 δ and the closely related paralog CK1 ϵ [8]. These clock-associated kinases are somewhat unusual, in that they remain stably anchored to PER1 and PER2 throughout the circadian cycle [2, 9] via a conserved Casein Kinase Binding Domain (CKBD) [10, 11]. Mutations in CK1 δ/ϵ (hereafter referred to jointly as CK1), as well as PER2, exert powerful control over circadian period, altering the intrinsic timing of circadian rhythms by hours *in vivo* [12-15]. Because circadian period is linked to the timing of sleep onset, PER2 or CK1-dependent alterations to human circadian period manifest as sleep phase disorders that influence behavior and wellbeing on a daily basis [16].

PER2 is regulated by a CK1-dependent phosphoswitch, where kinase activity at two antagonistic sites functionally interact to control PER2 stability [17, 18]. Two features define the CK1 phosphoswitch: degradation is initiated by phosphorylation of a Degron located several hundred residues upstream of the CKBD to recruit the E3 ubiquitin ligase, β -TrCP [10, 19]; this is counteracted by sequential phosphorylation of five serines embedded within the CBKD known as the FASP region [20]. This region is named for a Ser to Gly polymorphism in human PER2 that disrupts this stabilizing multi-site phosphorylation, shortens circadian period, and leads to Familial Advanced Sleep Phase Syndrome [13]. Mutation of the Degron phosphorylation site has the opposite effect, stabilizing PER2 to significantly compromise circadian rhythms [21] in a manner similar to its constitutive overexpression [22]. Therefore, the balance of stabilizing and degrading phosphorylation by CK1 leads to a complex temporal pattern of degradation in PER2 that is important for circadian timing [18].

Despite the importance of CK1 for circadian timing in eukaryotic organisms from humans to *Drosophila*, *Neurospora*, and green algae [14, 23-25], little is known about how its activity is regulated on clock protein substrates. CK1 is thought of as an anion- or phosphate-directed kinase, relying on negative charge on the substrate to template activity in the pSxxS consensus motif [26]. Consistent with this, biochemical studies exploring CK1 activity have primarily relied on the non-physiological acidic substrates casein [27] and phosvitin [12],

or used peptides harboring anion- or phosphate-driven motifs [28-30]. However, *in vitro* studies of clock-relevant kinase mutants using these non-physiological substrates have led to the puzzling conclusion that CK1 mutants that either decrease or increase period length all have reduced kinase activity [31, 32].

The importance of anion binding is highlighted by the CK1 ϵ *tau* allele that markedly speeds up the clock, leading to a ~20-hour period [12, 33]. The R178C mutation in *tau* alters a phosphate binding pocket on the surface of the kinase to block the ability of CK1 to further phosphorylate primed or acidic substrates. We discovered that *tau* has reduced activity on the FASP region *in vitro*, but exhibits a gain of function on the Degron site. Therefore, the *tau* allele inverts substrate selectivity on PER2 relative to the wild-type kinase to promote PER2 degradation. A mechanism for inverted substrate selectivity was suggested by the crystal structure of the *tau* kinase domain, which revealed the presence of a two-state conformational switch in the CK1 activation loop. Anion binding near the activation loop biases the switch towards a conformation that favors the FASP substrate, while mutations that disfavor anion binding enhance activity towards the Degron. Molecular dynamics simulations reveal that the alternate conformation is stabilized in *tau*, forming the basis for its enhanced activity on the Degron. A comprehensive analysis of other short period kinase mutants from *Drosophila* to humans finds that they differentially bias this intrinsic switch to enhance phosphorylation of the Degron and turnover of

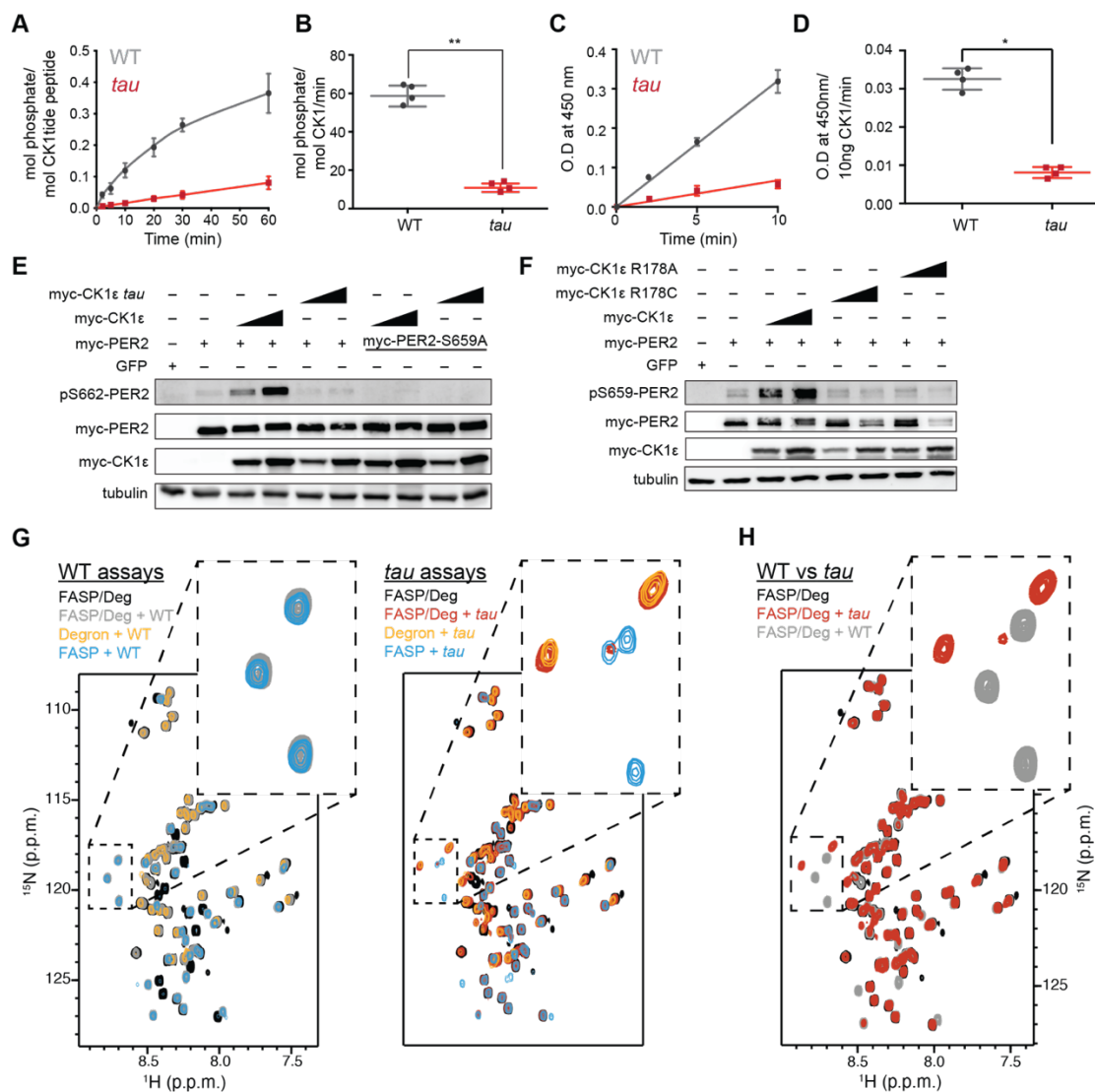
PER2. Therefore, the anion-triggered activation loop switch may be a general mechanism regulating CK1 substrate selection.

2.3 Results

2.3.1 The *tau* mutant has decreased activity on the FASP region

We recently demonstrated that CK1 primes FASP phosphorylation in a slow, rate-limiting step at serine 659 (mouse PER2 numbering, Figure 2.1A-B), with phosphorylation of the downstream consensus sites following rapidly in a sequential manner (dashed arrows at pSxxS consensus, Figure 2.1B) [20]. Because *tau* is a loss of function on the FASP domain, the prevailing model was that this disabled the phosphoswitch to allow for unchecked Degron phosphorylation to degrade PER2 [34]. The *tau* mutation eliminates a positively charged residue in the first of three CK1 family-specific anion-binding sites (Sites 1, 2, and 3) (Figure 2.1C) [35]. R178 sits at Site 1, located adjacent to the active site, and has been postulated to bind a phosphorylated priming site to position the downstream serine of the consensus motif near the active site [35, 36]. Based on this model, we predicted that *tau* should preferentially disrupt phosphorylation of the downstream consensus sites in the FASP region due to its inability to recruit the primed substrate.

bold) and two downstream phosphorylation sites (S662 and S665, bold) that are phosphorylated sequentially by CK1 δ (dashed arrows). Gray, polybasic motif included for ^{32}P kinase assay. C, CK1 δ kinase domain with 3 anion binding sites (PDB: 1CKJ with WO_4^{2-} anions). R178, blue. D, Kinase assay with 20 nM CK1 δ ΔC WT or *tau* on 200 μM of primed FASP peptide (pS659) (n = 4 with s.d.). E, Phosphorylation rates on primed FASP (n = 4 with s.d.). Significance assessed by unpaired Student's two-sided t-test: **, p < 0.01. F, Kinase assay as in D, but with 200 nM CK1 δ ΔC WT or *tau* on 200 μM of unprimed FASP (n = 4 with s.d.). G, Phosphorylation rates on the unprimed FASP peptide (n = 4 with s.d.). Significance assessed as above. H, Overlaid $^{15}\text{N}/^1\text{H}$ HSQC spectra at 3 hr timepoint in the NMR kinase assay on 200 μM ^{15}N FASP (black) \pm 1 μM WT (gray) or *tau* (red) CK1 δ ΔC . Arrows, phospho-specific peaks corresponding to pS659 and pS662. I, Phosphoserine peak intensities for pS659 and pS662 by WT and *tau* kinases from NMR kinase assay. J, Ratio of consensus to priming activity on the FASP (pS662/pS659) in the NMR kinase assay. Errors were estimated from the standard deviation of the noise in the spectrum. K-L, Western blot of FASP priming site, detecting pS659 (K) or the Degron, detecting pS478 (L) on mouse myc-PER2 in HEK293 cell lysates after transfection with indicated expression plasmids. Representative blot from n = 3 shown. Wedge, 10 or 50 ng of myc-CK1 ϵ plasmid used. *, non-specific band. M, Sequence of mouse PER2 Degron peptide with S478 (bold) and polybasic motif (gray). N, Kinase assay with 200 nM kinase on 200 μM Degron peptide (n = 4 with s.d.). O, Phosphorylation rates on Degron (n = 4 with s.d.). Significance assessed as above. See also Figure 2.1.1.



Supplemental Figure 2.1.1 (relates to Figure 2.1)

A, Kinase assay using 20 nM CK1 Δ C of WT or *tau* on 200 μ M of the synthetic primed substrate, CK1tide, KRRRALpSVASLPGL (n = 4 with s.d.). B, Phosphorylation rate of kinases on CK1tide (n = 4 with s.d.). Significance assessed by Student's two-sided t-test, **, p < 0.01. C, ELISA-based kinase assay on 200 μ M of the mouse FASP peptide detected with the anti-pS659 antibody with 10 ng of CK1 Δ C WT or *tau* (n = 4 with s.d.). D, Rate of phosphorylation measured by optical density (O.D.) at 450 nm at the indicated timepoints (n = 4 with s.d.). Significance assessed by unpaired Student's two-sided t-test: *, p < 0.05. E, Western blot of sequential phosphorylation of the FASP at S662 on mouse myc-PER2 in HEK293 cell lysates after transfection with indicated expression plasmids. Representative blot from n = 3 shown. Wedge, 10 or 50 ng of myc-CK1 ϵ plasmid used. F, Western blot of FASP priming phosphorylation at S659 on mouse myc-PER2 in HEK293 cell lysates after transfection with indicated expression plasmids as in panel E. Representative blot from n = 3 shown. G, Overlaid $^{15}\text{N}/^1\text{H}$

SOFAST HMQC spectra of NMR kinase assays with ^{15}N FASP, ^{15}N Degron, or both. WT and *tau* kinases were assayed for activity with 200 μM of both substrates (WT kinase, gray; *tau* kinase, red; no kinase, black), or with FASP or Degron peptides alone (FASP, blue; Degron, orange). H, Overlay of $^{15}\text{N}/^1\text{H}$ SOFAST HMQC spectra comparing WT and *tau* phosphorylation profiles for equimolar FASP/Degron substrate at 3 hours. Note the remarkably distinct substrate preferences for WT and *tau* kinases.

To test this idea, we used a FASP peptide based on the native mouse PER2 sequence (Figure 2.1B) that was primed synthetically by phosphorylation at S659. We used a constitutively active version of the isolated wild-type (WT) or *tau* (R178C) kinase lacking its autoinhibitory tail (CK1 δ Δ C, with 97% identity between CK1 δ and CK1 ϵ in the kinase domain). As expected, *tau* had significantly lower activity than the WT kinase on this primed substrate (Figure 2.1D-E). This was also true for a minimal, primed synthetic substrate CK1tide (Figure 2.1.1). We then asked if *tau* would influence priming phosphorylation using an unmodified FASP peptide. As we observed before, phosphorylation of the non-consensus priming site occurs with much slower kinetics than the downstream consensus sites (Figure 2.1F-G) [20]. To our surprise, we found that *tau* also had significantly diminished activity on an unprimed FASP substrate (Figure 2.1F-G), indicating that R178 is also important for the non-consensus priming event. The decrease in activity of *tau* on the priming site was also validated using an ELISA-based kinase assay with an antibody that is specific for phosphorylated S659 (Figure 2.1.1).

We used an NMR-based kinase assay to confirm that *tau* influences both priming and downstream events at the FASP region. In contrast to radiolabeled kinase assays, this assay provides site-specific information on the substrate by measuring new peaks that arise for phosphorylated serines over time [37]. We established the requirement for priming to initiate phosphorylation of downstream sites in the FASP by CK1 [20]. Therefore, if *tau* was simply

deficient in recruitment of primed substrate, we should observe a similar degree of phosphorylation at the priming site (pS659) compared to WT kinase, but a decreased peak volume for the downstream serine (pS662). By contrast, we observed that the peaks for both pS659 and pS662 were decreased in volume for *tau* (Figure 2.1H-I), revealing that the ratio of consensus to priming activity (pS662/pS659) was similar in WT CK1 and *tau* (Figure 2.1J).

To see if these findings held in the context of full-length protein, we expressed myc-PER2 and WT or *tau* myc-CK1 ϵ in HEK293 cells and assessed phosphorylation using an antibody specific for phosphorylation on the priming site at S659. Consistent with our *in vitro* studies, the activity of *tau* was much lower on the priming site relative to the WT kinase (Figure 2.1K). As expected, phosphorylation of the subsequent serine was also decreased with *tau* (Figure 2.1.1). To examine the possibility that loss of activity on the FASP region was specifically due to the cysteine mutation (R178C), we also tested an R178A mutant in the cell-based assay and found that it also exhibited much lower activity on the FASP priming site in a cell-based assay (Figure 2.1.1). Collectively, these data show that loss of R178 at the site 1 anion-binding pocket in *tau* leads to a reduction in both the slow priming step as well as the downstream sequential, primed phosphorylation of the FASP region.

2.3.2 *tau* exhibits a gain of function on the Degron

Using an antibody specific for phosphorylation of the CK1-dependent β -TrCP recruitment site at S478, we recapitulated the increased activity of *tau* on the Degron observed previously on myc-PER2 that was transiently expressed with the kinase in HEK293 cells (Figure 2.1L) [34]. Consistent with the phosphoswitch model that FASP phosphorylation antagonizes CK1 activity on the Degron (Figure 2.1A), we observed an increase in activity of WT kinase on the Degron with the S659A mutant that eliminates all phosphorylation of the FASP region (Figure 2.1L) [20]. We found that *tau* also had increased activity on the Degron in the S659A mutant, demonstrating that the *tau* mutant can still be regulated by the phosphoswitch. Given that kinase activity on the Degron is clearly linked to phosphorylation of the FASP region in cells, we sought to clarify whether *tau* truly exhibits increased activity at the Degron using a peptide-based kinase assay *in vitro* (Figure 2.1M). Here, we found that even on a peptide substrate *in vitro*, *tau* had significantly increased activity on the Degron relative to WT kinase (Figure 2.1N-O). Moreover, both *tau* and WT kinase maintain their distinct substrate preference in the presence of both FASP and Degron peptides *in vitro*, with *tau* showing enhanced activity for the Degron relative to WT kinase (Figure 2.1.1). These data demonstrate that in addition to any regulation imparted by the phospho-FASP on the Degron in cells, the *tau* mutation leads to a fundamental change in CK1 activity and substrate specificity.

2.3.3 The *tau* mutation disrupts anion binding at Site 1 and Site 2 on CK1

To explore the molecular basis for *tau*'s altered substrate specificity, we solved a crystal structure of the CK1 δ R178C kinase domain (Figure 2.2A and Table 2.1). Both WT and *tau* coordinate an anion at Site 3 similarly (Figure 2.2.1). However, the mutation disrupted anion binding at Site 1, although it led to only minor structural changes in this anion-binding pocket (Figure 2.2B). Unexpectedly, we observed a loss of anion binding at Site 2 in *tau*, mediated by an alternate conformation of the activation loop near this pocket that sterically blocks binding of the anion (Figures 2.2C). This alternate conformation initiates at G175, three residues upstream of the *tau* mutation (Figure 2.2C). A rotation of the backbone at G175 to a left-handed configuration dramatically alters the configuration of upstream residues to create a distinct conformation of the activation loop (Figures 2.2D and 2.2.1). A backbone flip of a glycine at this conserved position has been observed in other serine/threonine kinases, linking changes in conformation of the activation loop to regulation of kinase activity [38]; therefore, the 'loop up' conformation observed in *tau* may lead to different kinase activity than the 'loop down' conformation observed in the WT kinase.

Table 2.1 – X-ray crystallography data collection and refinement statistics

| | CK1δ ΔC <i>tau</i> R178C | CK1δ ΔC No Sulfate | CK1δ ΔC K171E |
|--------------------------------------|-----------------------------|----------------------------|-----------------------------|
| PDB | 6PXN | 6PXO | 6PXP |
| Data collection | | | |
| Space group | P2 ₁ | P2 ₁ | P2 ₁ |
| Resolution | 64.82-1.55 (1.58-1.55) | 65.24-2.00 (2.11- 2.00) | 47.38 – 2.35 (2.43-2.35) |
| a, b, c | 50.08, 129.64, 51.86 | 49.91, 130.49, 51.16 | 50.06, 130.35, 51.65 |
| α, β, γ | 90, 113.41, 90 | 90, 112.75, 90 | 90, 113.47, 90 |
| R _{merge} | 6.3 (60.1) | 10.5 (104.2) | 12.8 (65.2) |
| R _{pim} | 2.8 (27.0) | 4.5 (46.8) | 7.7 (40.4) |
| Total reflections | 588739 (27527) | 252539 (34017) | 109702 (10773) |
| Unique reflections | 85497 (4108) | 40494 (5884) | 25271 (2470) |
| I/σ | 13.1 (2.5) | 11.2 (1.7) | 6.7 (2.1) |
| CC1/2 | 0.99(0.89) | 0.99 (0.61) | 0.99 (0.77) |
| Completeness | 97.8(95.3) | 99.6 (99.7) | 99.9 (99.9) |
| Redundancy | 6.9 (6.7) | 6.2 (5.8) | 4.3 (4.4) |
| Wilson B-Factor | 19 | 28 | 32 |
| Refinement | | | |
| Resolution | 44.68-1.55 | 47.18-2.0 | 42.5-2.35 |
| R _{work} /R _{free} | 17.9/20.6 | 17.9/23.7 | 20.0/24.3 |
| No. of Atoms | 5057 | 5012 | 4922 |
| Protein | 4735 | 4727 | 4757 |
| Water | 297 | 285 | 115 |
| Ligands | 25 | - | 50 |
| RMS deviation | | | |
| Bond lengths | 0.01 | 0.008 | 0.009 |
| Bond angles | 1.2 | 0.94 | 1.15 |
| Ramachandran Favored/Outliers | 100.0/0.0 | 100.0/0.0 | 100/0.0 |
| Average B-Factor | 34 | 41 | 41 |

Values in parentheses are for highest resolution shell

The activation loop is a key feature that distinguishes the CK1 family from other serine/threonine kinases. There is little mechanistic insight into CK1 substrate selectivity because it deviates from the highly conserved APE motif in the P+1 region that helps to define substrate specificity in most kinases (Figure 2.2E) [39]. The activation loop and surrounding region also contain all of the residues that coordinate the three anions observed in nearly all CK1 structures: the residues that coordinate binding at Sites 1 and 3 are unique to the CK1 family, while R127 and K154, corresponding to Site 2, are broadly conserved in other kinase families. R127 is part of the highly conserved HRD motif that coordinates a phosphorylated residue in the activation loop of many kinases to regulate substrate binding and activity (Figure 2.2F) [40]. CK1 family kinases are generally considered to be constitutively active because they do not require phosphorylation of the activation loop [39]. However, CK1 δ and CK1 ϵ are inhibited by autophosphorylation of their disordered C-terminal tails [41, 42] and potentially by the phosphorylated FASP region (Figure 2.1L). Therefore, these anion binding sites could represent the basis for a CK1-specific regulatory mechanism by facilitating the binding of phosphorylated C-terminal tails or substrates, and/or anionic signaling molecules [43, 44].

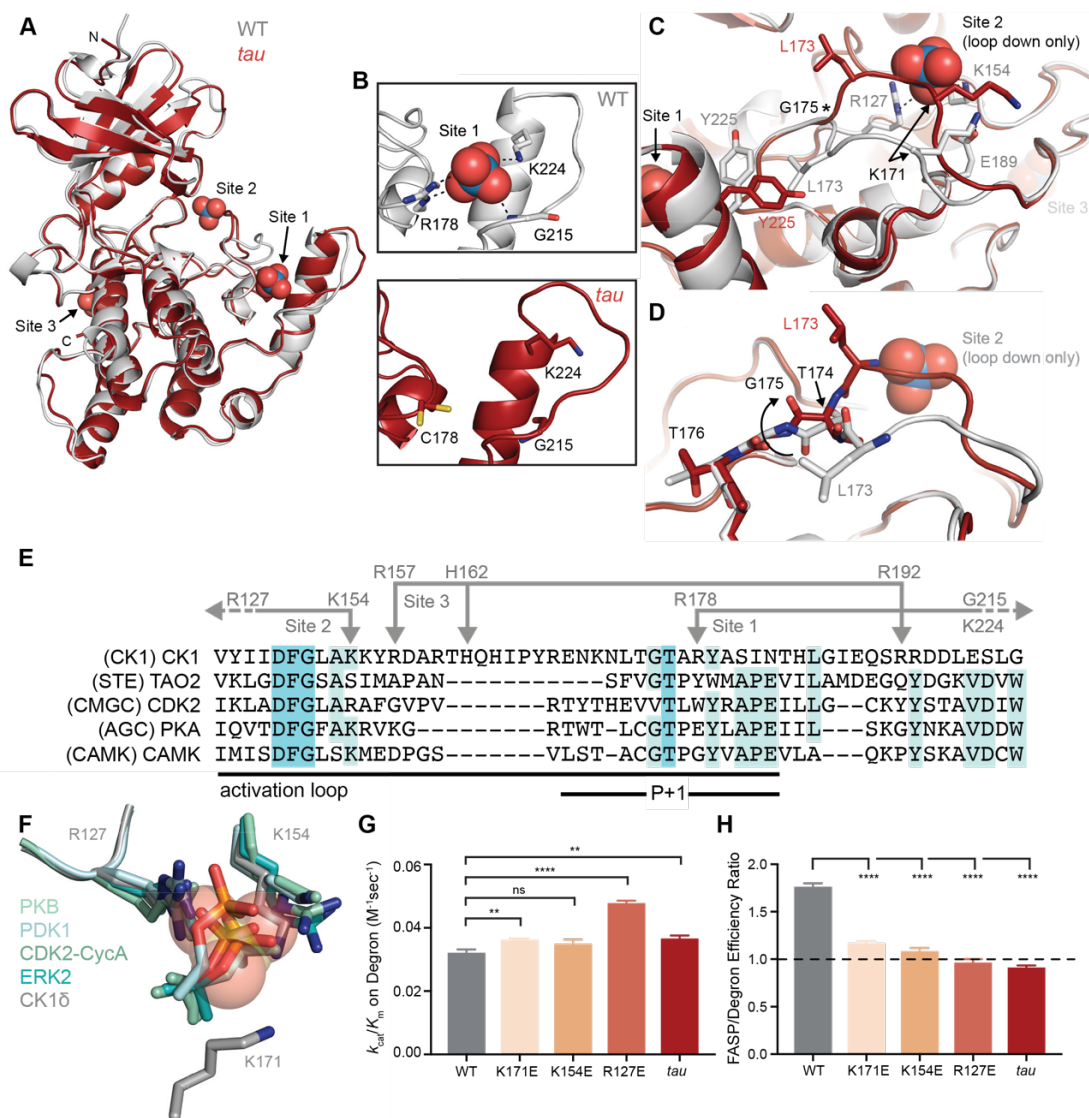
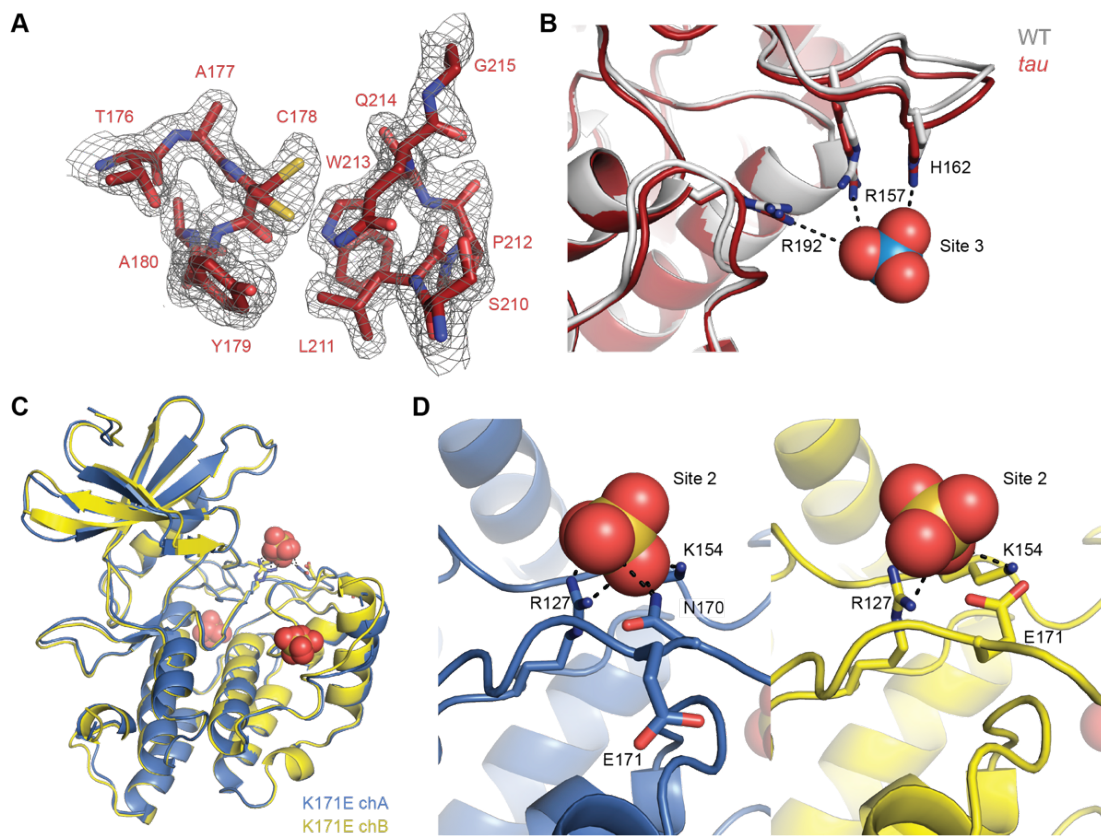


Figure 2.2 *tau* disrupts anion binding on CK15

A, Overlay of WT kinase domain (gray, PDB: 1CKJ, chain B) with *tau* (maroon, PDB: 6PXN, chain A). The 3 anion binding sites (WO_4^{2-} , from 1CKJ) are labeled. B, View of Site 1 in WT (top, gray) and *tau* (bottom, maroon). Polar interactions, dashed black lines. C, Overlaid view of Site 2 in WT and *tau* as above. Polar interactions, dashed black lines. Asterisk, hinge point for conformational change at G175. Note: Site 2 anion is only bound in WT, as it is blocked by the activation loop in *tau*. D, Representation depicting the left-hand configuration of G175 and subsequent rotation (solid arrow) of upstream residues T174 and L173. E, Alignment of the activation loop of CK15 with representatives of other serine/threonine kinase families. Residues that coordinate anion binding on CK1 are indicated above in gray. F, Superposition of the Site 2 anion binding site in CK1 with the binding site for the

phosphorylated activation loop of other serine/threonine kinases. Depicted are: PKB (PDB: 1O6K, pale cyan), PDK1 (1H1W, aquamarine), CDK2 (1QMZ, green cyan), ERK2 (2ERK, teal) and CK1 δ (5X17, dark gray). Residues that coordinate the anion are depicted in sticks, as are phosphoserine or phosphothreonine residues from other kinases; the SO₄²⁻ coordinated at Site 2 by CK1 δ (PDB: 5x17) is shown in transparent spheres. G, Enzymatic efficiency on the Degron (n = 3 with s.d.). Significance assessed relative to WT with an unpaired Student's two-sided t-test: **, p < 0.01; ***, p < 0.001; ****, p < 0.0001. H, Ratio of enzymatic efficiency on FASP relative to Degron (n = 3 with s.d.). Equivalent activity on FASP and Degron, dashed line. Significance assessed as above. See also Figure 2.2.1.



Supplemental Figure 2.2.1 (relates to Figure 2.1)

A, 2Fo-Fc omit map of the Site 1 anion binding pocket in the *tau* mutant (maroon, PDB: 6PXN, chain A) contoured at 1σ . B, View of the Site 1 anion binding pocket with WT (gray, PDB: 1CKJ, chain B) and *tau* (maroon, PDB: 6PXN, chain A) structures overlaid. Polar interactions that coordinate the anion are depicted with dashed black lines. Note, the anions depicted at Site 1 and 2 here are only present in the WT structure. C, Overlay of K171E CK1 δ Δ C (PDB: 6PXP; chain A, blue; chain B, yellow). The three conserved anion binding sites (sulfate) are depicted. D, Side-by-side overlaid view of the Site 2 anion binding pocket in the CK1 δ Δ C K171E crystal structure showing polar contacts to the bound sulfate (dashed black lines) from chain A (blue, left) and chain B (yellow, right).

2.3.4 Eliminating anion binding at Site 2 differentially regulates CK1 activity on the FASP and Degron

Mutation of the residues corresponding to positions R127 and K154 at Site 2 essentially eliminates the activity of kinases that depend on phosphorylation of the activation loop [45-47]. To test the role of Site 2 anion binding in regulation of CK1 activity, we made charge reversion mutants at positions R127 and K154, as well as at K171 located nearby on the activation loop, and measured enzymatic efficiency (k_{cat}/K_m) on FASP and Degron peptides *in vitro*. We observed a modest decrease (~25%) in activity towards the FASP peptide (Figure 2.2.1 and Table 2.2), suggesting that the 'loop down' conformation that is enforced by anion binding at Site 2 may be important for FASP activity. Strikingly, these mutants all increased activity towards the Degron, with a ~50% gain in efficiency for R127E (Figure 2.2.1 and Figure 2.2G). To further examine the role of K171 in regulation of anion binding, we solved a structure of the K171E mutant crystallized in high sulfate conditions and found a full complement of three anions bound (Figure 2.2.1), demonstrating that local flexibility in the activation loop allows it to retain sulfate binding at Site 2 to some degree. Overall, these data suggest that anion binding at Site 2 correlates with substrate selectivity on the FASP and Degron peptides. Notably, the change in selectivity with Site 2 mutants *in vitro* makes them much more *tau*-like (Figure 2.2H), consistent with a recent report that both *tau* and charge reversion mutants at Site 2 lead to decreased PER2 stability in cells [30].

2.3.5 The activation loop switch is intrinsic to the CK1 family of kinases

Two copies of the kinase are found in the asymmetric unit of the *tau* crystal. We discovered that the mutant kinase can take on either the ‘loop down’ or the ‘loop up’ conformation (Figure 2.3A). The activation loop is not stabilized by crystal contacts in the alternate ‘loop up’ conformation and was explicitly modeled based on good density in both conformations (Figure 2.3.1), suggesting that the kinase has an intrinsic ability to take on two discrete conformations in a switch-like manner. Since the first structure of CK1 δ published in 1996, nearly all CK1 structures have been determined after crystallization with high concentrations of sulfate or citrate anions [35, 48, 49]. Because anion binding at Site 2 is incompatible with the activation loop in its ‘loop up’ conformation, prior crystallographic conditions have likely disfavored this alternate conformation. The WT structure that we used for our analysis (PDB: 1CKJ) was first crystallized with a low concentration of anions, and then derivatized with tungstate as an analog for phosphate before data collection [35]. Importantly, this structure also displays the same two discrete conformations marked by translocation of residue L173 in the activation loop (Figure 2.3A), confirming that this switch is an intrinsic property of the CK1 δ kinase that has not been explored functionally.

Table 2.2 Enzymatic efficiency of CK1δ ΔC (WT and mutants)

| CK1δ ΔC | FASP k_{cat}/K_m ($M^{-1} s^{-1}$) | Degron k_{cat}/K_m ($M^{-1} s^{-1}$) | FASP/Degron Efficiency Ratio |
|--------------------|---|---|---------------------------------|
| wild-type | 0.0576 ± 0.0012 | 0.0322 ± 0.0009 | 1.77 ± 0.09 |
| T44A | 0.0447 ± 0.0007 | 0.0332 ± 0.0017 | 1.37 ± 0.08 |
| H46R | 0.0237 ± 0.0005 | 0.0235 ± 0.0009 | 1.01 ± 0.08 |
| P47S | 0.0349 ± 0.0008 | 0.0312 ± 0.0020 | 1.14 ± 0.09 |
| R127E | 0.0464 ± 0.0016 | 0.0479 ± 0.0011 | 0.969 ± 0.05 |
| K154E | 0.0381 ± 0.0008 | 0.0350 ± 0.0021 | 1.09 ± 0.05 |
| K171E | 0.0425 ± 0.0008 | 0.0363 ± 0.0005 | 1.17 ± 0.03 |
| L173A | 0.0358 ± 0.0037 | 0.0276 ± 0.0012 | 1.30 ± 0.06 |
| <i>tau</i> (R178C) | 0.0350 ± 0.0013 | 0.0368 ± 0.0008 | 0.918 ± 0.02 |
| <i>tau</i> L173A | 0.0203 ± 0.0007 | 0.0198 ± 0.0002 | 1.02 ± 0.03 |
| K224D | 0.0345 ± 0.0010 | 0.0319 ± 0.0009 | 1.08 ± 0.01 |

k_{cat}/K_m data are represented as mean ± s.d. from n = 3 assays.

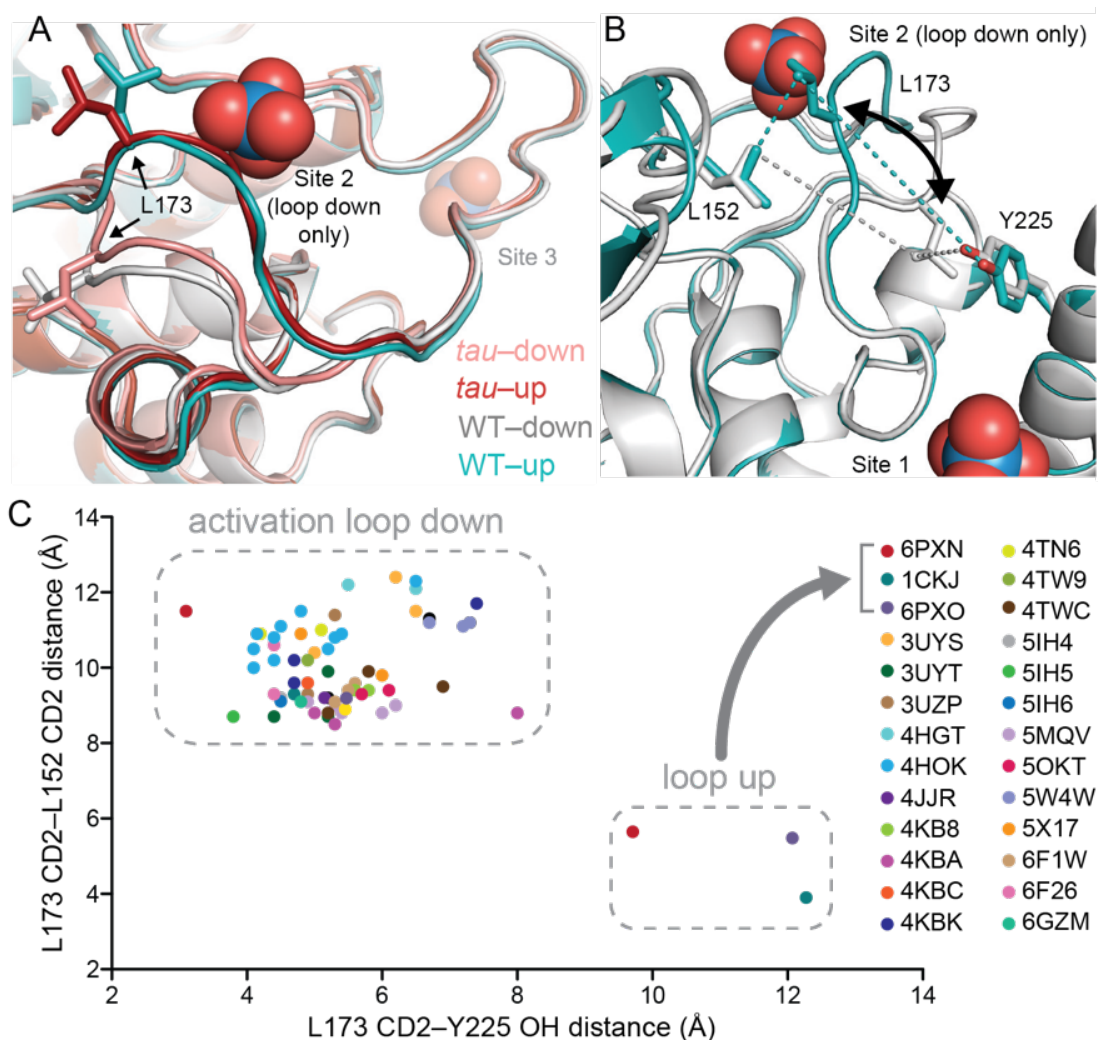
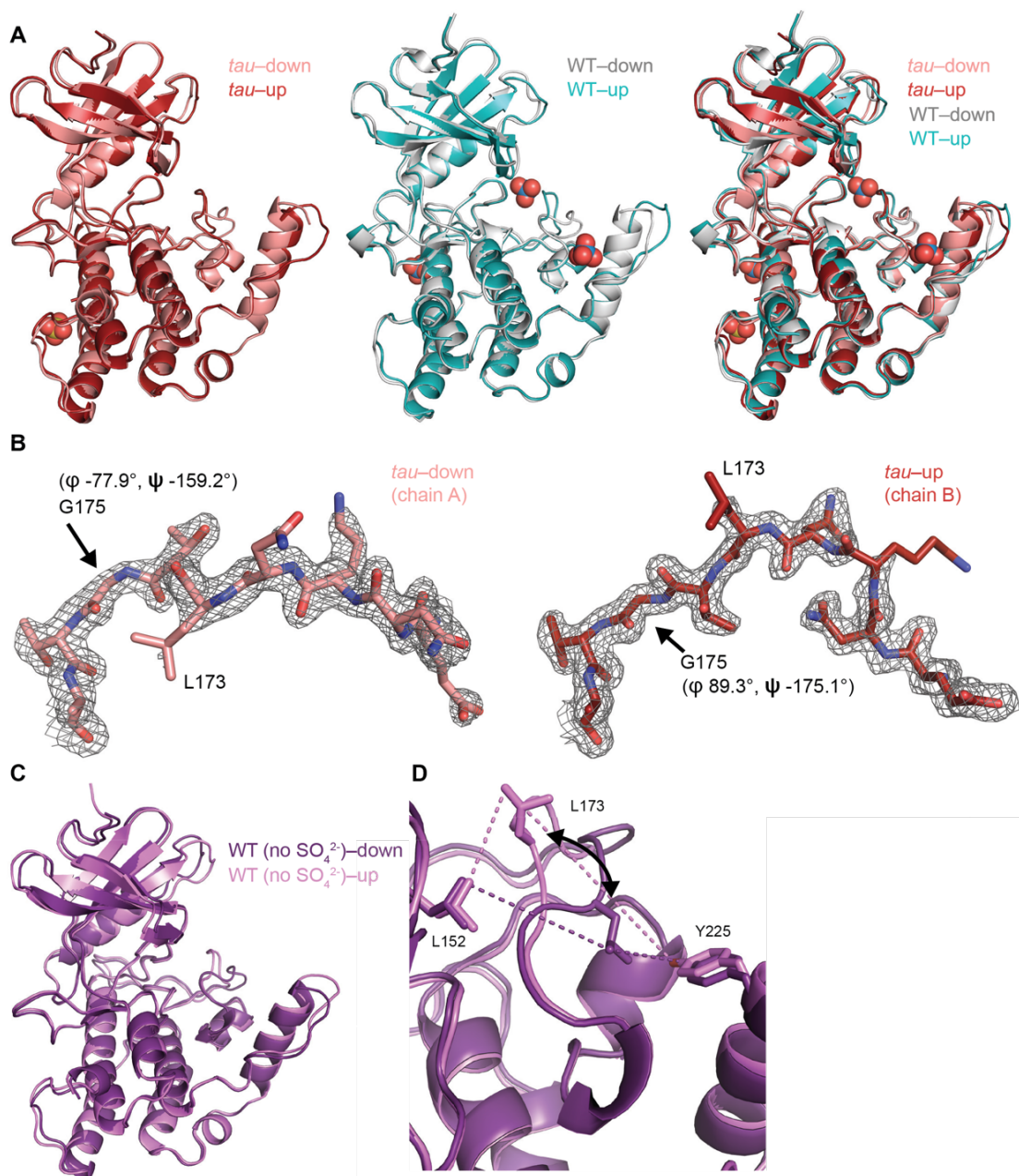


Figure 2.3 *tau* alters an intrinsic molecular switch in the activation loop of CK1 δ

A, View of the activation loop switch in WT (PDB: 1CKJ, chains A (cyan) and B (gray)) and *tau* (PDB: 6PXN, chains A (maroon) and B (salmon)). B, The position of L173 CD2 relative to either L152 CD2 or Y225 OH reports on the conformation of the activation loop in the 'loop down' (gray) or 'loop up' (cyan) conformation in WT CK1 δ (PDB: 1CKJ). C, Scatter plot of interatomic distances in Å (from panel B) measured in 68 chains from 26 different crystal structures of CK1 δ Δ C. See Figure 2.3.1 and Table 2.3 for more information.



Supplemental Figure 2.3.1 (relates to Figure 2.3)

A, Overlay of the kinase domain of individual chains from *tau* (left, PDB: 6PXN, chains A (maroon) and B (salmon) with SO₄²⁻), WT (center, PDB: 1CKJ, chains A (cyan) and B (gray) with WO₄²⁻), and a comparison of all four (right). Note: Anion binding occurs at Site 1 in both chains of the WT kinase, while anion binding at Site 2 only occurs when the activation loop switch is in the down conformation of WT (chain B, gray). B, 2Fo-Fc omit maps of the activation loop in *tau* chain A and B (residues 167-177) contoured at 1 σ . C, Overlaid view of the activation loop switch in the two chains of WT CK1 δ Δ C crystallized in sulfate-free conditions (PDB: 6PXO, chains A (purple) and B (violet)). D, The position of L173 CD2 relative to either L152 CD2 or Y225 OH

reports on the conformation of the activation loop in the 'loop down' (purple) or 'loop up' (violet) conformation in WT CK1 δ grown in sulfate-free conditions (PDB: 6PXO).

| PDB code | Species | Isoform | Res. (Å) | Space group | Site 1 Occ. [†] | Site 2 Occ. [†] | A-loop switch conformation | Mutation or ligand |
|----------|----------------------|----------|----------|--|--------------------------|--------------------------|----------------------------|--------------------|
| 1CKI | Rat | CK1δ | 2.3 | P 2 ₁ 2 ₁ 2 ₁ | no | no | down | |
| 1CKJ | Rat | CK1δ | 2.46 | P 2 ₁ 2 ₁ 2 ₁ | yes | yes/no | down/up | |
| 4HGT | Human | CK1δ | 1.8 | P 1 2 ₁ 1 | no | no | down | ligand |
| 4HNF | Human | CK1δ | 2.07 | C 1 2 1 | no | no | down | ligand |
| 3UYS | Human | CK1δ | 2.3 | P1 | yes | yes/no | down | |
| 3UYT | Human | CK1δ | 2 | P1 | yes | yes/no | down/poor density | ligand |
| 3UZP | Human | CK1δ | 1.94 | P 1 2 ₁ 1 | no | no | down | ligand |
| 4TWC | Human | CK1δ | 1.7 | P 1 2 ₁ 1 | yes | yes | down | ligand |
| 4JJR | Mouse | CK1δ | 2.41 | P 1 2 ₁ 1 | yes | yes | down | |
| 4KB8 | Human | CK1δ | 1.95 | P1 | yes | yes/no | down/poor density | ligand |
| 4KBA | Human | CK1δ | 1.98 | P1 | yes | yes/no | down/poor density | ligand |
| 4KBC | Human | CK1δ | 1.98 | P1 | yes | yes | down | ligand |
| 4KBK | Human | CK1δ | 2.1 | P1 | yes | yes | down | ligand |
| 4TW9 | Human | CK1δ | 2.4 | P 1 2 ₁ 1 | yes | yes | down | ligand |
| 4TN6 | Human | CK1δ | 2.41 | P 1 2 ₁ 1 | yes | yes | down | ligand |
| 5IH4 | Human | CK1δ | 1.9 | P 3 ₁ 2 1 | yes | yes | down | |
| 5IH5 | Human | CK1δ | 2.25 | P 3 ₁ 2 1 | yes | yes | down | ligand |
| 5IH6 | Human | CK1δ | 2.3 | P 3 ₁ 2 1 | yes | yes | down | ligand |
| 5W4W | Human | CK1δ | 1.99 | P1 | yes | yes/no | down | ligand |
| 5MQV | Human | CK1δ | 2.15 | C 1 2 1 | yes | yes/no | down | ligand |
| 5X17 | Human | CK1δ | 2 | P 1 2 ₁ 1 | yes | yes | down | ADP |
| 5OKT | Human | CK1δ | 2.13 | P 1 2 ₁ 1 | yes | yes | down | ligand |
| 6GZM | Human | CK1δ | 1.59 | P 1 2 ₁ 1 | yes | yes | down | ligand |
| 6F1W | Human | CK1δ | 1.86 | P 1 2 ₁ 1 | yes | yes | down | ligand |
| 6F26 | Human | CK1δ | 1.83 | P 1 2 ₁ 1 | yes | yes | down | ligand |
| 6PXN | Human | CK1δ | 1.55 | P2 ₁ | no | yes/no | down/up | R178C |
| 6PXO | Human | CK1δ | 2 | P2 ₁ | no | no | down/up | WT |
| 6PXP | Human | CK1δ | 2.35 | P2 ₁ | yes | yes | down | K171E |
| 4HOK | Human | CK1ε | 2.77 | C 1 2 1 | yes | no | down | |
| 5X18 | <i>S. cerevisiae</i> | CK1 | 1.8 | P 1 ₂ 1 1 | no | no | down | |
| 1CSN | <i>S.pombe</i> | CK1 | 2 | P 3 ₂ 2 1 | yes | yes | down | Mg-ATP |
| 2CSN | <i>S.pombe</i> | CK1 | 2.5 | P 3 ₂ 2 1 | yes | yes | down | ligand |
| 1EH4 | <i>S.pombe</i> | CK1 | 2.8 | P 6 ₁ | yes | yes | down | ligand |
| 4XH0 | <i>C.glabrata</i> | Hrr25 | 1.99 | P 2 ₁ 2 2 ₁ | yes | yes | down | ADP |
| 4XHG | <i>C.glabrata</i> | Hrr25 | 2.15 | P 2 ₁ 2 2 ₁ | no | no | down | ADP |
| 4XHH | <i>C.glabrata</i> | Hrr25 | 2.91 | P 2 ₁ 2 2 ₁ | yes | yes | down | |
| 4XHL | <i>C.glabrata</i> | Hrr25 | 3.1 | P 2 ₁ 2 2 ₁ | yes | yes | down | K38R |
| 2CMW | Human | CK1γ1 | 1.75 | P 2 ₁ 2 ₁ 2 ₁ | yes | no | down | |
| 2C47 | Human | CK1γ2 | 2.4 | P 2 ₁ 2 ₁ 2 ₁ | no | no | down | ligand |
| 2CHL* | Human | CK1γ3 | 1.95 | P 3 ₁ 2 1 | yes | yes | down | ligand |
| 3SV0 | <i>O. sativa</i> | CK1-like | 2 | C 1 2 1 | no | no | down | |

[†]Reflects anion occupancy (Occ.) at Site 1 or Site 2

*Other CK1γ3 structures with ligands (all activation loop switch down): 2IZR, 2IZS, 2IZT, 2IZU, 4G16, 4HGL, 4HGS

We probed the library of existing CK1 δ structures using the positioning of L173 as a quantitative metric for activation loop conformation by measuring interatomic distances of the L173 CD2 atom to either CD2 of L152 (short distance in the 'loop up' conformation, long in the 'loop down') or the hydroxyl of Y225 (long in the 'loop up', short in the 'loop down') (Figure 2.3B). A survey of 68 chains from 26 different crystal structures of CK1 δ (in at least 7 space groups) demonstrated that *tau* and the WT kinase from PDB entry 1CKJ are the only structures of CK1 δ to have ever been captured in the 'loop up' conformation (Figure 2.3C). Moreover, the residues that coordinate anion binding are broadly conserved in the CK1 family and anions are also found bound in these sites in other CK1 family kinases (e.g., CK1 ϵ , CK1 γ 3; Table 2.3). To determine if we could independently capture the two states of the activation loop switch in the native kinase, we optimized sulfate-free crystallographic conditions and solved a structure of anion-free CK1 δ . Similar to the 1CKJ structure, we observed both conformations of the activation loop in the two molecules of the asymmetric unit (Figure 2.3.1). Therefore, CK1 has an anion-dependent switch in its activation loop. However, the *tau* mutation appears to favor the 'loop up' conformation because it was observed in crystals that grew in the presence of high sulfate concentrations. Taken together, these data suggest that the *tau* mutation allosterically regulates anion binding at Site 2 via the activation loop.

2.3.6 *tau* stabilizes the rare ‘loop up’ conformation of the CK1 activation loop

To probe the dynamic behavior of CK1 and how this is perturbed by the *tau* mutation, we performed Gaussian Accelerated Molecular Dynamics (GaMD) simulations [50] on four systems: WT and *tau* CK1 with the activation loop in the crystallographically-defined ‘up’ or ‘down’ conformations (Table 2.4). By monitoring the Root Mean Square Deviation (RMSD) of the activation loop with respect to the ‘down’ or ‘up’ crystallographic conformations, we set out to assess its stability over the course of 500 ns simulations (Figure 2.4A-D). We found that the activation loop remained stably in position when simulations were started from the ‘loop down’ conformation for both *tau* and WT. Similar results were seen when the anion was computationally removed from Site 2, suggesting that this conformation of the activation loop is intrinsically stable (Figure 2.4.1). However, in simulations starting from the ‘loop up’ conformation, the WT activation loop rapidly underwent a conformational change, as shown by increased RMSD^{up} values. Because we did not see a concomitant decrease in the $\text{RMSD}_{\text{down}}$ values, we can conclude that this is not a complete transition from ‘loop up’ to ‘loop down’ on this timescale. Importantly, these transitions occurred more frequently in WT CK1 than in *tau* (Figure 2.4C-D). This confirms that the ‘loop up’ conformation is better tolerated in *tau*, consistent with our observation of this apparently rare conformation in our crystal structure. We also observed that Y225 displayed more conformational freedom in *tau*

compared to the WT kinase (Figure 2.4.1). Given that Y225 is directly adjacent to K224 in Site 1 and it also makes contact with L173 in the activation loop in its 'loop down' conformation, this suggests that Y225 could be poised to coordinate the conformation of the activation loop with activity at Site 1.

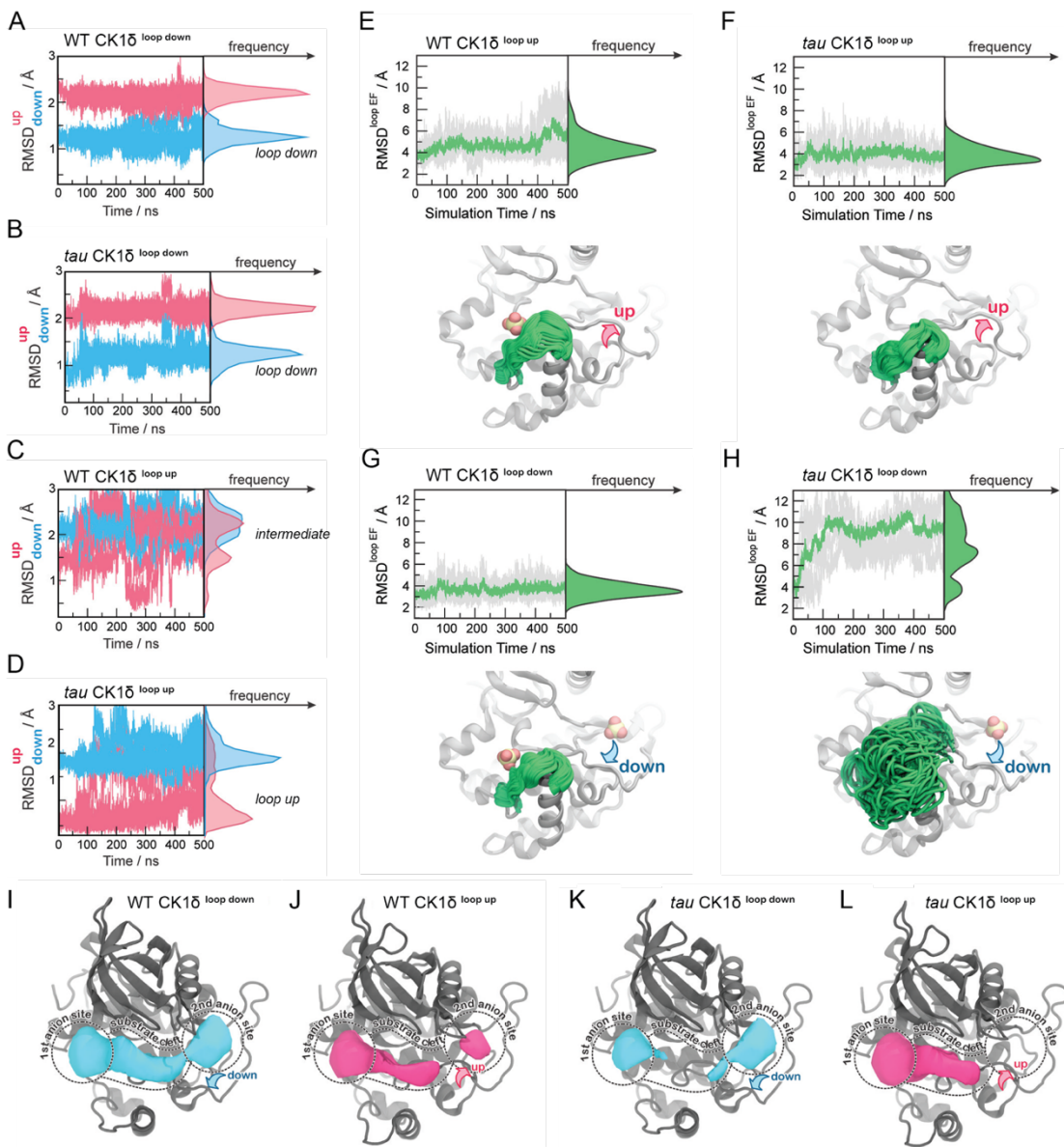
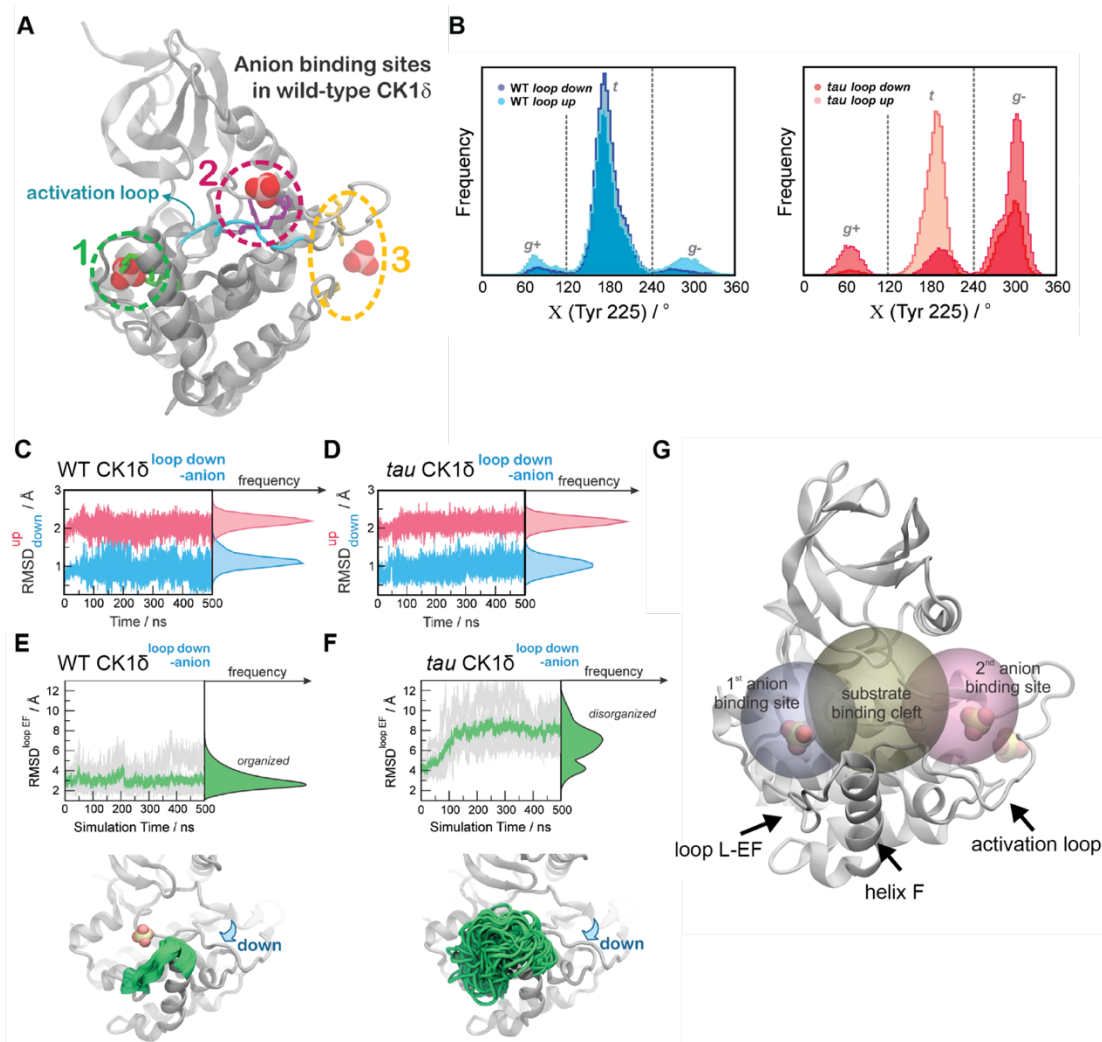


Figure 2.4 Probing the dynamics of CK1δ with GaMD simulations

A-D, Stability of the activation loop assessed by the RMSD of residues 168-175 with respect to the 'loop down' (RMSD_{down}, blue) or 'loop up' conformation (RMSD^{up}, pink), as observed in the crystal structure. For each system, the RMSDs from all five MD replicas are superimposed. Panel A, WT CK1δ^{loop down}; B, *tau* CK1δ^{loop down}; C, WT CK1δ^{loop up}; D, *tau* CK1δ^{loop up}. E-H, Dynamics of the EF loop assessed by the RMSD of residues 213-224 with respect to the initial structure. For each system, the RMSD was calculated for individual replica (gray lines, n = 5) and then averaged (green). The molecular representations in panels E-H show the crystallographic structure of CK1δ (gray) superimposed with snapshots of the L-EF loop extracted from the GaMD simulations (green).

When present in the crystal structure and the simulation, sulfate anions are represented by spheres. I-L, Alterations in anion and substrate-binding clefts arise from the activation loop switch and *tau* mutation. Volumes for the binding clefts were extracted and averaged from GaMD simulations in the four states: panel I, WT CK1 $\delta^{\text{loop down}}$; J, WT CK1 $\delta^{\text{loop up}}$; K, *tau* CK1 $\delta^{\text{loop down}}$; L, *tau* CK1 $\delta^{\text{loop up}}$. Water and anions were removed from the analysis. Volumetric maps are contoured at 0.1 and represent regions that were consistently open during the simulations. See also Figure 2.4.1.



Supplemental Figure 2.4.1 (relates to Figure 2.4)

A, Defining the localization of anion binding sites 1 (green), 2 (magenta) and 3 (yellow) for MD simulations. For reference, the loop down conformation of WT CK1 δ is represented as ribbons (cyan). B, Residue Y225 displays more conformational freedom in the *tau* mutant (right panel) than in WT CK1 δ (left panel). Populations of the gauche+ (g+), trans (t) and gauche- (g-) rotamers for Y225 from MD simulations of the loop up and loop down conformations of WT and *tau* kinase are depicted. C-D, Stability of the activation loop assessed by the Root Mean Square Deviation (RMSD) of residues 168-175 with respect to the loop down conformation (RMSD_{down}, blue) or to the loop up conformation (RMSD^{up}, magenta) as observed in the crystal structures. For both systems, the Site 2 anion was removed computationally before beginning MD simulations. Panel C, WT CK1 δ ^{loop down}; D, *tau* CK1 δ ^{loop down}; both show RMSDs superimposed from all five MD replicas. E-F, Dynamics of the L-EF loop obtained from Gaussian Accelerated MD simulations in WT CK1 δ (panel E) and *tau* mutant (panel F) when the activation loop in the 'down' conformation and the second anion binding site has been removed computationally. The RMSD was calculated for the backbone

atoms of residues 213-224 for each independent replica (gray, $n = 5$) and then averaged (green). The molecular representations show crystallographic structures of the enzyme (in gray) superimposed with several snapshots of the loop L-EF extracted from the Gaussian Accelerated MD (GaMD) simulations (in green). When present, sulfate anions are represented by van der Waals spheres. G, Volumetric analysis of the Site 1 binding site (gray sphere), substrate binding cleft (golden sphere) and Site 2 anion binding site (rose sphere) during the GaMD simulations. In each system, the volumes were calculated for snapshots extracted from the GaMD trajectories every 2 ns, using POVME 3.0 [51]. Water and ions were computationally removed prior to volume calculations.

2.3.7 The activation loop allosterically controls the dynamics of loop L-EF in *tau*

While monitoring the overall dynamics of WT and *tau* CK1, we detected a major difference in the dynamics of the loop connecting α -helices E and F (loop L-EF, Figure 2.4.1), part of the anion binding site disrupted by the *tau* mutation (Figure 2.4E-H). This is intriguing because temperature-dependent dynamics of loop L-EF were recently shown to be important for the temperature-compensated activity of CK1 on PER2 [30]. In our simulations of the WT kinase, this loop exhibited relatively restricted mobility, regardless of whether the activation loop was in the 'up' or 'down' conformation (Figure 2.4E and G). Similar results were observed when the anion was computationally removed from Site 2 (Figure 2.4.1). However, we observed that the 'loop down' conformation of the activation loop was accompanied by a strong disorganization of loop L-EF in *tau* (Figure 2.4H), leading to significantly larger conformational freedom compared to the WT kinase (Figure 2.4G). Surprisingly, the enhanced dynamics of loop L-EF was not observed when *tau* was in the 'loop up' conformation; instead, loop L-EF displayed the same restricted dynamics as the WT kinase (Figure E-F). These data suggest that the disruption of Site 1 by loop L-EF dynamics in the *tau* mutation may be due to allosteric communication with the activation loop, and by proxy, anion binding at Site 2.

2.3.8 *tau* dynamically reshapes the substrate-binding cleft in CK1

To investigate how the activation loop and dynamics of loop L-EF might influence substrate selectivity, we calculated the volume of the substrate binding cleft and adjacent anion binding sites throughout the 500 ns GaMD simulations (Figure 2.4 and S4). As expected, Site 2 was completely open only when the activation loop was in the ‘loop down’ conformation for the WT kinase (Figure 2.4I). Interestingly, this site became partially open in simulations of the WT kinase starting from the ‘loop up’ conformation (Figure 2.4J), indicating that the intermediate conformational state observed in our simulations might allow the kinase to recover, to some extent, the ability to bind an anion at Site 2. The conformation of the activation loop indirectly affects the volume of the substrate binding cleft with opposing effects in WT and *tau*. In WT, the substrate binding cleft was open more consistently with the activation loop in its preferred ‘down’ conformation (Figure 2.4I-J). By contrast, the substrate binding cleft was open more consistently in *tau* in the ‘loop up’ conformation (Figure 2.4L) and, due to the dynamic disordering of loop L-EF, often closed when in the ‘loop down’ conformation (Figure 2.4K). Because the activation loop does not contact the substrate binding cleft, it cannot directly affect the shape of the cleft by steric effects. Instead, closing of the substrate binding cleft in *tau* occurs due to the conformational disorganization in loop L-EF, which is allosterically induced when the activation loop is in the ‘down’ conformation.

2.3.9 *tau* influences the global dynamics of CK1

We next used principal component analysis to uncover effects of *tau* on the principal modes of motion displayed by CK1 during the GaMD simulations (Figure 2.5, S5 and Supplemental Movie 1). The 1st principal component consisted of a clear ‘open-and-close’ movement of the enzyme, achieved mainly by dislocation of the N-terminal lobe (N-lobe) with respect to the top of the helix F (Figure 2.5A). This mode of motion has been shown to control accessibility to the ATP-binding site and regulate substrate access in other kinases [52]. The histograms of the 1st principal component show that WT CK1 sampled more of the open conformations compared to *tau* (Figure 2.5C). The 2nd principal component consisted of a twisting movement of the N-lobe with respect to the top of helix F and a significant rearrangement of loop L-EF, which can either be extended or collapsed (Figure 2.5B). When collapsed, loop L-EF had the effect of sterically closing the substrate binding cleft. The histograms of the 2nd PCA illustrate that loop L-EF adopts more extended conformations in WT CK1 and more collapsed conformations in *tau* (Figure 2.5D). The collapsed conformations require loop L-EF to undergo a significant conformational change, which agrees with the high conformational freedom seen in this region when the *tau* activation loop is in the ‘loop down’ conformation. Altogether, the GaMD simulations suggest that the *tau* kinase never behaves fully like the WT enzyme; compared to WT, it stabilizes the rare, Degron-preferring conformation of the activation loop that remodels the substrate binding cleft and

excludes anion binding at Site 2. By contrast, when *tau* samples the 'loop down' conformation of the activation loop, it leads to a dynamic disordering of loop L-EF that favors conformations of the kinase that likely accounts for its decrease enzymatic efficiency on the FASP region.

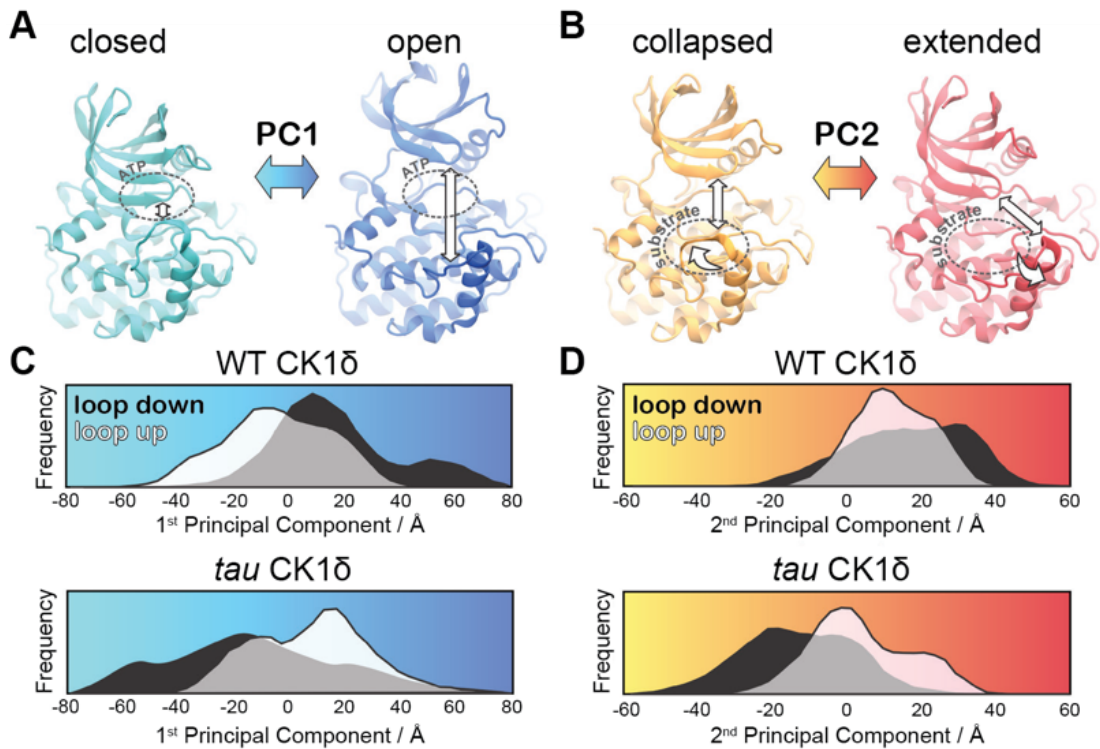
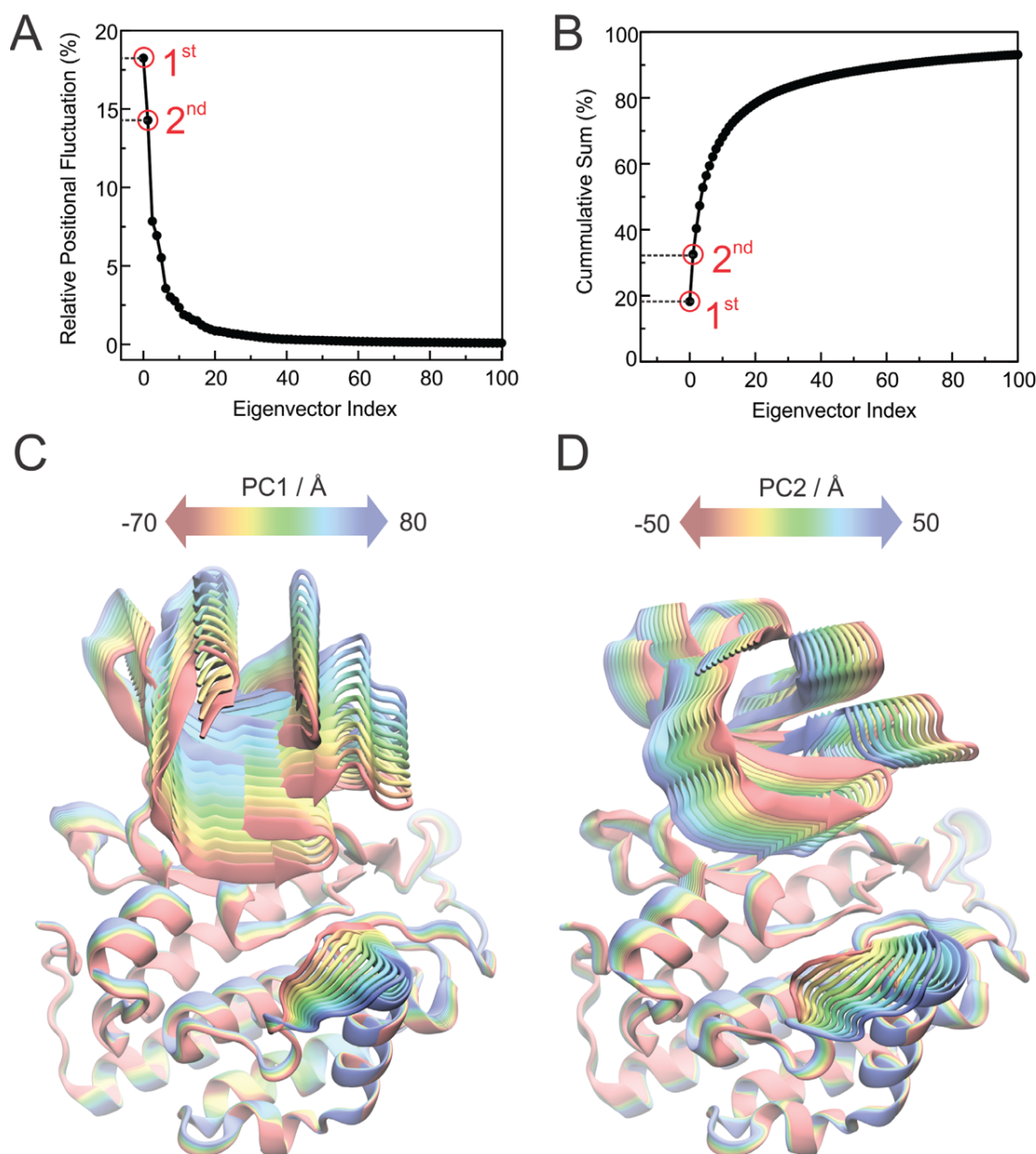


Figure 2.5 *tau* influences the principal modes of motion in CK1δ

Principal modes of motion obtained from Principal Component Analysis (PCA). A, PC1 consists of an ‘open-and-close’ movement achieved by dislocation of the N-lobe with respect to the top of the helix F to control accessibility of the ATP-binding site (dotted circle). B, PC2 consists of a twisting movement of N-lobe with respect to the top of helix F and significant rearrangement of the loop L-EF, which can be extended or collapsed against the substrate binding site (dotted circle). C-D, Structural representations correspond to (panel A) PC1 = -80 Å (cyan), PC1 = 80 Å (blue) and (panel B) PC2 = -60 Å (orange), and PC2 = 60 Å (red). The histograms represent projections of the accumulated GaMD trajectories along the 1st (C) or 2nd (D) principal components for WT CK1δ and the *tau* mutant, either in the activation ‘loop down’ (black) or ‘loop up’ (white) conformations. See also Figure 2.5.1 and Supplemental Movie 1.



Supplemental Figure 2.5.1 (relates to Figure 2.5)

A, Percent of atomic fluctuations contained in each of the principal modes of motion (eigenvectors) obtained from the Principal Component Analysis of the all GaMD trajectories. The 1st and 2nd modes of motions (highlighted in red) contain 18.2% and 14.3% of the total atomic fluctuations displayed by the backbone atoms, respectively. B, cumulative sum of the relative atomic fluctuations displayed in panel A, showing that, if combined, the 1st and 2nd modes of motions contain more than 30% of the total atomic fluctuations of the backbone atoms. C, 1st principal mode of motion corresponds to an 'open-and-close' movement of the enzyme, achieved mainly by dislocation of the N-terminal lobe (N-lobe) with respect to the top of the helix F. D, 2nd principal mode of motion corresponds to a twisting movement of the N-lobe with

respect to the top of helix F and significant rearrangement of loop L-EF, which can either be extended or collapsed.

2.3.10 Circadian alleles from *Drosophila* to humans occur throughout CK1

To gain further insight into CK1 function, we mapped known mutant alleles that influence circadian rhythms onto the CK1 structure (Figure 2.6). *Doubletime* (DBT), the CK1 δ/ϵ ortholog in *Drosophila*, has one allele that causes a short circadian period (*dbt^S*, P47S) while all others lead to a long period [24, 53, 54]. Many long period mutations occur at or near catalytically important residues like the catalytic DFG motif and the regulatory spine that controls kinase activity (Figure 2.6B) [55]. Moreover, two loss of function alleles occur in the activation loop: *dco¹⁸* (S181F) is located right behind the *tau* site (R178), linking it to the substrate binding channel and activation loop, while *dco²* (G175S) occurs at the hinge point for the activation loop switch [56]. Although *Drosophila* and mammalian PER proteins are somewhat functionally divergent, conservation of their Degrons [10, 57] and FASP-like stabilizing phosphorylation sites [15, 31, 58] suggests that there may be some conservation in their regulation by CK1 (Figure 2.6C). In line with this, expressing mammalian CK1 δ with the *tau* or *dbt^S* mutation leads to short period circadian rhythms in flies [59]. Consistent with this functional conservation, the entire surface-exposed area linking Sites 1 and 2 and the substrate binding cleft are $\geq 95\%$ identical in 20 species from humans to unicellular green alga where CK1 has been implicated in regulation of circadian clocks (Figure 2.6.1).

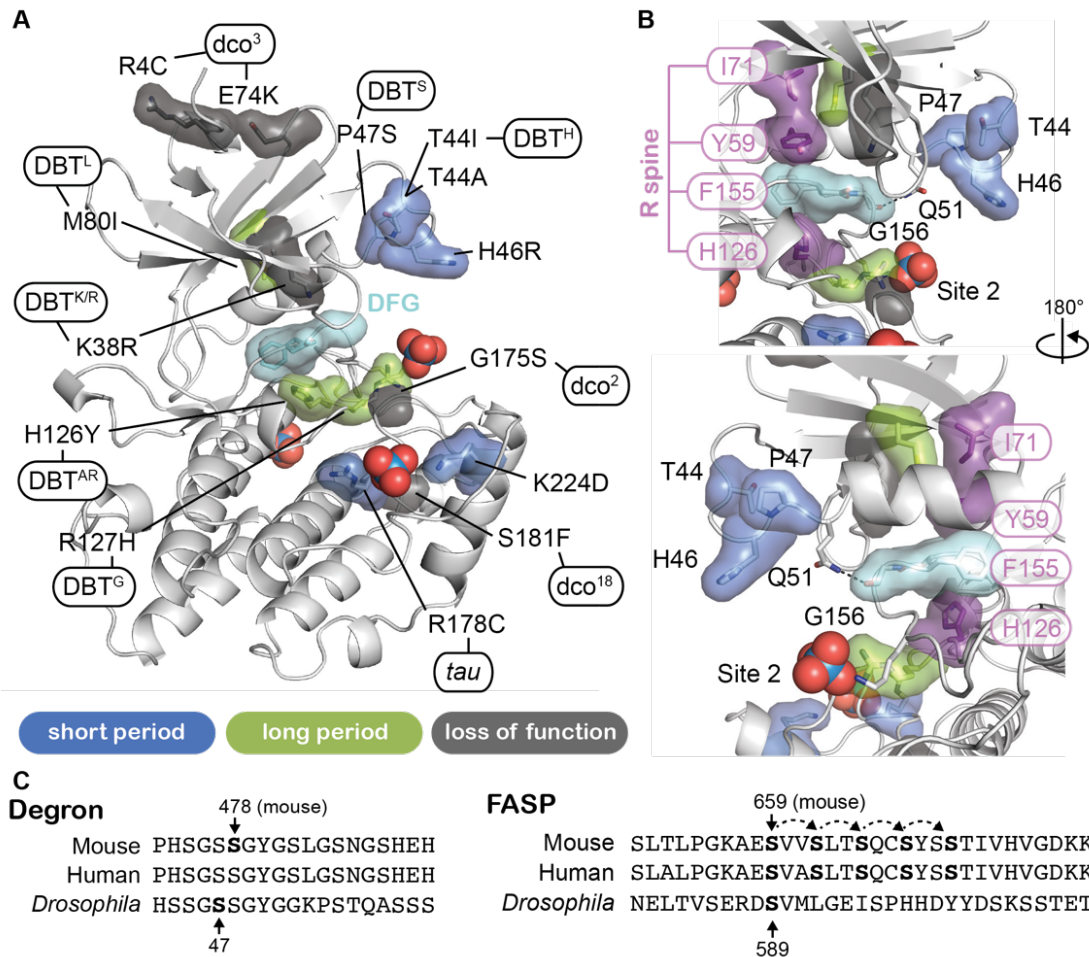
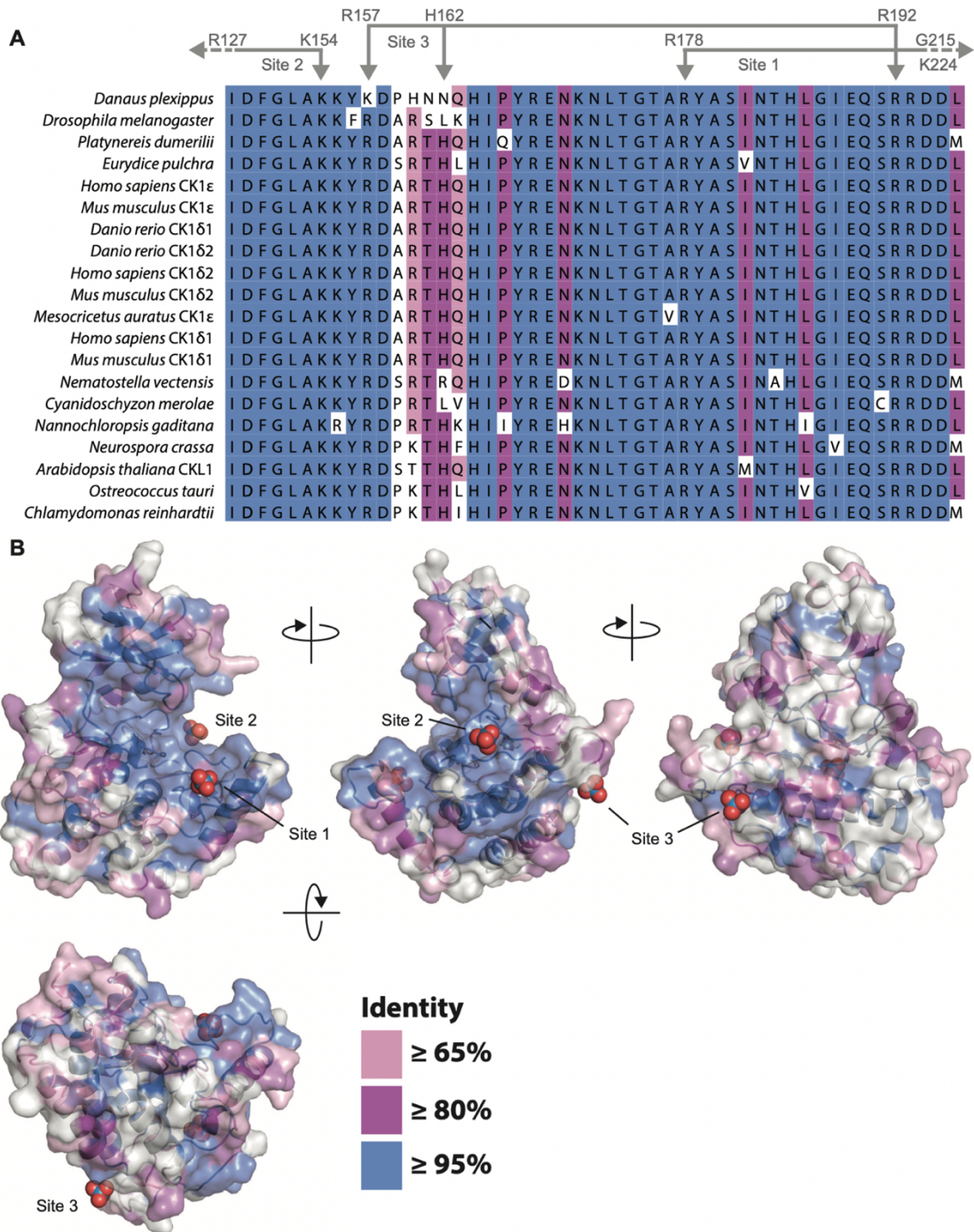


Figure 2.6 Proximity of CK1 alleles map to catalytic and substrate binding sites

A, Structure of CK1 δ (PDB: 1CKJ, chain B) clock relevant alleles mapped from mammalian CK1 or *Drosophila* DBT. Mutants are colored by phenotype: short period (blue), long period (green), loss of function (gray). DFG catalytic motif, cyan. B, View of N-lobe period mutants and the regulatory spine (R-spine, purple) with F155 of the DFG motif in cyan. Polar interactions between Q51 and G156 that link the N- and C-lobe are depicted with a dashed black line. C, Alignment of the mammalian and *Drosophila* Degron and FASP/stabilizing sequences. Residues in bold have experimental support for phosphorylation. Dashed arrows indicate sequential phosphorylation following the consensus pSxxS motif.



Supplemental Figure 2.6.1 (relates to Figure 2.6)

A, Alignment of the central catalytic DFG motif and activation loop of CK1ε and CK1δ (including isoforms δ1 and δ2 that differ only in the last 15 amino acids [20, 43]) that have been implicated in circadian regulation of the following species: *Danaus plexippus* [60]; *Drosophila melanogaster* [24, 61]; *Platynereis dumerilii* [62]; *Eurydice pulchra* [63]; *Homo sapiens* [13-15, 64]; *Mus musculus* [43, 65]; *Danio rerio* [66],

Mesocricetus auratus [33]; *Nematostella vectensis* [67]; *Cyanidoschyzon merolae* [68]; *Nannochloropsis gaditana* [69]; *Neurospora crassa* [23]; *Arabidopsis thaliana* [70]; *Ostreococcus tauri* [25]; and *Chlamydomonas reinhardtii* [71, 72]. When only one CK1 δ/ϵ -like homolog was identified in an organism, no gene name is shown in the alignment. Coloring indicates the degree of conservation, with $\geq 95\%$ identity in blue, $\geq 80\%$ identity in purple, $\geq 65\%$ identity in pink, and $<65\%$ identity in white. Residues that coordinate anion binding on CK1 are indicated above in gray. B, Conservation from the kinase domain alignment mapped onto the WT CK1 δ kinase domain (PDB: 1CKJ, chain B). The binding sites for three highly conserved anion are indicated.

2.3.11 Other short period mutants exhibit differential activity on the FASP and Degron

Three short period mutants from humans and *Drosophila* (T44A, H46R, and P47S) colocalize in the N-lobe right above Site 2 (Figure 2.6B). Given the changes in N- to C-lobe dynamics that we observed in our simulations of CK1 (Figure 2.5), we wondered how these mutations would influence substrate selectivity. We first tested the activity of these short period kinase mutants in cell-based transfection assays by monitoring both FASP priming (Figure 2.7A) and Degron (Figure 2.7B) phosphorylation. Similar to the Site 2 mutants we tested earlier (Figure 2.2.1), the short period mutants T44A, H46R, and P47S each retained substantially more kinase activity on the FASP priming site than *tau*. A triple mutant of all three short period mutants (3M) did not have additive effects. Likewise, they also appeared to retain kinase activity or even exhibited modest increases in Degron phosphorylation relative to WT (Figure 2.7B), although not to the same degree as *tau*. On balance, it appears that mutants near Site 2 might act differently from *tau* in that they retain FASP priming activity while increasing activity at the Degron relative to WT.

We also studied another short period mutant located at Site 1, K224D, which was recently reported to have a ~20-hour circadian period like *tau* [30]. Unlike *tau*, K224D retained FASP priming activity in HEK293 cells (Figure 2.7C), although it exhibited a sharp increase in Degron phosphorylation similar to *tau* (Figure 2.7D). This effect was not dependent on the charge inversion,

as we saw the same effect with a K224A mutant (Figure 2.7.1). Despite retaining priming activity in cells, we noticed that the enzyme efficiency of K224D was decreased on the FASP peptide, which contains multiple serines (Table 2.2). This suggested that while priming of the FASP site S659 might be intact, subsequent phosphorylation of the downstream sites might be compromised in K224D. To test this, we used the NMR-based kinase assay to provide information on the stepwise phosphorylation of the FASP region [20]. Consistent with the cellular data, K224D retained normal priming activity at S659, but phosphorylation of the downstream serines that conform to the pSxxS consensus motif was compromised relative to WT kinase (Figure 2.7E). Therefore, although *tau* and K224D both enhance Degron phosphorylation to a similar degree and lead to ~20-hour circadian periods [12, 30], this is likely achieved through different mechanisms on the kinase—*tau* reduces both priming and downstream phosphorylation of the FASP region, while K224D (and K224A) likely just disrupts the phosphorylation of the downstream pSxxS consensus motifs.

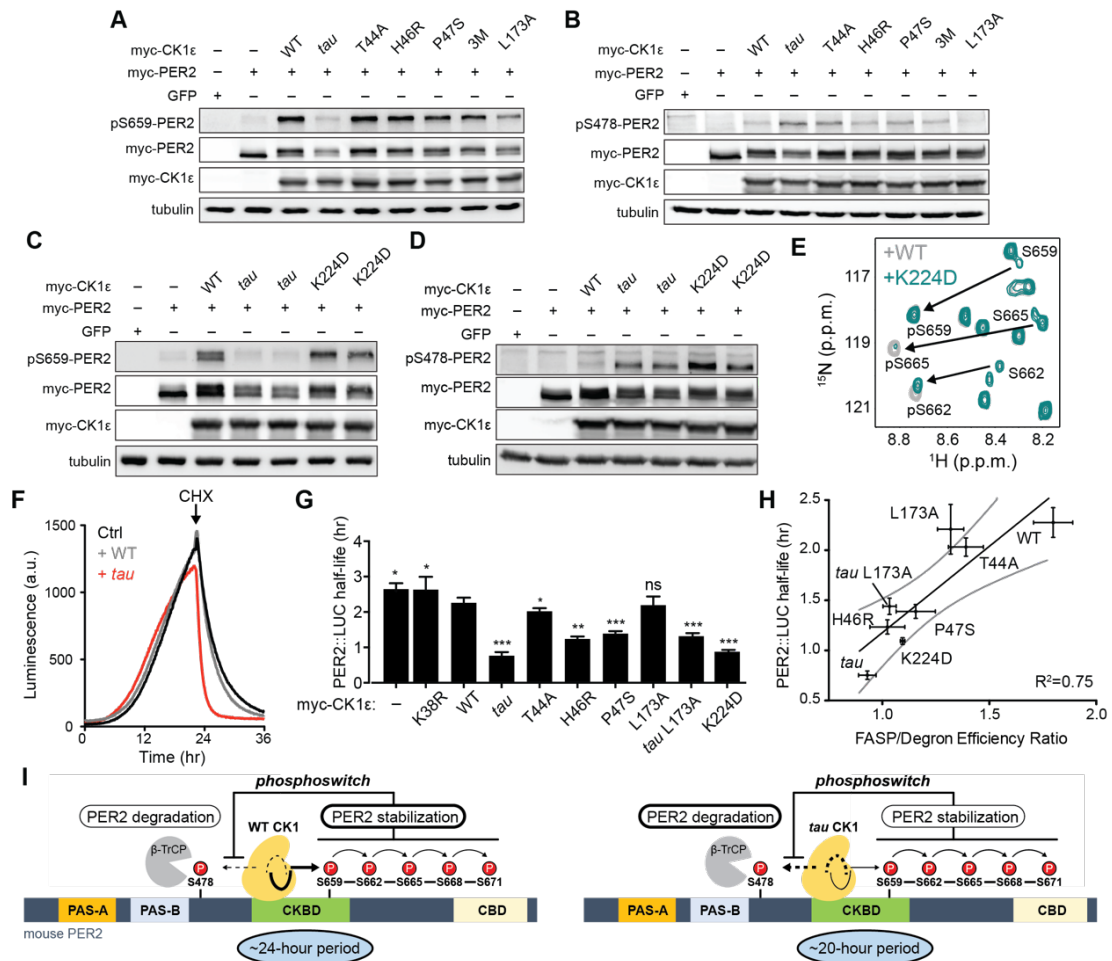


Figure 2.7 Substrate discrimination on the PER2 phosphoswitch is regulated by the CK1 activation loop switch

A,B Western blot of FASP priming site, detecting pS659 (A) or Degron site, detecting pS478 (B) phosphorylation on mouse myc-PER2 in HEK293 cell lysates after transfection with indicated myc-CK1ε expression plasmids. 3M triple mutant: T44A, H46R, P47S. Representative blot from n = 3 shown. C,D Western blot of FASP priming (C) or Degron (D) phosphorylation on PER2 as above with the myc-CK1ε K224D mutant. Representative blot from n = 3 shown with replicate samples loaded for *tau* and K224D. E, Overlaid ¹⁵N/¹H HSQC spectra at 3 hr timepoint in the NMR kinase assay on 200 μM ¹⁵N FASP + 1 μM K224D (teal) or WT (gray) CK1δ ΔC. Arrows, phospho-specific peaks corresponding to pS659, pS662, and pS665. F, Representative real-time luminescence data for PER2::LUC stability in HEK293 cells transfected with myc-PER2::LUC plus empty vector (black) or myc-CK1ε WT (gray) or *tau* (red) as indicated (n = 4). 40 μg/mL cycloheximide (CHX) added 24 hours post-transfection (arrow). G, Quantification of PER2::LUC half-life with different myc-CK1ε mutants. Data represent mean ± s.d. (n = 4) with significance assessed

as above. H, Scatterplot with linear regression analysis of the ratio of enzyme efficiencies (k_{cat}/K_m) for FASP and Degron relative to the PER2::LUC half-life determined in panel G and Figure 2.7.1. All data are plotted as mean \pm s.d. ($n = 4$ for PER2::LUC and $n = 3-4$ for enzyme efficiencies). Black, linear regression to data; gray, 95% confidence interval. I, The conformational switch of the CK1 δ/ϵ activation loop is coupled to substrate selection in the PER2 phosphoswitch. Left, the activation loop of the WT kinase is stable in the 'loop down' conformation, leading to preferential phosphorylation the FASP region, which stabilizes PER2 by reducing phosphorylation of the Degron. Right, the activation loop of *tau* kinase is better tolerated in the alternate 'loop up' conformation leading to an intrinsic gain of kinase function on the Degron and loss of kinase function on the stabilizing FASP region. This switch in substrate preference promotes PER2 degradation and leads to a shorter circadian period. CKBD, CK1 binding domain; CBD, CRY binding domain. See also Figure 2.7.1.

Representative blot from $n = 3$ shown. F, Quantification of PER2::LUC half-life from transfection assays (as in panel A) with myc-CK1 ϵ mutants from panel E. Data represent mean \pm s.d. ($n = 4$).

2.3.12 The ratio of FASP/Degron enzyme efficiency correlates with PER2 stability

One commonality of short period mutants is enhanced Degron phosphorylation in cells, as both cellular [19, 34] and *in vivo* studies of short period mutants demonstrate that PER2 stability is decreased in a CK1-dependent manner [15, 61]. We measured the effect of CK1 mutants on the half-life of PER2::LUC in real-time after cycloheximide treatment (Figure 2.7F and S7). All of the mutants, apart from L173A, lead to a shorter half-life of PER2::LUC (Figure 2.7G). We initially mutated L173 because it appears to serve as a latch for the activation loop in both its 'loop up' and 'loop down' conformations (Figure 2C). We found that the mutant substantially decreased kinase activity at both the FASP priming and Degron sites in the transfection-based assay and *in vitro* (Figure 2.7A-B and Table 2.2), and a double mutant with *tau* decreased its activity on the Degron to a similar degree (.27). We hypothesized that the L173A mutant might have a half-life similar to WT because its reduced activity on the stabilizing FASP region was offset to a similar degree on the Degron (Figure 2.7G and Table 2.2). Indeed, we observed a significant correlation between PER2::LUC half-life and the intrinsic ratio of CK1 kinase activity on these two key sites that establish the phosphoswitch mechanism (Figure 2.7H). Collectively, these data support a new model for CK1 regulation whereby activation loop dynamics orchestrate

substrate specificity and contribute directly to the phosphoswitch regulation of PER2 stability, and therefore, the timing of circadian rhythms (Figure 2.7I).

2.4 Discussion

Despite its powerful control over the timing of circadian rhythms in eukaryotes from humans to green algae [14, 25], very little is known about the molecular determinants of CK1 δ substrate selectivity and activity. We discovered a conformational switch in the activation loop of CK1 that regulates its activity on two regulatory regions in PER2 that control its stability and circadian timing in mammals [18]. We show that anion binding regulates the conformation of this switch to reshape the substrate binding cleft and thereby control substrate selectivity. Short period mutants in CK1 from *Drosophila* to mammals reveal that all exhibit an intrinsic increase in kinase activity on the Degron, consistent with an earlier observation in cells [34]. However, the *tau* mutant disrupts the apparent allosteric regulation between anion binding sites; our MD simulations revealed that *tau* alters the dynamics of the activation loop and adjacent loop L-EF that likely underlie the decreased activity of *tau* on the stabilizing FASP region.

Allosteric regulation is a common feature of protein kinases, often based on dynamic changes in ensembles of residues that can occur in the absence of major changes in conformation [73]. CK1 has remarkable, histone-like

conservation ($\geq 95\%$ identity) of the entire surface-exposed area linking the two key anion binding sites and substrate binding cleft, suggesting that the mechanisms we discovered here likely apply broadly to circadian rhythms as well as other CK1-regulated processes in other eukaryotes. Binding of regulatory anions at these conserved sites could arise from phosphorylated CK1 itself in *cis* via its autoinhibitory tail [42], or in *trans* from the binding of phosphorylated substrates like the FASP region, to allow for the generation of feedback regulation directly on the kinase. In line with this, changes in the sequence [43] or phosphorylation [74] of the autoinhibitory tail of CK1 δ/ϵ could alter the balance of PER2 phosphorylation at the FASP or Degron to control circadian period. Therefore, our study demonstrates that the dynamics of CK1 δ/ϵ directly encode its activity in the PER2 phosphoswitch [18]. The conformational equilibrium of the activation loop may also play a role in the temperature-compensated activity of CK1 δ/ϵ observed *in vitro* that is linked to loop L-EF, an insertion in the clock-relevant kinases CK1 δ and CK1 ϵ that plays a role in maintaining its relative insensitivity to temperature [30].

We used PER2 stability here as a cellular proxy to study the effect of mutations in CK1 on circadian timing. PER proteins seem to have a special role in the mammalian clock as state variables that define both the timing and phase of circadian rhythms through changes in their abundance [75, 76]. CK1-dependent changes in PER abundance likely affect circadian period based on their role as stoichiometrically limiting factors in the assembly of transcriptional

repressive complexes in the feedback loop of the molecular clock [2, 5, 77]. Recent studies have shown that CK1 may allow target other clock proteins for phosphorylation in the repressive complexes [2], a property that seems to be conserved in *Drosophila* [78]. Therefore, more studies are needed to fully understand the interplay between PER2 stability, PER-CK1 interactions and its regulation by post-translational modifications, including by phosphatases [79] and other kinases [80-82] that ultimately control circadian rhythms.

There is still much more to be learned about the factors that dictate CK1 substrate selectivity. CK1 is clearly highly active on primed (pSxxS) sites [20], supporting its designation as the canonical consensus motif of the kinase. However, we find it compelling that many of the biologically important roles of CK1 δ/ϵ and the related kinase CK1 α as key regulators of Wnt signaling [83], the DNA damage response [84], cell cycle [85], and circadian rhythms [12, 24] depend on their activity at non-consensus sites. The ability of these kinases to phosphorylate lower affinity, non-consensus sites on PER2 is likely dependent on the formation of a stable, stoichiometric complex with PER2 via highly conserved sites that flank the FASP phosphorylation region in the CKBD [10, 11]. The generally low activity of CK1 that we observe on clock-relevant non-consensus sequences may also be important for the slow timescale of circadian rhythms. This property is also conserved in KaiC, the enzyme that controls circadian timing in the cyanobacterial system [86], suggesting commonalities in the biochemical origins of building slow biological clocks.

2.5 Materials and Methods

Cell culture, reagents and transfection

myc-mPer2, myc-mPer2 S659A, mPer2::Luc, and myc-CK1 ϵ expression plasmids were described previously [10, 18, 74]. Mutations of the kinase domain were introduced by Quikchange site-directed mutagenesis (Stratagene) and validated by sequencing.

HEK293 cells (from American Type Culture Collection) were cultured in Dulbecco's Modified Eagle's Medium (DMEM, Gibco) supplemented with 10% FBS (Gibco), 50 units/mL penicillin, 50 μ g/mL streptomycin (Invitrogen) and maintained at 37°C in a 5% CO₂ environment. Cells were transfected using Lipofectamine 2000 transfection reagent (Life Technologies) following the manufacturer's instructions. For transfections titrating expression of myc-CK1 ϵ , either 10 or 50 ng of plasmid was used; total plasmid DNA of either 1 or 2 μ g was used for each well of a 12 or 6-well-plate respectively. 10 μ M MG132 was added to cultures 24 hours prior to harvest to prevent proteasomal degradation for experiments shown in Figure 2.7A and B.

PER2::LUC half-life measurement

Mouse PER2::LUC expression plasmids (10 ng) were transiently transfected alone or with myc-CK1 ϵ (100 ng) in 35 mm dishes of HEK293 cells in phenol red-free DMEM in the presence of 100 mM D-luciferin (122799,

PerkinElmer), 10 mM HEPES and 1.2 g/L sodium bicarbonate. Dishes were sealed with 40 mm cover glasses and vacuum grease, and incubated in the LumiCycle (Actimetrics). The next day, 40 µg/mL cycloheximide (Sigma) was added per 35 mm dish. Luminescence data were used to calculate PER2::LUC half-life in Prism (GraphPad) using one-phase decay algorithm as described previously [18]. Briefly, half-lives were calculated using the one-phase decay algorithm in Prism (GraphPad) using the raw luciferase activity, beginning from the point of cycloheximide addition to the plateau at minimum luciferase activity (n = 4).

SDS-PAGE and western blotting

Whole cell extracts of transfected HEK293 cells lysed on ice with cell lysis buffer (50 mM Tris-HCl pH 8.0, 150 mM NaCl, 1% (vol/vol) Nonidet P-40 and 0.5% deoxycholic acid containing Complete Protease Inhibitors (Roche) and PhosStop Phosphatase Inhibitors (Roche)) were analyzed by denaturing SDS-PAGE gel, which was transferred on PVDF membrane (Immobilon, Millipore). The blot was probed using the indicated primary antibodies: anti-myc (9E10) (sc-40, Santa Cruz Biotechnology) and anti-tubulin (ab52623, Abcam) were purchased from commercial providers, while rabbit polyclonal antibodies were generated against phospho-Ser478, phospho-Ser659 or phospho-Ser662 of mouse PER2 and purified against the phosphopeptides by Abfrontier (Young In Frontier Co.). The phosphopeptides for phospho-Ser478 and phospho-

Ser659 have been described elsewhere [18, 20]; the phosphopeptide KAESVVpSLTSQ-Cys was used to generate the phospho-Ser662 antibody. HRP-conjugated goat secondary antibodies for anti-rabbit (1706515, Bio-Rad) and anti-mouse (1706516, Bio-Rad) were with standard ECL reagents (Thermo Fisher Scientific). Densitometric analysis of western blot bands was performed using ImageJ software (National Institutes of Health).

Expression and purification of recombinant proteins

All proteins were expressed from a pET22-based vector in *Escherichia coli* Rosetta2 (DE3) cells based on the Parallel vector series [87]. The extended wild-type FASP peptide (residues 645-687) and Degron peptide (residues 475-505) from human PER2, and a short wild-type mouse FASP peptide (residues 642-666) all contain an N-terminal WRKKK polybasic motif for *in vitro* kinase assays and a tryptophan for UV detection during purification. All peptides were expressed downstream of an N-terminal TEV-cleavable His-NusA tag. Human CK1 δ catalytic domains (CK1 δ Δ C, residues 1-317) were all expressed in Rosetta2 (DE3) cells with a TEV-cleavable His-GST tag. Mutations were made using standard site-directed mutagenesis protocols and validated by sequencing. All proteins and peptides expressed from Parallel vectors have an additional N-terminal vector artifact of "GAMDPEF" remaining after TEV cleavage. Cells were grown in LB media (for natural abundance growths) or M9 minimal medium with the appropriate stable isotopes (^{15}N , ^{13}C for NMR, as

done before [20]) at 37 °C until the O.D.₆₀₀ reached ~0.8; expression was induced with 0.5 mM IPTG, and cultures were grown for approximately 16-20 hours more at 18 °C.

For CK1δ kinase domain protein preps, cells were lysed in 50 mM Tris pH 7.5, 300 mM NaCl, 1 mM TCEP, and 5% glycerol using a high-pressure extruder (Avestin). HisGST-CK1δ ΔC fusion proteins were purified using Glutathione Sepharose 4B resin (GE Healthcare) using standard approaches and eluted from the resin using Phosphate Buffered Saline with 25 mM reduced glutathione. His₆-TEV protease was added to cleave the His-GST tag from CK1δ ΔC at 4 °C overnight. Cleaved CK1δ ΔC was further purified away from His-GST and His-TEV using Ni-NTA resin (Qiagen) and subsequent size exclusion chromatography on a HiLoad 16/600 Superdex 75 prep grade column (GE Healthcare) in 50 mM Tris pH 7.5, 200 mM NaCl, 5 mM BME, 1 mM EDTA, and 0.05% (vol/vol) Tween 20. Purified CK1δ ΔC proteins used for *in vitro* kinase assays were buffer exchanged into storage buffer (50 mM Tris pH 7.5, 100 mM NaCl, 1 mM TCEP, 1 mM EDTA, and 10% glycerol) using an Amicon Ultra centrifugal filter (Millipore) and frozen as small aliquots in liquid nitrogen for storage at -80 °C.

For PER2 peptide preps, cells were lysed in 50 mM Tris pH 7.5, 500 mM NaCl, 2 mM TCEP, 5 % glycerol and 25 mM imidazole using a high-pressure extruder (Avestin). His-NusA-FASP or His-NusA -Degron fusion proteins were purified using Ni-NTA resin using standard approaches and eluted from the

resin using 50 mM Tris pH 7.5, 500 mM NaCl, 2 mM TCEP, 5 % glycerol and 250 mM imidazole. His-TEV protease was added to cleave the His₆-NusA tag from the PER2 peptides at 4 °C overnight. The cleavage reaction was subsequently concentrated and desalted into low imidazole lysis buffer using a HiPrep 26/10 Desalting column. Peptides were purified away from His-NusA and His-TEV using Ni-NTA resin with 50 mM Tris pH 7.5, 500 mM NaCl, 2 mM TCEP, 5 % glycerol and 25 mM imidazole. Peptides were purified by size exclusion chromatography on a HiLoad 16/600 Superdex 75 prep grade column, using NMR buffer (25 mM MES pH 6.0, 50 mM NaCl, 2 mM TCEP, 1 mM EDTA, 11 mM MgCl₂) or 1x kinase buffer (25 mM Tris pH 7.5, 100 mM NaCl, 10 mM MgCl₂, and 2 mM TCEP) for NMR or ADP-Glo kinase assays, respectively.

Radioactive and ELISA-based kinase assays

Mouse PER2 FASP region peptides (primed, RKKKTEVSAHLSSLTPGKAEPpSVVSLTSQ, or unprimed, RKKKTEVSAHLSSLTPGKAESVSLTSQ), mouse PER2 Degron peptide (RKKKPHSGSSGYGSLGNSGHEHMSQTSSSDSN, from [28]) and the CK1tide peptide (KRRRALpSVASLPGL, from [28, 30]) were synthesized and purified to 95% or higher (SABio).

For the radioactive kinase assay, two independent reaction mixtures of 50 µL containing 200 µM of the FASP or Degron peptides in reaction buffer (25

mM Tris pH 7.5, 7.5 mM MgCl₂, 1 mM DTT, 0.1 mg/mL BSA) were preincubated for 5 minutes with or without 20 nM CK1δ ΔC (for primed FASP substrate) or 200 nM CK1δ ΔC (for unprimed FASP or Degron) and the reaction was started by addition of 750 μM of UltraPure ATP (Promega) containing 1-2 μCi of γ-³²P ATP (Perkin Elmer). After incubation of the reaction mix at 30 °C, an 8 μL aliquot of the reaction mix was transferred to P81 phosphocellulose paper (Reaction Biology Corp) at the indicated timepoints. The P81 paper was washed three times with 75 mM of orthophosphoric acid and once with acetone. The air-dried P81 paper was counted for P_i incorporation using a scintillation counter (Perkin Elmer) by Cherenkov counting. Results shown are from four independent assays.

For the ELISA kinase assay, unprimed FASP peptide was diluted to 2 μg/mL in Carbonate buffer, pH 9.5 (0.1 M sodium carbonate) and coated onto a 96 well plate (100 μL/well). The next day, wells were washed three times with wash buffer (PBS with 0.05% Tween, PBS-T) and once with kinase buffer (25 mM Tris pH 7.5, 5 mM beta glycerol phosphate, 2 mM DTT and 0.1 mM sodium orthovanadate). Reaction mixture (50 μL) containing 10 ng of CK1δ ΔC purified protein in the kinase buffer including 10 mM MgCl₂ and 200 μM ATP was added onto each well and the plate was incubated at 30 °C for 1 hour. Next, the reaction mixture was removed and the wells were washed with three times with wash buffer and incubated with blocking buffer (PBS-T with 5% BSA) for 1 hour at room temperature. Subsequently, wells were incubated with pS659 Ab, anti-

rabbit antibody conjugated to Biotin and Streptavidin-HRP for 1 hour at room temperature with a washing step after each incubation as above. For signal detection, TMB (1-Step Ultra TMB-ELISA, Thermo Scientific) was added, incubated for color development at room temperature and stopped with the addition of STOP solution (Thermo Scientific). The plate was read at 450 nm using an xMark Spectrophotometer plate reader (Biorad). Results shown are from four independent assays.

NMR-based kinase assay

NMR spectra were collected on a Varian INOVA 600 MHz or a Bruker 800 MHz spectrometer equipped with a ^1H , ^{13}C , ^{15}N triple resonance z-axis pulsed-field-gradient cryoprobe. Spectra were processed using NMRPipe [88] and analyzed using CCPNmr Analysis [89]. Backbone assignments were obtained previously for the mouse FASP (BMRB entry: 27306) [20]. NMR kinase reactions were performed at 30 °C with 0.2 mM ^{15}N -mouse FASP and/or Degron, 2.5 mM ATP and 1 μM CK1 δ ΔC (WT or *tau*). SOFAST HMQC spectra (total data acquisition = 6 min) were collected at the indicated intervals for 3 hours and relative peak volumes were calculated and normalized as described previously [20]. Data analysis was performed using Prism (GraphPad), with data fit to either a one-phase exponential or linear regression.

ADP-Glo kinase assay

Kinase reactions were performed on the indicated peptides (Degron or extended FASP) using the ADP-Glo kinase assay kit (Promega) according to manufacturer's instructions. All reactions were performed in 30 μ L volumes using 1x kinase buffer (25 mM Tris pH 7.5, 100 mM NaCl, 10 mM MgCl₂, and 2 mM TCEP) supplemented with ATP and PER2 substrate peptides as indicated. To determine the apparent 2nd-order rate constants, triplicate reactions containing 10 μ M substrate, 100 μ M ATP, and 0.2 μ M CK1 δ Δ C kinase were incubated in 1x kinase buffer at room temperature for 3 hours (and repeated for n = 3 independent assays). Linearity of the reaction rate with respect to time was determined by performing larger reactions (50 μ L) with wild-type and *tau* CK1 δ Δ C and either the FASP or Degron substrate; 5 μ L aliquots were taken and quenched with ADP-Glo reagent at discrete time points up to 3 hours (data not shown). Luminescence measurements were taken at room temperature with a SYNERGY2 microplate reader in 384-well microplates. Data analysis was performed using Excel (Microsoft) or Prism (GraphPad).

Statistical analyses

All statistical analyses were done using Prism (GraphPad). p-values were calculated using unpaired two-tailed Students t-tests. In all figures, * indicates p<0.05, ** p<0.01, *** p<0.001, **** p<0.0001; ns, not significant.

Crystallization and structure determination

Crystallization was performed by hanging-drop vapor-diffusion method at 22 °C by mixing an equal volume of CK1δ ΔC with reservoir solution. The reservoir solution for CK1δ ΔC *tau* (R178C) (8.5 mg/mL) was 50 mM sodium acetate pH 6.0, 300 mM ammonium sulfate, and 17.5% (vol/vol) PEG 2000. The reservoir solution for crystallizing CK1δ ΔC wild-type (8 mg/mL) without sulfate was 150 mM succinic acid pH 5.5 and 17% (vol/vol) PEG 3350. The reservoir solution for CK1δ ΔC K171E (7.7 mg/mL) was 50 mM sodium acetate pH 6.0, 350 mM ammonium sulfate, and 17.5% (vol/vol) PEG 3500. The crystals were looped and briefly soaked in a drop of reservoir solution and then flash-cooled in liquid nitrogen for X-ray diffraction data collection. For CK1δ ΔC *tau*, a cryopreservant of reservoir solution with 20% (vol/vol) glycerol was used. Data sets were collected at the APS beamline 23-ID-D, and the ALS beamline 8.3.1. Data were indexed, integrated and merged using the CCP4 software suite [90]. Structures were determined by molecular replacement with Phaser MR [91] using the ADP-bound structure of wild-type CK1δ ΔC (PDB: 5X17). Model building was performed with Coot [92] and structure refinement was performed with PHENIX [93]. All structural models and alignments were generated using PyMOL Molecular Graphics System 2.0 (Schrödinger).

Molecular dynamics

Initial structures: To simulate *tau* CK1 δ , we used the crystallographic structure reported herein (PDB: 6PXN), using chain A to simulate the ‘loop up’ conformation and chain B to simulate the ‘loop down’ conformation. As starting structures for the WT CK1 δ simulations, we selected an apo structure (PDB: 1CKJ) of 2.46Å resolution, which has the activation loop crystallized both in ‘up’ (chain A) and ‘down’ (chain B) conformations [35]. This structure contained two (chain A) or three (chain B) WO_4^{2-} anions, which were computationally replaced by SO_4^{2-} anions at the same positions, to make the simulations of WT CK1 δ more comparable to the *tau* simulations. The initial backbone conformation of loop L-EF was similar in all of the structures used as starting points for the MD simulations with a backbone RMSD for residues 210 to 230 of < 3.7Å between initial structures. Using these structures, we created the systems to be simulated, described in Supplemental 2.4.

| System | Activation loop conformation | Presence of SO_4^{2-} ions | | | Chain | PDB |
|--|------------------------------|-------------------------------------|--------|--------|-------|------|
| | | Site 1 | Site 2 | Site 3 | | |
| WT CK1 $\delta^{\text{loop down}}$ | Down | Yes | Yes | Yes | B | 1CKJ |
| WT CK1 $\delta^{\text{loop up}}$ | Up | Yes | No | Yes | A | 1CKJ |
| <i>tau</i> CK1 $\delta^{\text{loop down}}$ | Down | No | Yes | Yes | B | 6PXN |
| <i>tau</i> CK1 $\delta^{\text{loop up}}$ | Up | No | No | Yes | A | 6PXN |
| WT CK1 $\delta^{\text{loop down}}_{\text{-anion}}$ | Down | Yes | No* | Yes | B | 1CKJ |
| <i>tau</i> CK1 $\delta^{\text{loop down}}_{\text{-anion}}$ | Down | No | No* | Yes | B | 6PXN |
| The nomenclature of the anion binding sites is defined in Figure S4. | | | | | | |
| * SO_4^{2-} ions were computationally removed | | | | | | |

Systems set up and equilibration: The systems described in Table 2.4 were refined by (i) position restrained energy minimization followed by (ii) full energy minimization, using Maestro (Schrödinger). The protonation states of the minimized models were estimated using the H++ server [94] and hydrogens were added using pdb2pqr [95].

All systems were solvated in a pre-equilibrated cubic TIP3P [96] water box with at least 15 Å between the protein and the box boundaries. The net charge of the system was neutralized with Na⁺ or Cl⁻ counterions. Parameters for protein atoms and counterions were extracted from the ff14SB forcefield [97], while parameters for the SO₄²⁻ anions were extracted from the Generalized Amber Force Field (GAFF) [98] and adjusted as proposed by [99].

Minimization and equilibration were performed with AMBER 16 [100], using the following protocol: (i) 2000 steps of energy minimization with a 500 kcal mol⁻¹ Å⁻¹ position restraint on protein and SO₄²⁻ anions; (ii) 1000 steps of energy minimization with a 500 kcal mol⁻¹ Å⁻¹ position restraint on protein atoms only; (iii) 2000 steps of energy minimization without position restraints; (iv) 50 ps of NVT simulation, with gradual heating to a final temperature of 300 K, with 10 kcal mol⁻¹ Å⁻¹ position restraint on protein and SO₄²⁻ anions; (v) 1 ns of NPT simulation to equilibrate the density (or final volume of the simulation box).

Conventional (cMD) and Gaussian Accelerated MD (GaMD) simulations

Before running the GaMD simulations, we ran 100 ns of conventional MD simulations for each system, using AMBER 16 [100]. These simulations were performed in the NVT regime, with a time step of 2 fs, and all bonds involving hydrogen atoms were restrained with SHAKE [101]. The PME method [102] was used to calculate electrostatic interaction using periodic boundary conditions, and a 12 Å cutoff was used to truncate non-bonded short-range interactions.

The final conformations produced by the cMD simulations were used as starting configurations for the GaMD simulations, which were performed with AMBER 17 [103]. For these simulations, additional acceleration parameters were used to boost the exploration of the conformational space, as described in [50]. All systems had a threshold energy $E = V_{\max}$ and were subjected to a dual boost acceleration of both the dihedral and the total potential energies. To optimize the acceleration parameters we first ran 2 ns of MD simulations with no boost potential, during which the minimum, maximum, average and standard deviation (V_{\min} , V_{\max} , V_{av} , σ_{avg}) of the total potential and dihedral energies were estimated and used to derive boost potentials as detailed in [50]. These potentials were used to start 50 ns of Gaussian accelerated MD simulations, during which the boost statistics and boost potentials were updated until the maximum acceleration was achieved. The maximum

acceleration was constrained setting the upper limit of the standard deviation of the total boost potential to be 6 kcal/mol.

We ran 5 replicas of production GaMD simulations for each system with fixed acceleration parameters derived from the previous equilibration stage. Each replica started from the same initial conformation, but the atoms were given different initial velocities, consistent with a Maxwell-Boltzmann distribution at 300 K. Each production simulation ran for 500 ns, totalizing 2.5 μ s of sampling for each system, and 15 μ s in total.

Analysis of GaMD simulations

Conformational dynamics of loops: The RMSD of the activation loop (Figure 2.4A-D) or loop L-EF (Figure 2.4E-H) was measured throughout the GaMD trajectories with CPPTRAJ using the *rms* module [104].

Volumetric analysis of the substrate binding cleft: The volume and shape of the substrate binding cleft and adjacent anion binding sites were obtained from the GaMD trajectories using POVME 3.0 [51]. For each trajectory, conformations of WT or *tau* CK1 δ were extracted every 2 ns, stripping all water molecules, counter-ions and sulfate anions. All protein conformations were superimposed to the same reference frame and the substrate binding cleft and adjacent anion binding sites were encompassed by three overlapping spheres as shown in Supplemental Figure 2.4G. POVME was then used to estimate the free (or empty) volume within the three overlapping spheres for all

conformations extracted from the GaMD trajectories. The resulting volumes were averaged to produce three-dimensional density maps, as showed in Figure 2.4 (panels I-L). The maps in Figure 2.4 were contoured at 0.10 and represent regions that are found more frequently ‘open’ during the simulations.

Principal Modes of Motion: To detect the principal modes of motion displayed by WT and *tau* CK1 δ , we used atomic fluctuations sampled during the GaMD simulations to perform Principal Component Analysis (PCA) [105, 106]. Before performing PCA, we stripped the trajectories of all solvent, ions and protein side-chains, keeping the backbone atoms only. We then concatenated and aligned these new trajectories to the same reference frame. To construct and diagonalize the co-variance matrix of atomic fluctuations, we used the *matrix* and *analyze* modules, respectively, in CPPTRAJ [104]. For each system (WT CK1 $\delta^{\text{loop down}}$, WT CK1 $\delta^{\text{loop up}}$, *tau* CK1 $\delta^{\text{loop down}}$, *tau* CK1 $\delta^{\text{loop up}}$), we projected their respective trajectories into the obtained eigenvector space using the *projection* function in CPPTRAJ [104]. The projections of each system along the subset of the eigenvector space formed by the 1st and 2nd principal components are shown in Figures 5 and S5.

All visualization of the GaMD simulations was performed with VMD [107].

References

1. Bass, J. and M.A. Lazar, *Circadian time signatures of fitness and disease*. Science, 2016. **354**(6315): p. 994-999.
2. Aryal, R.P., et al., *Macromolecular Assemblies of the Mammalian Circadian Clock*. Mol Cell, 2017. **67**(5): p. 770-782 e6.
3. Michael, A.K., et al., *Formation of a repressive complex in the mammalian circadian clock is mediated by the secondary pocket of CRY1*. Proc Natl Acad Sci U S A, 2017. **114**(7): p. 1560-1565.
4. Xu, H., et al., *Cryptochrome 1 regulates the circadian clock through dynamic interactions with the BMAL1 C terminus*. Nat Struct Mol Biol, 2015. **22**(6): p. 476-84.
5. Lee, Y., et al., *Stoichiometric relationship among clock proteins determines robustness of circadian rhythms*. J Biol Chem, 2011. **286**(9): p. 7033-42.
6. Kojima, S., D.L. Shingle, and C.B. Green, *Post-transcriptional control of circadian rhythms*. J Cell Sci, 2011. **124**(Pt 3): p. 311-20.
7. Takahashi, J.S., *Transcriptional architecture of the mammalian circadian clock*. Nat Rev Genet, 2017. **18**(3): p. 164-179.
8. Hirano, A., Y.H. Fu, and L.J. Ptacek, *The intricate dance of post-translational modifications in the rhythm of life*. Nat Struct Mol Biol, 2016. **23**(12): p. 1053-1060.
9. Lee, C., et al., *Posttranslational mechanisms regulate the mammalian circadian clock*. Cell, 2001. **107**(7): p. 855-67.
10. Eide, E.J., et al., *Control of mammalian circadian rhythm by CKepsilon-regulated proteasome-mediated PER2 degradation*. Mol Cell Biol, 2005. **25**(7): p. 2795-807.
11. Lee, C., D.R. Weaver, and S.M. Reppert, *Direct association between mouse PERIOD and CKepsilon is critical for a functioning circadian clock*. Mol Cell Biol, 2004. **24**(2): p. 584-94.

12. Lowrey, P.L., et al., *Positional syntenic cloning and functional characterization of the mammalian circadian mutation tau*. Science, 2000. **288**(5465): p. 483-92.
13. Toh, K.L., et al., *An hPer2 phosphorylation site mutation in familial advanced sleep phase syndrome*. Science, 2001. **291**(5506): p. 1040-3.
14. Xu, Y., et al., *Functional consequences of a CKIdelta mutation causing familial advanced sleep phase syndrome*. Nature, 2005. **434**(7033): p. 640-4.
15. Xu, Y., et al., *Modeling of a human circadian mutation yields insights into clock regulation by PER2*. Cell, 2007. **128**(1): p. 59-70.
16. Jones, C.R., et al., *Genetic basis of human circadian rhythm disorders*. Exp Neurol, 2013. **243**: p. 28-33.
17. Masuda, S., et al., *Mutation of a PER2 phosphodegron perturbs the circadian phosphoswitch*. bioRxiv, 2019.
18. Zhou, M., et al., *A Period2 Phosphoswitch Regulates and Temperature Compensates Circadian Period*. Mol Cell, 2015. **60**(1): p. 77-88.
19. Vanselow, K., et al., *Differential effects of PER2 phosphorylation: molecular basis for the human familial advanced sleep phase syndrome (FASPS)*. Genes Dev, 2006. **20**(19): p. 2660-72.
20. Narasimamurthy, R., et al., *CK1delta/epsilon protein kinase primes the PER2 circadian phosphoswitch*. Proc Natl Acad Sci U S A, 2018. **115**(23): p. 5986-5991.
21. Reischl, S., et al., *Beta-TrCP1-mediated degradation of PERIOD2 is essential for circadian dynamics*. J Biol Rhythms, 2007. **22**(5): p. 375-86.
22. Chen, R., et al., *Rhythmic PER abundance defines a critical nodal point for negative feedback within the circadian clock mechanism*. Mol Cell, 2009. **36**(3): p. 417-30.

23. Gori, M., et al., *A PEST-like element in FREQUENCY determines the length of the circadian period in Neurospora crassa*. EMBO J, 2001. **20**(24): p. 7074-84.
24. Kloss, B., et al., *The Drosophila clock gene double-time encodes a protein closely related to human casein kinase Iepsilon*. Cell, 1998. **94**(1): p. 97-107.
25. van Ooijen, G., et al., *Functional analysis of Casein Kinase 1 in a minimal circadian system*. PLoS One, 2013. **8**(7): p. e70021.
26. Flotow, H., et al., *Phosphate groups as substrate determinants for casein kinase I action*. J Biol Chem, 1990. **265**(24): p. 14264-9.
27. Venerando, A., M. Ruzzene, and L.A. Pinna, *Casein kinase: the triple meaning of a misnomer*. Biochem J, 2014. **460**(2): p. 141-56.
28. Isojima, Y., et al., *CKIepsilon/delta-dependent phosphorylation is a temperature-insensitive, period-determining process in the mammalian circadian clock*. Proc Natl Acad Sci U S A, 2009. **106**(37): p. 15744-9.
29. Marin, O., F. Meggio, and L.A. Pinna, *Design and synthesis of two new peptide substrates for the specific and sensitive monitoring of casein kinases-1 and -2*. Biochem Biophys Res Commun, 1994. **198**(3): p. 898-905.
30. Shinohara, Y., et al., *Temperature-Sensitive Substrate and Product Binding Underlie Temperature-Compensated Phosphorylation in the Clock*. Mol Cell, 2017. **67**(5): p. 783-798 e20.
31. Kivimae, S., L. Saez, and M.W. Young, *Activating PER repressor through a DBT-directed phosphorylation switch*. PLoS Biol, 2008. **6**(7): p. e183.
32. Venkatesan, A., et al., *The Circadian tau Mutation in Casein Kinase 1 Is Part of a Larger Domain That Can Be Mutated to Shorten Circadian Period*. Int J Mol Sci, 2019. **20**(4).

33. Ralph, M.R. and M. Menaker, *A mutation of the circadian system in golden hamsters*. Science, 1988. **241**(4870): p. 1225-7.
34. Gallego, M., et al., *An opposite role for tau in circadian rhythms revealed by mathematical modeling*. Proc Natl Acad Sci U S A, 2006. **103**(28): p. 10618-23.
35. Longenecker, K.L., P.J. Roach, and T.D. Hurley, *Three-dimensional structure of mammalian casein kinase I: molecular basis for phosphate recognition*. J Mol Biol, 1996. **257**(3): p. 618-31.
36. Zeringo, N.A. and J.J. Bellizzi, 3rd, *A PER2-derived mechanism-based bisubstrate analog for casein kinase 1epsilon*. Chem Biol Drug Des, 2014. **84**(6): p. 697-703.
37. Theillet, F.X., et al., *Site-specific NMR mapping and time-resolved monitoring of serine and threonine phosphorylation in reconstituted kinase reactions and mammalian cell extracts*. Nat Protoc, 2013. **8**(7): p. 1416-32.
38. Nolen, B., S. Taylor, and G. Ghosh, *Regulation of protein kinases; controlling activity through activation segment conformation*. Mol Cell, 2004. **15**(5): p. 661-75.
39. Goldsmith, E.J., et al., *Substrate and docking interactions in serine/threonine protein kinases*. Chem Rev, 2007. **107**(11): p. 5065-81.
40. Johnson, L.N., M.E. Noble, and D.J. Owen, *Active and inactive protein kinases: structural basis for regulation*. Cell, 1996. **85**(2): p. 149-58.
41. Graves, P.R. and P.J. Roach, *Role of COOH-terminal phosphorylation in the regulation of casein kinase I delta*. J Biol Chem, 1995. **270**(37): p. 21689-94.
42. Rivers, A., et al., *Regulation of casein kinase I epsilon and casein kinase I delta by an in vivo futile phosphorylation cycle*. J Biol Chem, 1998. **273**(26): p. 15980-4.

43. Fustin, J.M., et al., *Two Ck1delta transcripts regulated by m6A methylation code for two antagonistic kinases in the control of the circadian clock*. Proc Natl Acad Sci U S A, 2018. **115**(23): p. 5980-5985.
44. Kawakami, F., K. Suzuki, and K. Ohtsuki, *A novel consensus phosphorylation motif in sulfatide- and cholesterol-3-sulfate-binding protein substrates for CK1 in vitro*. Biol Pharm Bull, 2008. **31**(2): p. 193-200.
45. Gibbs, C.S. and M.J. Zoller, *Rational scanning mutagenesis of a protein kinase identifies functional regions involved in catalysis and substrate interactions*. J Biol Chem, 1991. **266**(14): p. 8923-31.
46. Leon, B.C., I. Tsigelny, and J.A. Adams, *Electrostatic environment surrounding the activation loop phosphotyrosine in the oncoprotein v-Fps*. Biochemistry, 2001. **40**(34): p. 10078-86.
47. Skamnaki, V.T., et al., *Catalytic mechanism of phosphorylase kinase probed by mutational studies*. Biochemistry, 1999. **38**(44): p. 14718-30.
48. Long, A.M., H. Zhao, and X. Huang, *Structural basis for the potent and selective inhibition of casein kinase 1 epsilon*. J Med Chem, 2012. **55**(22): p. 10307-11.
49. Minzel, W., et al., *Small Molecules Co-targeting CKIalpha and the Transcriptional Kinases CDK7/9 Control AML in Preclinical Models*. Cell, 2018. **175**(1): p. 171-185 e25.
50. Miao, Y., V.A. Feher, and J.A. McCammon, *Gaussian Accelerated Molecular Dynamics: Unconstrained Enhanced Sampling and Free Energy Calculation*. J Chem Theory Comput, 2015. **11**(8): p. 3584-3595.
51. Wagner, J.R., et al., *POVME 3.0: Software for Mapping Binding Pocket Flexibility*. J Chem Theory Comput, 2017. **13**(9): p. 4584-4592.
52. McClendon, C.L., et al., *Dynamic architecture of a protein kinase*. Proc Natl Acad Sci U S A, 2014. **111**(43): p. E4623-31.

53. Rothenfluh, A., M. Abodeely, and M.W. Young, *Short-period mutations of per affect a double-time-dependent step in the Drosophila circadian clock*. *Curr Biol*, 2000. **10**(21): p. 1399-402.
54. Suri, V., J.C. Hall, and M. Rosbash, *Two novel doubletime mutants alter circadian properties and eliminate the delay between RNA and protein in Drosophila*. *J Neurosci*, 2000. **20**(20): p. 7547-55.
55. Taylor, S.S. and A.P. Kornev, *Protein kinases: evolution of dynamic regulatory proteins*. *Trends Biochem Sci*, 2011. **36**(2): p. 65-77.
56. Zilian, O., et al., *double-time is identical to discs overgrown, which is required for cell survival, proliferation and growth arrest in Drosophila imaginal discs*. *Development*, 1999. **126**(23): p. 5409-20.
57. Chiu, J.C., et al., *The phospho-occupancy of an atypical SLIMB-binding site on PERIOD that is phosphorylated by DOUBLETIME controls the pace of the clock*. *Genes Dev*, 2008. **22**(13): p. 1758-72.
58. Top, D., et al., *CK1/Doubletime activity delays transcription activation in the circadian clock*. *Elife*, 2018. **7**.
59. Fan, J.Y., et al., *Drosophila and vertebrate casein kinase Idelta exhibits evolutionary conservation of circadian function*. *Genetics*, 2009. **181**(1): p. 139-52.
60. Reppert, S.M., P.A. Guerra, and C. Merlin, *Neurobiology of Monarch Butterfly Migration*. *Annu Rev Entomol*, 2016. **61**: p. 25-42.
61. Price, J.L., et al., *double-time is a novel Drosophila clock gene that regulates PERIOD protein accumulation*. *Cell*, 1998. **94**(1): p. 83-95.
62. Zantke, J., et al., *Circadian and circalunar clock interactions in a marine annelid*. *Cell Rep*, 2013. **5**(1): p. 99-113.
63. Zhang, L., et al., *Dissociation of circadian and circatidal timekeeping in the marine crustacean Eurydice pulchra*. *Curr Biol*, 2013. **23**(19): p. 1863-73.

64. Beale, A.D., et al., *Casein Kinase 1 Underlies Temperature Compensation of Circadian Rhythms in Human Red Blood Cells*. J Biol Rhythms, 2019. **34**(2): p. 144-153.
65. Meng, Q.J., et al., *Setting clock speed in mammals: the CK1 epsilon tau mutation in mice accelerates circadian pacemakers by selectively destabilizing PERIOD proteins*. Neuron, 2008. **58**(1): p. 78-88.
66. Smadja Storz, S., et al., *Casein kinase 1delta activity: a key element in the zebrafish circadian timing system*. PLoS One, 2013. **8**(1): p. e54189.
67. Oren, M., et al., *Profiling molecular and behavioral circadian rhythms in the non-symbiotic sea anemone Nematostella vectensis*. Sci Rep, 2015. **5**: p. 11418.
68. Matsuzaki, M., et al., *Genome sequence of the ultrasmall unicellular red alga Cyanidioschyzon merolae 10D*. Nature, 2004. **428**(6983): p. 653-7.
69. Poliner, E., et al., *Identification of circadian rhythms in Nannochloropsis species using bioluminescence reporter lines*. Plant J, 2019. **99**(1): p. 112-127.
70. Uehara, T.N., et al., *Casein kinase 1 family regulates PRR5 and TOC1 in the Arabidopsis circadian clock*. Proc Natl Acad Sci U S A, 2019. **116**(23): p. 11528-11536.
71. Boesger, J., et al., *Application of phosphoproteomics to find targets of casein kinase 1 in the flagellum of chlamydomonas*. Int J Plant Genomics, 2012. **2012**: p. 581460.
72. Boesger, J., et al., *Comparative phosphoproteomics to identify targets of the clock-relevant casein kinase 1 in C. reinhardtii Flagella*. Methods Mol Biol, 2014. **1158**: p. 187-202.
73. Kornev, A.P. and S.S. Taylor, *Dynamics-Driven Allostery in Protein Kinases*. Trends Biochem Sci, 2015. **40**(11): p. 628-647.

74. Eng, G.W.L., Edison, and D.M. Virshup, *Site-specific phosphorylation of casein kinase 1 delta (CK1delta) regulates its activity towards the circadian regulator PER2*. PLoS One, 2017. **12**(5): p. e0177834.
75. Balsalobre, A., L. Marcacci, and U. Schibler, *Multiple signaling pathways elicit circadian gene expression in cultured Rat-1 fibroblasts*. Curr Biol, 2000. **10**(20): p. 1291-4.
76. Zylka, M.J., et al., *Three period homologs in mammals: differential light responses in the suprachiasmatic circadian clock and oscillating transcripts outside of brain*. Neuron, 1998. **20**(6): p. 1103-10.
77. Kim, J.K. and D.B. Forger, *A mechanism for robust circadian timekeeping via stoichiometric balance*. Mol Syst Biol, 2012. **8**: p. 630.
78. Yu, W., et al., *PER-dependent rhythms in CLK phosphorylation and E-box binding regulate circadian transcription*. Genes Dev, 2006. **20**(6): p. 723-33.
79. Lee, H.M., et al., *The period of the circadian oscillator is primarily determined by the balance between casein kinase 1 and protein phosphatase 1*. Proc Natl Acad Sci U S A, 2011. **108**(39): p. 16451-6.
80. Hayasaka, N., et al., *Salt-inducible kinase 3 regulates the mammalian circadian clock by destabilizing PER2 protein*. Elife, 2017. **6**.
81. Hirota, T. and S.A. Kay, *High-throughput screening and chemical biology: new approaches for understanding circadian clock mechanisms*. Chem Biol, 2009. **16**(9): p. 921-7.
82. Oshima, T., et al., *Cell-based screen identifies a new potent and highly selective CK2 inhibitor for modulation of circadian rhythms and cancer cell growth*. Sci Adv, 2019. **5**(1): p. eaau9060.
83. Marin, O., et al., *A noncanonical sequence phosphorylated by casein kinase 1 in beta-catenin may play a role in casein kinase 1 targeting of important signaling proteins*. Proc Natl Acad Sci U S A, 2003. **100**(18): p. 10193-200.

84. Knippschild, U., et al., *p53 is phosphorylated in vitro and in vivo by the delta and epsilon isoforms of casein kinase 1 and enhances the level of casein kinase 1 delta in response to topoisomerase-directed drugs*. *Oncogene*, 1997. **15**(14): p. 1727-36.
85. Penas, C., et al., *Casein kinase 1delta is an APC/C(Cdh1) substrate that regulates cerebellar granule cell neurogenesis*. *Cell Rep*, 2015. **11**(2): p. 249-60.
86. Abe, J., et al., *Circadian rhythms. Atomic-scale origins of slowness in the cyanobacterial circadian clock*. *Science*, 2015. **349**(6245): p. 312-6.
87. Sheffield, P., S. Garrard, and Z. Derewenda, *Overcoming expression and purification problems of RhoGDI using a family of "parallel" expression vectors*. *Protein Expr Purif*, 1999. **15**(1): p. 34-9.
88. Delaglio, F., et al., *NMRPipe: a multidimensional spectral processing system based on UNIX pipes*. *J Biomol NMR*, 1995. **6**(3): p. 277-93.
89. Vranken, W.F., et al., *The CCPN data model for NMR spectroscopy: development of a software pipeline*. *Proteins*, 2005. **59**(4): p. 687-96.
90. Winn, M.D., et al., *Overview of the CCP4 suite and current developments*. *Acta Crystallogr D Biol Crystallogr*, 2011. **67**(Pt 4): p. 235-42.
91. McCoy, A.J., et al., *Phaser crystallographic software*. *J Appl Crystallogr*, 2007. **40**(Pt 4): p. 658-674.
92. Emsley, P., et al., *Features and development of Coot*. *Acta Crystallogr D Biol Crystallogr*, 2010. **66**(Pt 4): p. 486-501.
93. Adams, P.D., et al., *The Phenix software for automated determination of macromolecular structures*. *Methods*, 2011. **55**(1): p. 94-106.
94. Anandakrishnan, R., B. Aguilar, and A.V. Onufriev, *H++ 3.0: automating pK prediction and the preparation of biomolecular structures for atomistic molecular modeling and simulations*. *Nucleic Acids Res*, 2012. **40**(Web Server issue): p. W537-41.

95. Dolinsky, T.J., et al., *PDB2PQR: expanding and upgrading automated preparation of biomolecular structures for molecular simulations*. Nucleic Acids Res, 2007. **35**(Web Server issue): p. W522-5.
96. Jorgensen, W.L., et al., *Comparison of simple potential functions for simulation liquid water*. J Phys Chem B, 1983. **79**: p. 926.
97. Maier, J.A., et al., *ff14SB: Improving the Accuracy of Protein Side Chain and Backbone Parameters from ff99SB*. J Chem Theory Comput, 2015. **11**(8): p. 3696-713.
98. Wang, J., et al., *Development and testing of a general amber force field*. J Comput Chem, 2004. **25**(9): p. 1157-74.
99. Kashefolgheta, S. and A. Vila Verde, *Developing force fields when experimental data is sparse: AMBER/GAFF-compatible parameters for inorganic and alkyl oxoanions*. Phys Chem Chem Phys, 2017. **19**: p. 20593-20607.
100. Case, D.A., et al., *AMBER 16*. 2016, University of California, San Francisco.
101. Rykckaertr, J.P., G. Ciccotti, and H.J.C. Berendsen, *Numerical integration of the Cartesian equations of motion of a system with constraints: molecular dynamics of n-alkanes*. J Comput Phys, 1977. **23**: p. 327-341.
102. Darden, T., D.M. York, and L. Pedersen, *Particle mesh Ewald: An $N\log(N)$ method for Ewald sums in large systems*. Chem Phys, 1993. **98**: p. 10089-10092.
103. Case, D.A., et al., *AMBER 17*. 2017: University of California, San Francisco.
104. Roe, D.R. and T.E. Cheetham, *J. PTAJ and CPPTAJ: Software for processing and analysis of molecular dynamics trajectory data*. Theory Comput, 2013. **9**: p. 3084-3095.

105. Amadei, A., A.B. Linssen, and H.J. Berendsen, *Essential dynamics of proteins*. Proteins, 1993. **17**(4): p. 412-25.
106. Amadei, A., et al., *An efficient method for sampling the essential subspace of proteins*. J Biomol Struct Dyn, 1996. **13**(4): p. 615-25.
107. Humphrey, W., A. Dalke, and K. Schulten, *VMD: visual molecular dynamics*. J Mol Graph, 1996. **14**(1): p. 33-8, 27-8.

CHAPTER 3

PERIOD phosphorylation leads to feedback inhibition of CK1 activity to control circadian period

Acknowledgments

Philpott JM, Freeberg AM, Park J, Lee K, Ricci CG, Hunt SR, Narasimamurthy R, Segal DH, Robles R, Cai YD, Tripathi S, McCammon AJ, Virshup DM, Chiu JC, Lee C, Partch CL. *PERIOD phosphorylation leads to feedback inhibition of CK1 activity to control circadian period*. bioRxiv, 2022: p. 2022.06.24.497549.

The following co-authors are acknowledged for their contributions to the published work: JMP, AMF, JP, KL, CGR, SRH, RN, DHS, RR, and YDC provided investigation. JMP, JP, KL, CGR, RN and YDC provided formal analysis. JMP, CGR, DMV, JCC, CL and CLP provided conceptualization. JMP, CGR, JK and KL provided visualization. JMP, AMF and ST provided validation. AJM, DMV, JCC, CL and CLP provided funding acquisition, supervision, and project administration.

3.1 Summary

PERIOD (PER) and Casein Kinase 1 δ regulate circadian rhythms through a phosphoswitch that controls PER stability and repressive activity in the molecular clock. CK1 δ phosphorylation of the Familial Advanced Sleep Phase (FASP) serine cluster embedded within the Casein Kinase 1 binding domain (CK1BD) of mammalian PER1/2 inhibits its activity on phosphodegrons to stabilize PER and extend circadian period. Here, we show that the phosphorylated FASP region (pFASP) of PER2 directly interacts with and inhibits CK1 δ . Co-crystal structures in conjunction with accelerated molecular dynamics simulations reveal how pFASP phosphoserines dock into conserved anion binding sites near the active site of CK1 δ . Limiting phosphorylation of the FASP serine cluster reduces product inhibition, decreasing PER2 stability and shortening circadian period in human cells. We found that *Drosophila* PER also regulates CK1 δ via feedback inhibition through the phosphorylated dPER-Short domain, revealing a conserved mechanism by which PER phosphorylation near the CK1BD regulates CK1 kinase activity.

3.2 Introduction

The mammalian circadian clock is driven by a set of interlocked transcription-translation feedback loops (TTFLs) [1]. The core feedback loop is driven by the heterodimeric transcription factor, CLOCK:BMAL1, that promotes the transcription of multiple clock-controlled genes including its own repressors, Period (PER) and Cryptochrome (CRY) [2]. PER proteins nucleate formation of a complex with CRYs and the clock-associated kinase, Casein Kinase 1 δ/ϵ (CK1) [3-5] that ultimately bind to and inhibit CLOCK:BMAL1 activity [6], so the relative abundance of PER proteins is tightly regulated [7, 8] by transcriptional, post-transcriptional, and post-translational mechanisms [9]. The abundance of PER proteins is critical, as constitutive overexpression of PER proteins disrupts circadian rhythms [8] while the inducible regulation of PER expression on a daily basis can establish circadian rhythms *de novo* with tunable periods [10].

The post-translational control of PER stability by its cognate kinase, CK1, has been widely studied. CK1 remains stably bound, or anchored, to PER1 and PER2 throughout the circadian cycle [3, 4] via a conserved Casein Kinase 1 Binding Domain (CK1BD) [11, 12]. CK1 regulates PER2 stability through a phosphoswitch mechanism, whereby the anchored kinase phosphorylates antagonistic sites on PER2 that, on balance, control its stability [13]. CK1 phosphorylation of a Degron located several hundred residues upstream of the CK1BD, near the tandem PAS domains of PER2, leads to recruitment of the E3 ubiquitin ligase, β -TrCP, and subsequent proteasomal

degradation [11, 14-16]. Activity at this PAS-Degron is counteracted somehow by CK1-dependent phosphorylation of a multiserine cluster within the CK1BD known as the FASP region. This region is named for a Ser to Gly polymorphism in human *Per2* (S662G) that disrupts CK1 activity at this cluster [17], destabilizing PER2 and shortening circadian period, leading to Familial Advanced Sleep Phase Syndrome [18] that impacts the timing of sleep onset in humans [19]. Mutations in CK1 can also alter the balance of its activity on these two regions to significantly shorten circadian period *in vivo* [20-22].

Similar to the FASP region of mammalian PER1/2, phosphorylation of the PER-Short domain of *Drosophila* PER (dPER) by DOUBLETIME (DBT, the *Drosophila* homolog of CK1 δ/ϵ) and NEMO/NLK attenuates DBT-dependent phosphorylation at an N-terminal Degron to stabilize dPER and regulate circadian period [23, 24]. In particular, DBT-dependent phosphorylation of S589, the site of the classic *per^S* mutation (S589N) within the PER-Short domain [25], stabilizes PER in its inhibition-active form while mutation of this residue is sufficient to destabilize PER and shorten circadian period [26]. Phosphorylation of S596 by the NEMO/NLK kinase is required for DBT-dependent phosphorylation of nearby sites within the PER-Short domain, including S589, suggesting a hierarchical phosphorylation program that acts as a time-delay in the regulation of dPER abundance and repressive activity [23].

In this study, we discovered how CK1 phosphorylation of the stabilizing FASP or PER-Short domains leads to feedback inhibition of the kinase. First,

we found that multisite phosphorylation of the human PER2 FASP region is gated by rate-limiting phosphorylation of the first of five sequential serines in the FASP cluster by CK1. After this slow priming, CK1 rapidly phosphorylates the remaining serines in the FASP cluster following an ordered-distributive kinetic mechanism. Phosphorylation of C-terminal sites within the FASP region leads to product inhibition of CK1, reducing the overall rate of priming phosphorylation. Consistent with this, we show that phosphorylated FASP (pFASP) peptides inhibit CK1 activity on the PAS-Degron *in vitro*. Crystal structures and molecular dynamics simulations of the pFASP-bound kinase reveal the mechanism of product inhibition, driven by the interaction between pFASP and highly conserved anion binding sites on CK1. Leveraging newly developed U2OS *PER1^{Luc}* and *PER2^{Luc}* reporter cell lines [27], we used CRISPR-generated indels to disrupt phosphorylation within the FASP region of *Per1* or *Per2*, observing shorter circadian periods and demonstrating conservation of the pFASP phosphoswitch in PER1 and PER2. Likewise, we discovered that phosphorylation of the PER-Short domain of *Drosophila* PER, located just upstream of the CK1BD, also inhibits CK1 activity *in vitro*. A structure of CK1 bound to a PER-Short domain phosphopeptide reveals a similar mechanism of product inhibition. Taken together, these results establish a conserved mechanism by which CK1 activity is regulated by feedback inhibition of PER to control PER stability and kinase activity within the molecular clock.

3.3 Results

3.3.1 CK1 phosphorylates the serine cluster in the PER2 FASP region in a sequential manner

The FASP region is an intrinsically disordered stretch of ~50 highly conserved residues embedded within the CK1BD of PER1 and PER2 that contains a cluster of 5 serine residues with the repeated spacing of SxxS (**Figure 3.1a**). We previously showed that CK1 is necessary and sufficient to initiate phosphorylation of the FASP region in mouse PER2 by targeting the first serine within this cluster in a rate-limiting step known as priming [17]. We sought to extend this analysis to study the mechanism of multisite phosphorylation within the intact human PER2 FASP region using an NMR-based kinase assay that provides site-specific resolution of kinase activity on an ^{15}N -labeled peptide substrate [17, 28]. Using a constitutively active version of CK1 δ lacking its autoinhibitory C-terminal tail, we found that CK1 phosphorylated all 5 serines within the FASP region (**Figure 3.1b**, **Supplementary Figure 3.1a**). Based on the CK1 consensus recognition motif, pSxxS [29], we expected that CK1 would phosphorylate serines downstream of the priming site in a sequential manner. To test this, we introduced alanine mutations at each successive serine within the FASP cluster and assayed CK1 activity in the NMR kinase assay (**Figure 3.1c-f**). As expected, each Ser/Ala substitution selectively disrupted CK1 activity at downstream serines,

confirming that the kinase acts in a sequential manner and generating a set of variably phosphorylated FASP peptides to study the functional consequences of kinase activity on this region.

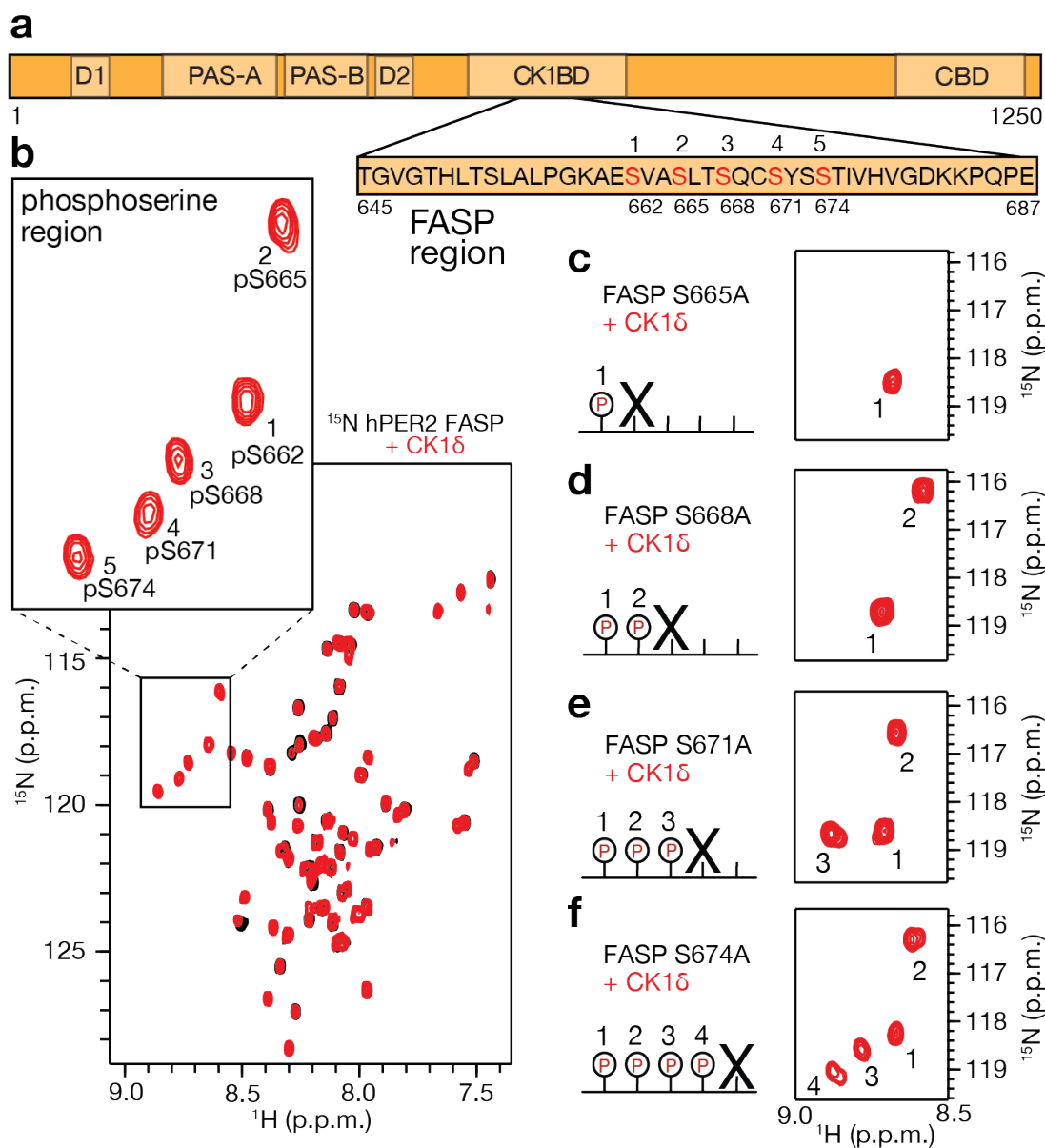


Figure 3.1. CK1 phosphorylates the human PER2 FASP region sequentially.

a, Domain map of hPER2 with tandem PAS domains, phosphodegrons (D1/D2), Casein Kinase 1 binding domain (CKBD), and CRY binding domain (CBD). Zoom, the FASP peptide used in NMR assays with CK1 phosphorylation sites (red). **b**, $^{15}\text{N}/^1\text{H}$ HSQC of 200 μM hPER2 FASP used for kinetic assays (black), overlaid with 16 hr timepoint in kinase assay (red). Zoom/boxed region, the phosphoserine region. Numbering (1-5) corresponds to the order in the FASP peptide. **c-f**, Schematic representation of Ser/Ala mutations introduced to the FASP peptide. X, indicates position of the alanine substitution within the FASP serine cluster. Zoom of phosphoserine region for

the $^{15}\text{N}/^1\text{H}$ HSQC of FASP mutants (red) at 3 hr timepoint in the kinase assay, with numbering showing the sequential order of reaction.

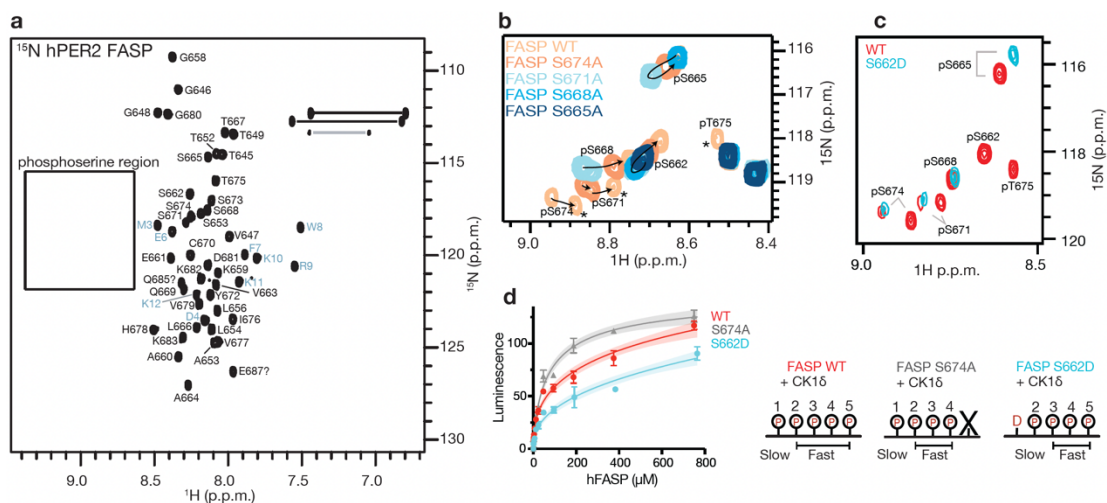


Figure 3.1.1 (relates to Figure 3.1 and Figure 3.2).

a, $^{15}\text{N}/^1\text{H}$ HSQC of hPER2 FASP peptide with assignments. Boxed region indicates area within the spectra where phosphoserines appear. **b**, Overlaid $^{15}\text{N}/^1\text{H}$ HSQC spectra of FASP Ser/Ala mutant peptides. Arrows indicate movement of unique chemical shifts corresponding to extent of FASP phosphorylation. Asterisk indicates peaks with chemical shift due to phosphorylation of T675. **c**, Zoom into phospho-serine region of $^{15}\text{N}/^1\text{H}$ HSQC of hPER2 FASP peptide (WT) overlaid with the S662D phosphomimetic mutant after a 3 hr incubation with CK1 δ and ATP at 25 °C. **d**, ADP-Glo kinase assay with titration of FASP mutant peptides with mean and SD from 2 replicates, representative of $n = 3$ independent assays. Shaded area indicates 95% C.I. of the fit. Schematic represents the different combination of non-consensus and consensus-based phosphorylation events for each of the mutants. Note how the S674A and S662D mutants have an equivalent number of consensus-based phosphorylation sites.

3.3.2 CK1 follows an ordered distributive mechanism gated by slow, non-consensus priming

Due to the sequential nature of FASP phosphorylation by CK1, we propose that the kinase follows an ordered distributed kinetic mechanism (**Figure 3.2a**). The transient accumulation of intermediates can theoretically be observed by NMR, depending on the rate constants for intermediate states (**Figure 3.2b-c**) [30]. Since we previously determined that phosphorylation of the non-consensus priming serine was much slower than consensus-based activity on subsequent serines [17], we expected that phosphorylation of the FASP would appear to be an all-or-none event by NMR, represented by state F in **Figure 3.2b**. When phosphorylation sites are in close proximity to one another, the chemical shift of a particular residue can change over the course of a reaction as nearby sites become modified [28]. Using the distinct phosphospecies generated with alanine substitutions in the FASP, we were able to assign unique chemical shifts for each phosphopeak that arises as a function of sequential phosphorylation (**Figure 3.1.1b**). However, in a kinase reaction with the native FASP, we did not observe accumulation of any intermediate states over the course of the reaction, only a set of peaks corresponding to the 5 phosphoserines defined as species C in **Figure 3.2d** and **e**. We did observe a second slow step due to phosphorylation of T675 (peak 6D in **Figure 3.2d**) that was dependent on phosphorylation of the upstream residue S671 (**Figure 3.1.1b**), consistent with the less optimal CK1

consensus motif of pSxxxS/T [29]. The peaks corresponding to phosphoserines 4 and 5 (pS671 and pS674) were split depending on whether or not T675 was phosphorylated (4C and 4D, 5C and 5D, **Figure 3.2d**).

We confirmed the overall kinetic scheme by collecting a series of 6-minute SoFast HMQC NMR spectra over the course of a 3-hr real-time kinase reaction in the magnet (**Figure 3.2f**). Combining the total intensities for phosphoserines 4 and 5 from states C and D (**Figure 3.2g**) confirms that the reaction kinetics proceed as predicted by the model outlined in **Figure 3.2b**. To probe the ordered distributive mechanism, we utilized a mutant form of the kinase, K224D [31], that disrupts the anion binding pocket Site 1 near the active site thought to anchor primed substrates and facilitate kinase activity on downstream consensus sites [32-34]. The K224D mutant retains its ability to prime the FASP region with kinetics similar to the WT kinase but has decreased activity on subsequent consensus-based sites [35]. By reducing the relative difference in rates for priming and sequential phosphorylation with this mutant, we were able to resolve a distinct peak corresponding to the transient accumulation of the primed, singly phosphorylated FASP, like that observed in the PER2 S665A mutant (**Figure 3.2h**), which exhibited a clear lagging phase for kinase activity on subsequent phosphorylation sites (**Figure 3.2i**).

Mutation of the priming serine in the human FASP region to an aspartate, S662D, rescues downstream kinase activity within the FASP region [18] and increases circadian period by promoting the stabilization of PER2 in

mice [22]. Other CK1 substrates are constitutively primed by D/E residues upstream that can act as phosphomimetics [36, 37]. Using the NMR kinase assay, we observed that while the S662D mutation can prime kinase activity on downstream serines within the FASP region, it is a relatively poor mimetic of pS662, leading to a reduction in the overall kinase activity on the FASP peptide (**Figure 3.1.1c-d**). Therefore, the ability of the S662D mutant to promote PER2 stability and period lengthening *in vivo* [22] likely rests on the weak but constitutive priming by the aspartate.

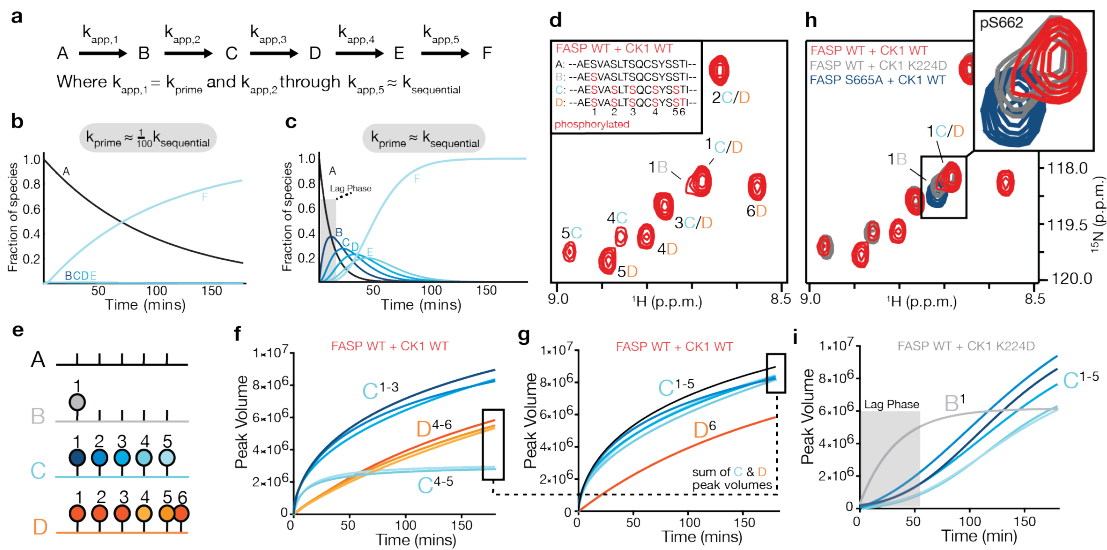


Figure 3.2. CK1 follows an ordered distributive mechanism on the human PER2 FASP region.

a, Schematic of ordered distributive kinetic model used for panels **b** and **c** (modeled using Wolfram Mathematica, see Supplement). **b**, Reaction coordinate for ordered distributive kinetic mechanism with differential rates for priming and sequential kinase activity. **c**, Reaction coordinate for ordered distributive kinetic mechanism with similar rates for priming and sequential kinase activity. **d**, Zoom of $^{15}\text{N}/^1\text{H}$ HSQC hPER2 FASP phosphoserine region looking at peaks corresponding to different states arising from at 3 hr incubation with CK1 WT (red). States A-D (inset) correspond to unique chemical shift states observed throughout the kinase assay. **e**, Schematic of unique states A-D observed in **d**: A, unphosphorylated FASP; B, primed FASP; C, all serines in FASP phosphorylated; D, all serines plus T675 phosphorylated. Numbering indicates order of phosphorylation. **f**, Traces of accumulating peak volume from the NMR kinase assay. Letters C-D with superscript numbers correspond to specific phosphoserines observed in the NMR assay. **g**, Same traces as in **f**, with peak volumes corresponding to states C and D for the last two serines (4-5) summed to show that all phosphoserines in the FASP report on state C with similar kinetics. **h**, Phosphoserine region showing unique chemical shift environment for singly phosphorylated (priming only) FASP S665A (blue) overlaid with WT FASP with CK1 WT (red) or K224D (gray) after 3 hr incubation. B-D lettering corresponds to unique states observed in NMR kinase assay as in **d**. **i**, Traces of accumulating peak volume from NMR kinase assay with CK1 K224D, resolving the transient accumulation of primed FASP and a clear lagging phase for subsequent phosphorylation states.

3.3.3 Sequential phosphorylation of FASP leads to feedback inhibition of CK1

Disrupting phosphorylation of the FASP region by mutating the priming serine increases CK1 activity at a phosphodegron in PER2 [35], consistent with increased PER2 turnover in the human FASPS S662G mutant [18]. However, no mechanistic model has been robustly demonstrated yet for how FASP phosphorylation influences CK1 activity. Monitoring both the loss of peak intensity for S662 and the concomitant increase in peak intensity for pS662, we made the striking observation that the fraction of primed WT FASP plateaued at approximately 50% completion over the course of a 3-hr real-time NMR kinase assay (**Figure 3.3a**). This suggested to us that some or all of the phosphoserines in the FASP cluster might work to reduce CK1 activity via feedback inhibition. To dissect the role of successive phosphoserines in this inhibition, we monitored the kinetics of FASP priming by NMR using the alanine-substituted mutants that limit the extent of sequential phosphorylation in a stepwise manner (**Figure 3.3b-e**). We found that reducing the extent of possible phosphosites in the FASP led to a stepwise increase in priming activity, resulting in near complete priming of the S668A mutant limited to just 2 phosphoserines (**Figure 3.3d**) and a several-fold increase in the rate of priming (k_{prime}) relative to the WT FASP (**Figure 3.3f**).

To confirm that the observed inhibition of FASP priming was due to feedback inhibition, we performed substrate titration experiments using an

ADP-Glo assay that measures bulk kinase activity. Here, we observed that WT FASP had the lowest overall rate of phosphorylation, despite having the most consensus-based phosphosites available for the kinase (**Figure 3.3e,g**). Moreover, kinase activity began to decrease on WT FASP at higher substrate concentrations, consistent with substrate/product inhibition. As in the NMR based assay, we observed a rank-order increase in overall kinase activity and decrease in apparent inhibition as the extent of possible phosphosites in FASP was successively limited with the alanine substitutions (**Figure 3.3g**), shifting the Michaelis constant higher for each of these peptides (**Figure 3.3h, Figure 3.3.1a**). Together, these data are consistent with the rapid generation of a pFASP product that inhibits kinase activity in *trans*. To test this, we performed a kinase assay on a peptide corresponding to the PAS-Degron of PER2 (**Figure 3.3.1b**) [38] in the presence or absence of synthetically phosphorylated FASP peptides (pFASP). The doubly phosphorylated FASP peptide (2pFASP) inhibited the kinase in *trans*, with the 3pFASP peptide further increasing the potency of inhibition (**Figure 3.3i**). Addition of the 4pFASP peptide in *trans* also inhibited phosphorylation of the priming serine in an *in vitro* kinase assay, where full-length mouse PER2 immunoprecipitated from HEK293 cells was dephosphorylated *in vitro* and then treated with CK1 δ kinase that had been pre-incubated with 4pFASP peptide (**Figure 3.3j-k**).

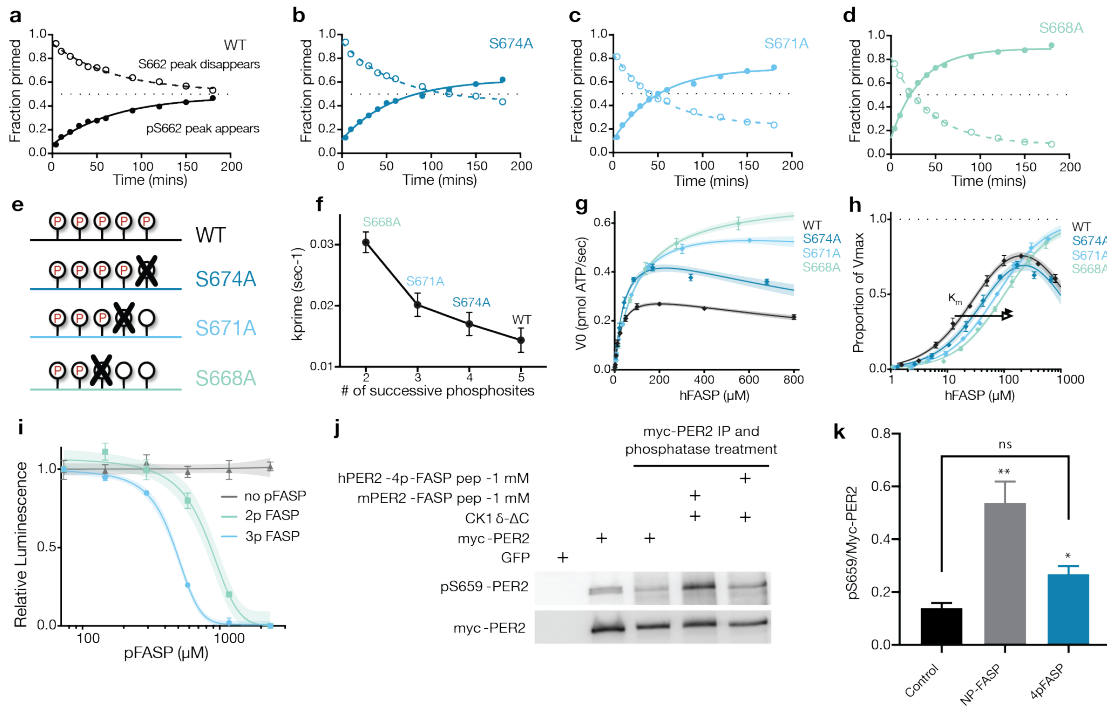


Figure 3. Phosphorylation of the human PER2 FASP region inhibits CK1 activity.

a-d, NMR kinase assay for the WT FASP or indicated mutant peptides monitoring the reaction kinetics of priming phosphorylation at S662 by NMR. **e**, Schematic of FASP alanine mutations and resulting discrete phosphostates. **f**, Plot of priming rate constant (k_{prime}) as a function of the possible successive phosphosites in the FASP. Error bars represent SEM from fits in panels **a-d**. **g**, ADP-Glo kinase assay with titration of FASP mutant peptides with mean and SD from 2 replicates, representative of $n = 3$ independent assays. Shaded area indicates 95% C.I. of the fit. **h**, Data from panel **f** normalized by V_{max} values calculated from the preferred kinetic model (see Supplementary Figure 3.3.1a). **i**, ADP-Glo kinase assay of hPER2 PAS-degron peptide (see Figure 3.3.1b) with titration of pFASP peptides corresponding to 2 (2p) or 3 (3p) phosphoserines (see Figure 3.4.1c) with mean and SD from 2 replicates, representative of $n = 3$ independent assays. Shaded area indicates 95% C.I. of the fit. **j-k**, Western blot and quantification of the phosphorylation of the FASP priming site (pS659 in mouse PER2). Full-length mouse PER2 was immunoprecipitated from transfected HEK293T cells, dephosphorylated, and subjected to an *in vitro* kinase assay with 200 ng CK1 in the presence and absence of added NP or 4pFASP peptides as indicated.

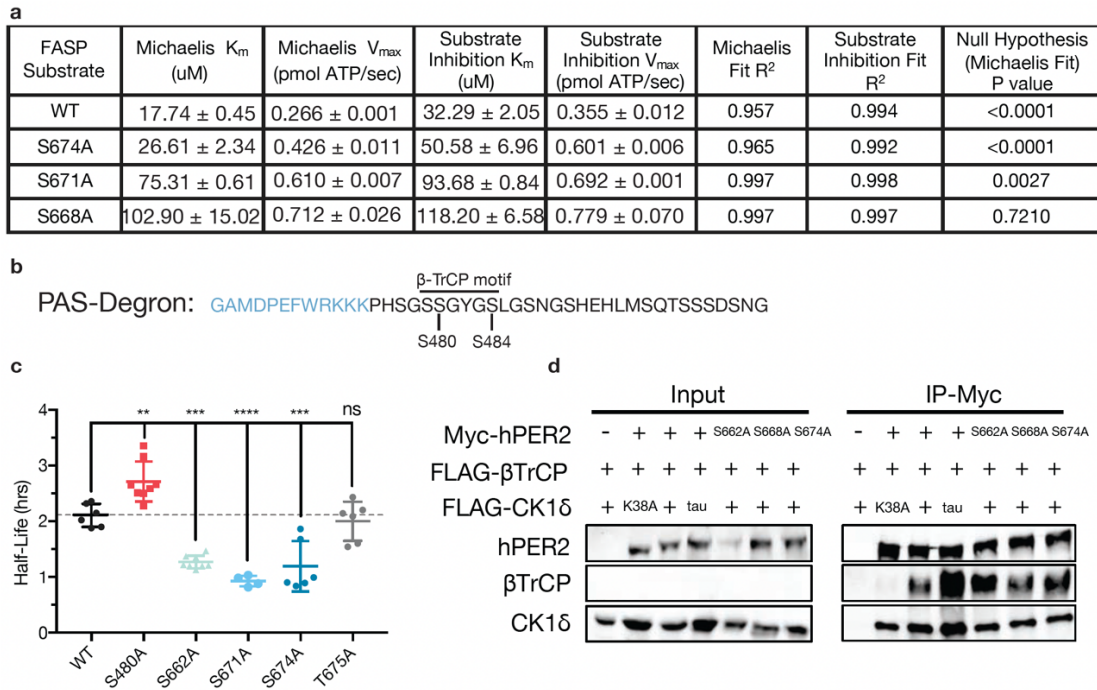


Figure 3.3.1 (relates to Figure 3).

a, Table of kinetic analysis for ADP-Glo assay in Figure 3, panel **f**. **b**, The sequence of the PAS-Degron peptide used for kinase substrate in pFASP inhibition assays (Figure 3.3, panel **h**) in black (blue, non-native amino acids). **c**, Quantification of real-time luciferase traces treated with cycloheximide 48 hrs after co-transfection of HEK293T cells with hPER2-LUC and CK1δ expression plasmids ($n \geq 4$ with SD). Significance assessed relative to WT with ordinary one-way ANOVA: **, $p < 0.01$; ***, $p < 0.001$; ****, $p < 0.0001$; ns, not significant. **d**, Co-immunoprecipitation assay from transiently transfected HEK293T cells assessing CK1δ-mediated β-TrCP recruitment to PER2 ($n = 3$).

We performed real-time bioluminescence measurements of HEK293T cells transiently transfected with hPER2::LUC and CK1 δ expression plasmids to monitor the half-life of hPER2::LUC in the context of Ser/Ala mutations that modulate PER2 phosphorylation. Consistent with prior results, mutation of the PAS-Degron site (S480) to an alanine increased hPER2::LUC stability (**Figure 3.3.1c**), where S480 corresponds to the first phosphorylated residue of the β -TrCP consensus recognition motif, DpSGYGpS (**Figure 3.3.1b**) [11, 39, 40]. Mutation of either the priming serine (S662A) or downstream serines (i.e., S671A or S674A) decreased PER2::LUC half-life, while mutation of the threonine residue at the end of the FASP cluster (T675A) showed no significant effect on PER2 stability (**Figure 3.3.1c**). To further link the Ser/Ala mutations in FASP to β -TrCP recognition of PER2, we performed co-immunoprecipitation experiments from HEK293T cells co-transfected with PER2, β -TrCP and CK1 δ expression plasmids and observed increased CK1 δ -dependent β -TrCP binding to PER2 with mutants that reduce FASP phosphorylation (**3.3.1d**).

3.3.4 pFASP binds to CK1 via conserved anion binding sites to occlude the substrate binding cleft

CK1 has several highly conserved anion binding sites located around the substrate binding cleft (**Figure 3.4a**) [32, 35]. Given their location and the distance between phosphosites within pFASP, we hypothesized that these anion binding sites might mediate interaction of the phosphorylated peptide

with CK1. To test this prediction, we solved crystal structures of phosphorylated FASP peptides bound to the catalytic domain of CK1 δ (**Table 3.1**). Indeed, in three distinct complexes with 2pFASP, 3pFASP, or 4pFASP peptides, we observed a consistent binding mode (**Figure 3.4.1a-b**) with the phosphorylated peptides coordinating the two anion binding sites (Site 1 and Site 2) to fully occlude the substrate binding cleft (**Figure 3.4b**). Interestingly, a substrate motif analysis derived from a dataset of 101 known CK1 δ substrate sequences from PhosphoSitePlus aligns well with this pFASP binding mode, suggesting that the first 3 sites of the FASP region conform to an ideal CK1 δ recognition sequence (**Figure 3.4.1c**). In Site 1, R178 and the backbone amide of G215 coordinate pS662 of the pFASP peptide (**Figure 3.4c**). Site 1 harbors the location of the *tau* mutation (R178C) that shortens circadian period [20]. We did not observe strong density for K224, the other basic residue that could coordinate an anion in Site 1, suggesting flexibility in the Fa helix consistent with previous studies [31, 35, 41]. Moving down the pFASP peptide, we observed additional backbone-backbone interactions and docking of the pFASP side chains of V663 & A664 into small hydrophobic pockets within the substrate binding cleft (**Figure 3.4b, d**).

Table 3.1 X-ray crystallography data collection and refinement statistics

| | 2pFASP:CK1 | 3pFASP:CK1 | 4pFASP:CK1 | pS589:CK1 |
|--|-------------------------------|-----------------------------|-------------------------------|-------------------------------|
| | δ | δ | δ | δ |
| Data collection | | | | |
| PDB Id. | 8D7M | 8D7N | 8D7O | 8D7P |
| Beam line | APS(23IDD) | APS(23IDD) | APS(23IDD) | APS(23IDD) |
| Resolution Range (Å) (highest shell)* | 46.15 - 2.25 (2.32 - 2.25) | 68.01-1.66 (1.69 - 1.66) | 67.70 - 1.65 (1.68 - 1.65) | 60.77 - 2.25 (2.32 - 2.25) |
| Space group | C 1 2 1 | C 1 2 1 | C 1 2 1 | P1 |
| a, b, c | 55.7, 135.97, 91.14 | 55.90, 136.03, 90.54 | 55.33, 135.40, 90.35 | 48.78, 56.74, 65.94 |
| α, β, γ | 90, 94.3, 90 | 90, 94.60, 90 | 90, 94.41, 90 | 108.93, 95.63, 108.69 |
| Wavelength (Å) | 1.03 | 1.03 | 1.03 | 1.03 |
| Total observations | 176957 (15319) | 480416 (23861) | 468136 (24113) | 85303 (7506) |
| Unique reflections | 31319 (2767) | 79274 (3942) | 78946 (4059) | 27457 (2505) |
| Completeness (%) | 97.8 (94.5) | 100 (99.9) | 99.4 (99.2) | 93.7 (91.8) |
| R _{merge} | 15.2 (127.4) | 9.3 (55.6) | 6.4 (54.2) | 11.6 (31.2) |
| <I/σ> | 9.4 (2.5) | 9.9 (2.7) | 13.6 (2.9) | 5.5 (2.7) |
| CC1/2 | 0.99 (0.55) | 0.99 (0.82) | 0.99 (0.84) | 0.98 (0.85) |
| Redundancy | 5.7 (5.5) | 6.1 (6.1) | 5.9 (5.9) | 3.1 (3.0) |
| Refinement | | | | |
| R _{work} / R _{free} (%) | 17.9 (22.9) | 18.8 (21.3) | 17.4 (21.1) | 19.7 (25.4) |
| Number of non-hydrogen atoms | 5075 | 5388 | 5342 | 4999 |
| Protein | 4820 | 4840 | 4840 | 4864 |
| Water | 255 | 548 | 502 | 135 |
| B-factor (Wilson) | 36.95 | 33.32 | 32.9 | 29.93 |
| RMSD Bond length (Å) | 0.008 | 0.01 | 0.011 | 0.009 |
| RMSD Bond angle | 1.05 | 1.18 | 1.18 | 1.04 |
| Ramachandran favored (%)/ Ramachandran outliers (%) | 97.04/0.0 | 96.17/0.0 | 96.34/0.26 | 96.23/0.0 |

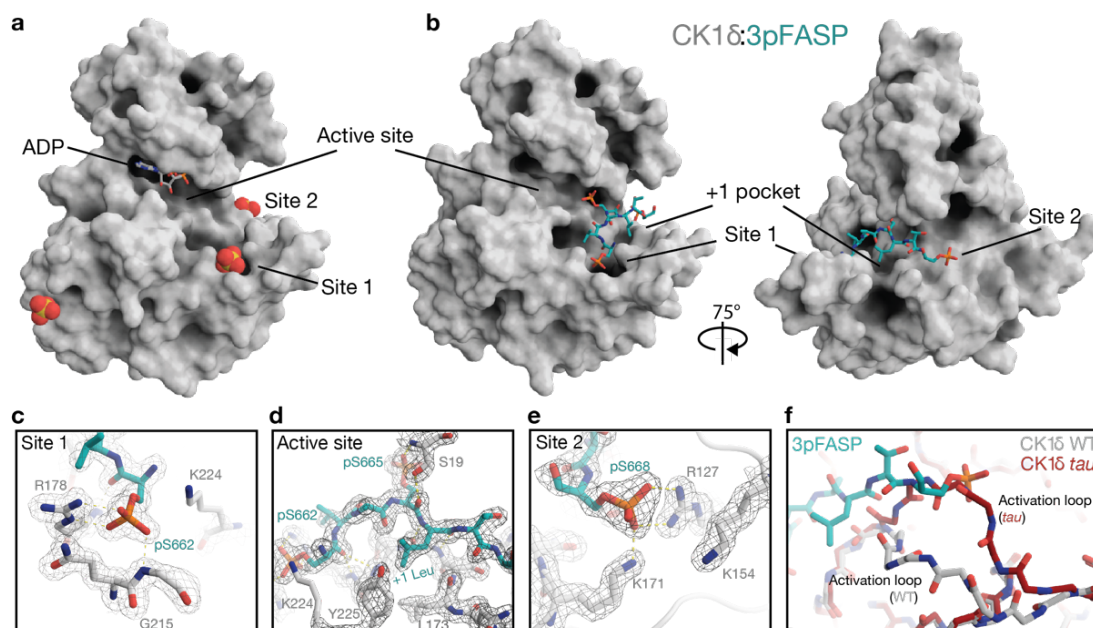


Figure 3.4. The human PER2 pFASP binds to the active site of CK1.

a, Surface representation of CK1 catalytic domain bound to ADP (PDB 5X17). Spheres, sulfate anions from the crystallization condition bound at anion binding sites as indicated. **b**, Surface representation of the CK1 catalytic domain bound to a 3pFASP peptide (see Figure 3.4.1). **c**, Zoom of 3pFASP interactions within anion binding site 1. **d**, Zoom of 3pFASP interactions within active site region. **e**, Zoom of 3pFASP interactions within anion binding site 2. **f**, Structural alignment showing the main chain for the activation loop of CK1 WT (gray) and the *tau* mutant (red) showing a clash of the 3pFASP (teal) with the conformation of the activation loop stabilized by the *tau* mutation.

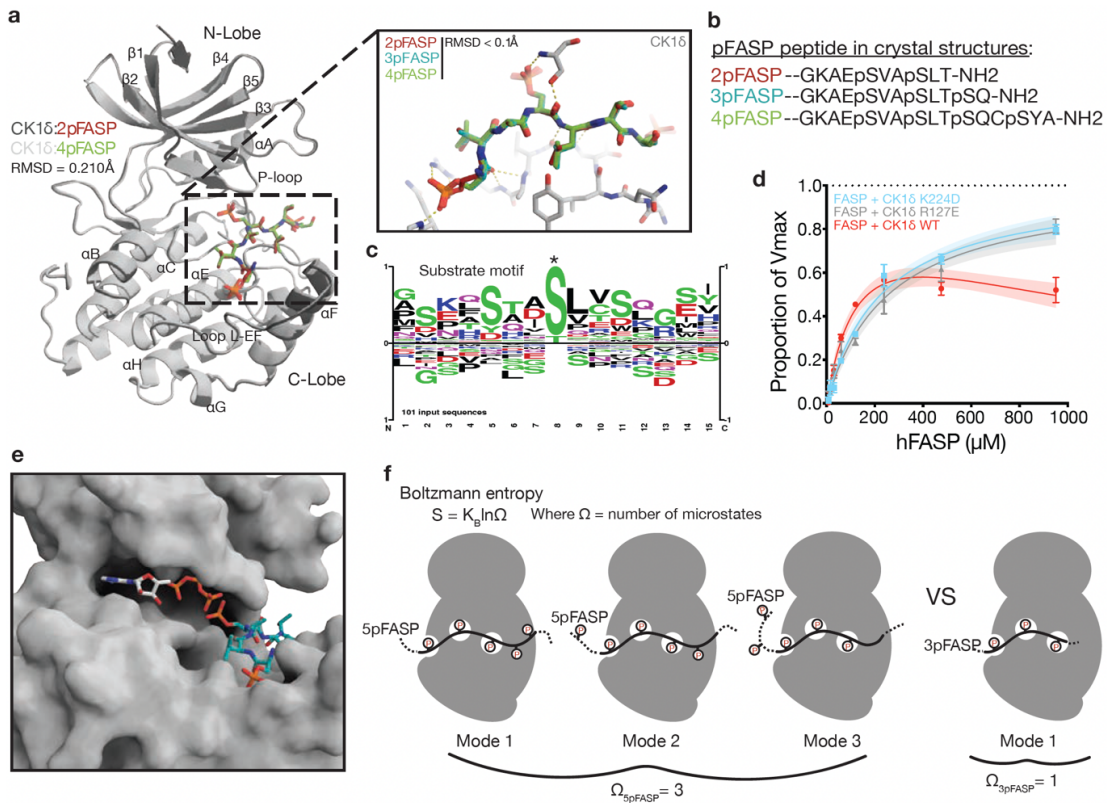


Figure 3.4.1 (relates to Figure 3.4).

a, Cartoon representation of CK1δ:2pFASP and CK1δ:4pFASP aligned structures to show overall similarity (RMSD indicated). Boxed region represents activation loop zoom. 2pFASP, 3pFASP, and 4pFASP aligned based on overall structural alignment of CK1δ:2pFASP and CK1δ:4pFASP complexes with CK1δ:3pFASP, with RMSD of peptides indicated. **b**, Synthetic peptides used for soaking into CK1δ crystals and ADP-Glo inhibition assays. **c**, Substrate motif analysis (pLogogram) generated with dataset of 101 known CK1δ substrates from PhosphositePlus. Relative size of residue-letter indicates relative frequency of that residue at that position. Asterisk indicates site of phosphorylation. **d**, ADP-Glo kinase assay with titration of hFASP peptide showing that anion binding site 1 (K224D) and anion binding site 2 (R127E) contribute to pFASP inhibition. Data (mean and SD of 2 replicates) are normalized to V_{max} calculated from the preferred model fit (Michaelis or Substrate Inhibition). Shaded area indicates 95% C.I. of the fit. **e**, Zoom in of CK1δ:3pFASP active site. ATP is shown in active site based on alignment of the CK1δ:3pFASP catalytic domain with an ATP bound structure of CK1δ, 1CSN. **f**, Schematic representation of entropic differences between 3pFASP and 5pFASP binding modes. The higher number of accessible microstates in 5pFASP could contribute to the observed increase in inhibition of kinase activity.

The 2nd phosphoserine of pFASP, pS665, projected into the active site of CK1, positioned close to where the gamma phosphate would be in ATP-bound CK1 (**Figure 3.4.1e**). We also observed that S19 of the N-terminal lobe P-loop of CK1 clamped down on pS665, suggesting a stabilizing mechanism for transfer of phosphate from the nucleotide to the substrate, with the +1 Leu after pS665 fitting into a small hydrophobic pocket on the kinase. As previously noted, this small hydrophobic pocket is formed between L173 and Y225 of CK1 (the +1 pocket, **Figure 3.4b, d**) in the downward conformation of the CK1 activation loop [35]. The +1 pocket is just large enough to accommodate small residues such as Ala, Leu, or Val, and could contribute to CK1 recognition of the non-consensus SLS motif [37] or the FASP priming site, where the +1 residue is a valine.

Moving towards the C-terminal end of the peptide, the 3rd phosphoserine of pFASP, pS668, is coordinated by anion binding Site 2, comprising basic residues R127, K154, and K171 (**Figure 3.4e**). R127 is part of the conserved HRD motif involved in the regulation of Ser/Thr kinases by coordinating a phosphorylated residue within the activation loop [42]. To further validate the significance of these anion binding sites in the binding of pFASP and product inhibition, we introduced charge inversion mutations in Site 1 (K224D) or Site 2 (R127E) and performed substrate titrations with FASP peptide, observing a decrease in the level of product inhibition (**Figure 3.4.1d**).

The highly specific sequential mechanism of FASP phosphorylation also strongly suggests that the FASP peptide translates through the substrate binding cleft, with each phosphoserine anchoring into Site 1 to facilitate the next phosphorylation event in the active site. The phosphorylated serines in pFASP all share the same approximate atomic distance between each other that is consistent with the spacing between Site 1, the active site, and Site 2. Therefore, product inhibition may continue to increase as a function of sequential phosphorylation at least partially due to changes in entropy, where 3pFASP can occupy each of the aforementioned sites on the kinase in one way (1 microstate), 4pFASP in two ways (2 microstates), and 5pFASP in three ways (3 microstates) (**Figure 3.4.1f**).

The *tau* mutation in Site 1 of CK1 δ prevents anion coordination at this site and alters the global dynamics of CK1 as well as significantly changing the local dynamics in and around the activation loop and Site 2 via an allosteric mechanism [35]. We note that the alternate conformation of the activation loop stabilized in the *tau* mutant sterically clashes with the 3pFASP binding mode (**Figure 3.4f**). This incompatibility suggests that the *tau* mutant is less susceptible to feedback product inhibition, perhaps also contributing to the increased phosphorylation of the PAS-Degron and degradation of PER2 by this kinase mutant [13, 35, 43].

3.3.5 Molecular dynamics simulations support stable binding mode of pFASP:CK1 crystal structures

To investigate how CK1 might be inhibited by a fully phosphorylated FASP peptide, we modeled and simulated the interaction of CK1 and a 5pFASP peptide using Gaussian accelerated Molecular Dynamics (details in Supplementary Material) [44]. We found that the first three phosphoserines (pS662, pS665, and pS668) remain stably bound in the substrate binding cleft of CK1, while the 4th and 5th phosphoserines (pS671 and pS674) display higher mobility (**Figure 3.5a-b**). As expected, pS662 forms stable electrostatic interactions in Site 1 (**Figure 3.5c**). In addition to being close to R178 and K224, pS662 also engages in stable electrostatic interactions with Q214, located in the highly flexible loop-EF [31, 41]. In the active site, pS665 is locked in place by a cluster of electrostatic interactions involving D128, K130, D148 and a Na⁺ ion (**Figure 3.5d**). The presence of this ion in the active site suggests that at least one cation (likely Mg²⁺) could be important for product inhibition. The third phosphoserine (pS668) is held in place in Site 2 by stable electrostatic interactions with R127, K154, K171, and, to a lesser extent, R168 (**Figure 3.5e**). Finally, we found that the 5th phosphoserine (pS674) often engages in electrostatic interactions with R160 (close to anion binding Site 3, which precedes the activation loop) and with K155 (just after the DFG motif) (**Figure 3.5f**). We refer to this herein as Site 3'. These interactions provide additional

product stabilization, perhaps contributing to stronger inhibition when the FASP region is fully phosphorylated.

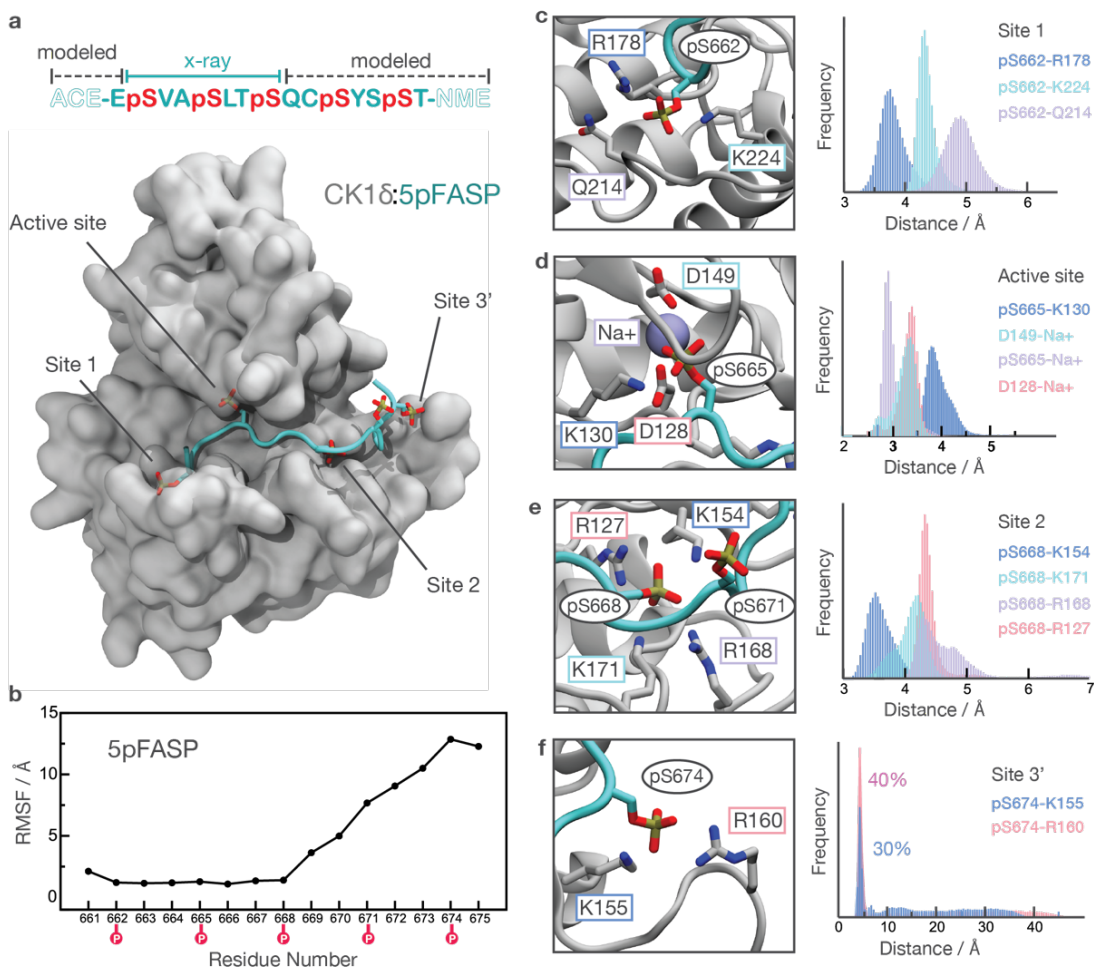


Figure 3.5. Molecular dynamics simulations of CK1:5pFASP.

a, Structural model of CK1 bound to a 5p FASP peptide obtained by Gaussian accelerated Molecular Dynamics (GaMD). The molecular representation corresponds to one snapshot from the MD trajectories. **b**, Root Mean Square Fluctuation (RMSF) of the 5pFASP peptide with respect to its average conformation after aligning the MD trajectories with respect to CK1 backbone. **c-f**, Characterization of key interactions that stabilize the 5pFASP product in **(c)** Site 1, **(d)** the active site, **(e)** Site 2, and **(f)** an additional anion binding site located proximal to Site 2 (Site 3'). Histograms were computed based on distances sampled during the GaMD simulations.

3.3.6 Circadian rhythms are shortened by small deletions in the conserved FASP region of PER

To address the regulatory role of the FASP region on circadian period, small amino acid deletions were introduced in the human *Per2* FASP region encoded by exon 17 (E17) by targeting the priming serine (S662) with CRISPR (**Figure 3.6a**). This CRISPR-mediated strategy utilized human U2OS cells with endogenous *Per2-luc* and *Per1-luc* knock-in reporter genes that produced robust rhythms in bioluminescence and clock proteins [27]. As out-of-frame mutations would disrupt LUC expression and eliminate bioluminescence, we could select for small in-frame deletions in PER2::LUC protein based on intact bioluminescence signals followed by molecular characterization. Small in-frame deletions that removed the priming serine led to rhythms in PER2::LUC abundance that were phase-advanced relative to WT PER2::LUC after synchronization by serum shock (**Figure 3.6b**). Additionally, PER1 also showed phase-advanced rhythms in abundance in these mutant lines relative to the parental cell line (**Figure 3.6.1a**).

Immunoblots for priming-disrupted PER2 mutants showed similar levels of gross phosphorylation as WT PER2::LUC (**Figure 3.6c-d, Figure 3.6.1b**). To quantify differences in period, real-time bioluminescence measurements were collected on the clonal cell lines, which exhibited robust circadian rhythms with a significantly shorter period relative to the parental cell line (**Figure 3.6e, Figure 3.6.1c**). Mutants that left the priming serine intact but removed one or

more of the downstream serines (i.e., P2E17-25) also showed robust rhythms in bioluminescence with short periods (**Figure 3.6f**), but they were not as short as the priming-disrupted mutants that eliminate all FASP phosphorylation ($P < 0.05$). This suggests a role for the downstream phosphorylation sites in regulation of CK1 activity on PER2. Disruption of the FASP region led to decreased stability of PER2 after treatment with cycloheximide (**Figure 3.6g**) and also exhibited accelerated phosphorylation kinetics relative to WT, based on mobility shift, on the *de novo* PER2 synthesized after washout of cycloheximide (**Figure 3.6h**). The FASP region is highly conserved in PER1, and similar CRISPR-mediated edits to the PER1 FASP region by targeting the priming serine S714 also exhibited short period rhythms characterized by destabilized PER1 (**Figure 3.6.2a-f**). NMR studies of the human PER1 FASP demonstrate that CK1 phosphorylates it similarly to PER2 and that indels disrupting the priming serine eliminate kinase activity on the region (**Figure 3.6.2g**), demonstrating that the phosphorylated FASP region of both mammalian PERs likely act in a similar manner to constrain CK1 activity.

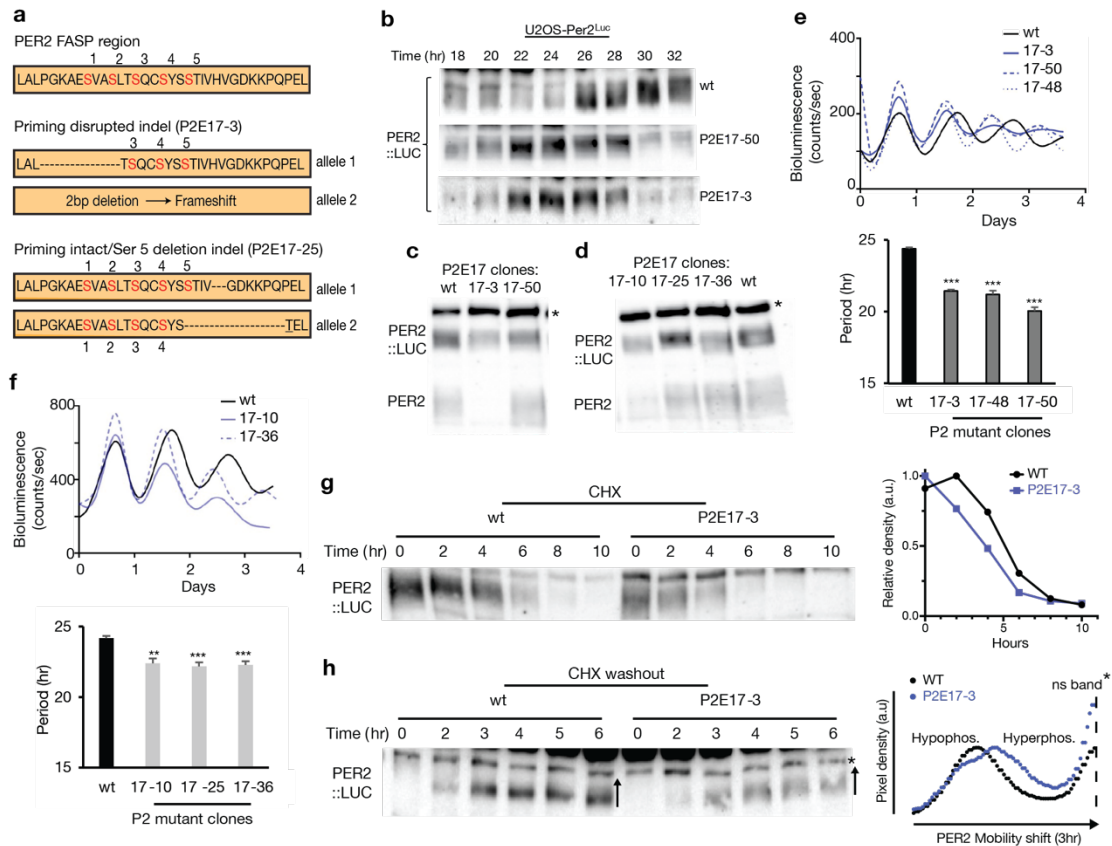


Figure 3.6. Circadian rhythms are shortened by small deletions in the conserved FASP domain of human PER2.

a, Schematic representation of select in-frame deletions within the human PER2 FASP region are separated into 2 classes: priming-disrupted (P2E17-3) or priming intact (P2E17-25). **b**, Immunoblot of select priming-disrupted PER2::LUC mutants compared to WT PER2::LUC. Blot representative of two independent experiments. **c,d**, Representative immunoblots for **(c)** priming-disrupted or **(d)** priming intact PER2 mutants. *nonspecific band. The *Per2* allele in clone 17-3 has a frame-shifting mutation leading to deletion of the untagged PER2. **e,f**, Real-time bioluminescence traces of circadian rhythms from WT and mutant *Per2* clones (**e**, priming-disrupted; **f**, priming intact) with quantification of mean period and SD from $n = 3$ cultures. Periods from mutant clones were compared to WT with an unpaired t-test: ***, $p < 0.001$. *Per2* priming intact mutants (clones 17-25 and 17-36) exhibited rhythms that were shortened to a lesser degree than the priming-disrupted mutants in **e**, $p < 0.05$. In both graphs, the first peaks are aligned to show differences in period clearly. **g**, Western blot and quantification of degradation of WT PER2::LUC and clone 17-3 after cycloheximide treatment. Blot representative of two independent assays ($n = 2$). **h**, Western blot and quantification of phosphorylation of *de novo* PER2 after protein depletion by 10 hr CHX treatment and washout. Blot representative of two independent assays ($n = 2$).

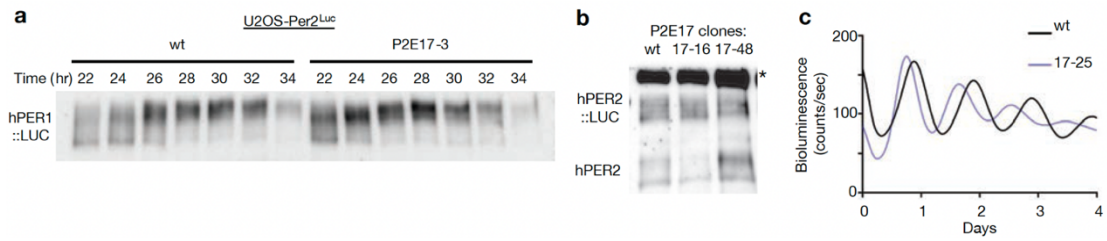


Figure 3.6.2 (relates to Figure 3.6).

a, PER1 in the PER2-LUC mutant clone 17-3 shows phase-advanced rhythms in abundance and phosphorylation (n = 2).

b. Two mutant clones 17-16 and 17-48 are shown. * non-specific band. **c**, Clone P2E17-25 showed shorter period bioluminescence rhythms.

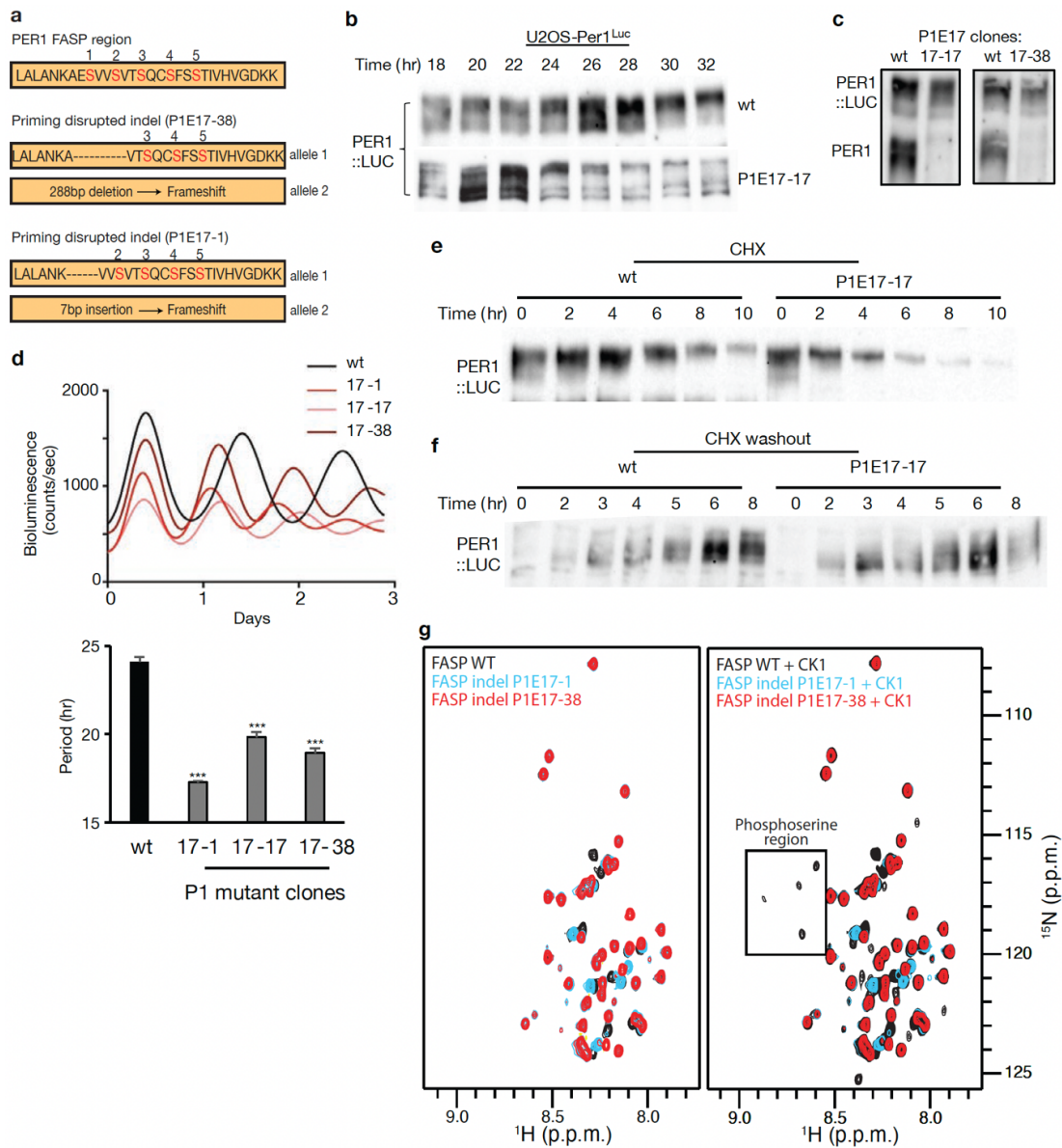


Figure 3.6.2 (relates to Figure 3.6).

a, Schematic representation of select in-frame deletions within the PER1 FASP region. **b**, Targeting S714 with CRISPR produced PER1 mutants with rhythms in protein abundance that peak earlier relative to wt. The PER1 blot for 17-17 is shown. **c**, Representative immunoblots for mutants and wt PER1. **d**, Real-time bioluminescence traces of *Per1* mutants and quantification of periods. Each period represents the mean and SD calculated from $n = 3$ cultures, compared to wt cells with an unpaired t-test. **e**, Degradation of PER1 wt and clone 17-17 after cycloheximide treatment ($n = 2$). **f**, Phosphorylation of *de novo* PER1 was monitored after existing protein was depleted by 10 hr CHX treatment and washout. Mutant PER1 exhibited accelerated phosphorylation

kinetics in gross phosphorylation based on mobility shift (n = 2). **g**, $^{15}\text{N}/^1\text{H}$ HSQC of PER1 FASP peptides corresponding to select indel mutants, with and without CK1 δ .

3.3.7 The phosphorylated *Drosophila* PER-Short region binds CK1 to inhibit kinase activity

Mammalian and *Drosophila* PER proteins both possess the two conserved motifs comprising the CK1 binding domain (CK1BD) that stably anchors the kinase to PER throughout its daily life cycle [11, 45-47] (**Figure 3.7a-b**). Phosphorylation of S589 on dPER by the *Drosophila* CK1 homolog DBT reduces kinase activity at a phosphodegron upstream to increase dPER stability and lengthen circadian period [23, 46] in a manner similar to the FASP-associated S662 on human PER2 [18] (**Figure 3.7a**). Loss of this phosphorylation site with the classic *per-Short* mutation [25] (*per^S*, S589N) or other mutants nearby in the PER-Short domain result in predominantly short period phenotypes [23, 48-50]. Because this CK1-dependent phosphosite is in close proximity to the CK1BD (**Figure 3.7c**) [12, 45, 47], we wondered if it would work similarly to the FASP region to attenuate CK1 activity. Phosphorylation of S589 by CK1 (i.e., DBT) has been invoked as a potential mechanism by which dPER could control CK1 activity in *trans* to regulate dPER turnover and repressive activity [23, 24, 26, 46]. Phosphorylation of S589 is preceded *in vivo* by phosphorylation of S596 by NEMO kinase, and the S596A mutation eliminates phosphorylation of S589, suggesting a hierarchical regulation of the PER-Short region by multiple kinases [23].

To determine if the phosphocluster in the PER-Short domain regulates CK1 activity on the N-terminal dPER Degron, we examined the progressive

phosphorylation of this region in *Drosophila* S2 cells using a full-length dPER construct that contains a TEV-cleavable 100-residue N-terminal fragment encompassing the Degron (PER/T100) [23, 24]. PER/T100 was co-expressed with full length dPER or a C-terminal fragment containing the kinase binding domain (residues 560-1034), with or without the S596A mutant, along with an inducible DBT construct. We observed that inhibition of dPER Degron phosphorylation is lost with the S596A mutant in full-length dPER (**Figure 3.7d, f**) or a fragment of dPER containing just the kinase binding domain in *trans* (**Figure 3.7e, f**). To test for direct inhibition of CK1 activity by the phosphorylated PER-Short domain, we also performed kinase assays *in vitro* using the human CK1 δ kinase domain and a PER2 PAS-Degron substrate in the presence of unphosphorylated and phosphorylated dPER-Short peptides (**Figure 3.7g**). CK1 phosphorylates only S589 in this peptide *in vitro* [46], although it is dependent upon NEMO kinase phosphorylation of S596 *in vivo* [23]. Here, we observed that peptides containing pS589, pS596, or both pS589/pS596 inhibited CK1 kinase activity similarly to the 3pFASP peptide (**Figure 3.7g**).

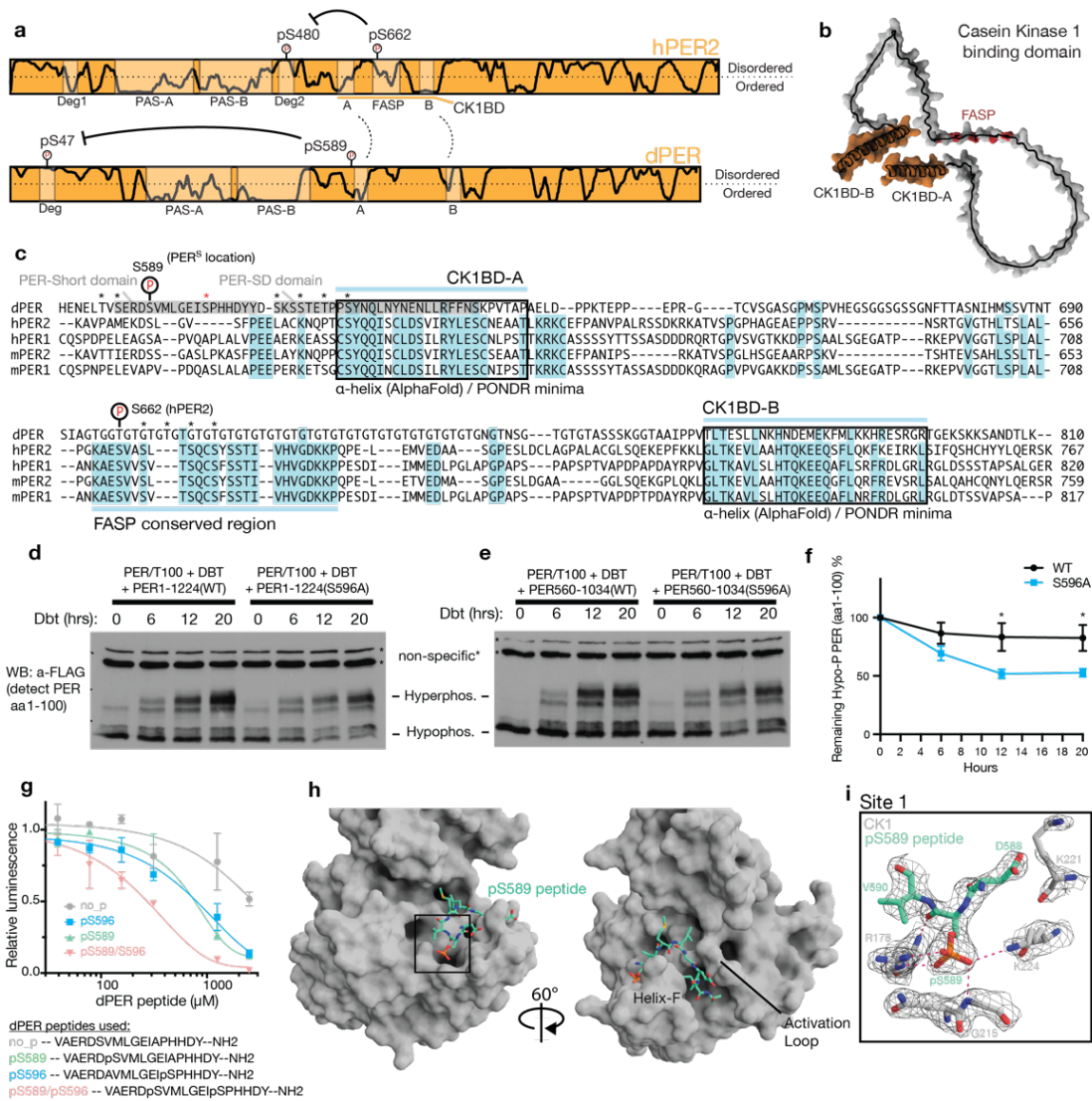


Figure 3.7. The phosphorylated PER-Short domain of *Drosophila* PER binds CK1 Site 1 to inhibit kinase activity.

a, Schematic of human and *Drosophila* PER proteins, illustrating similar mechanisms of Degron regulation by phosphoserines proximal to the two conserved motifs of the CK1BD (see panel **c**). **b**, AlphaFold2 structural prediction of the human PER2 CK1BD with helical motifs A and B (orange) and FASP phosphorylation sites (red). **c**, Alignment of *Drosophila* PER, human and mouse PER1/2 proteins showing conservation and the dPER-Short and Short-Downstream (SD) domains. *, phosphorylation by either CK1 (black) or NEMO (red). **d-e**, Western blot of dPER fragment (aa1-100). Samples collected at indicated timepoints after kinase induction, followed by protein extraction and TEV cleavage. **f**, Quantification of hypophosphorylated band (n=4). WT and S596A compared with Two-way ANOVA with Sidak multiple comparisons test:

*****, $p < 0.05$. **g**, ADP-Glo kinase assay of CK1 on the human PER2 PAS-Degron substrate in the presence of indicated peptides from dPER. Data are mean and SD from 2 replicates, representative of $n = 3$ independent assays. **h**, Structure of human CK1 (gray) bound to the dPER-Short peptide with pS589 (light green). **i**, Close-up view of dPER pS589 coordinated by CK1 residues in anion binding Site 1.

We then sought to characterize the structural basis for this inhibition with a crystal structure of CK1 in complex with the pS589 dPER-Short domain peptide (**Figure 3.7g-h**). This structure revealed a binding mode similar to the pFASP, where the substrate binding cleft was largely occluded by the peptide (**Figure 3.7h**) and anchored by the coordination of pS589 at anion binding Site 1 (**Figure 3.7i**). However, the activation loop of the kinase took on the rare 'loop up' conformation in this complex, which disrupts the second anion binding pocket [35]. This alternate conformation exposes a new channel that runs from the active site down towards the bottom of the kinase between the activation loop and helix-F that is bound by the dPER-Short peptide (**Figure 3.7h**), constricting at its narrowest point around dPER residue G593. We did not have density for residues after 595, including for pS596 in structures solved with the doubly phosphorylated peptide (data not shown). Therefore, although both mammalian and *Drosophila* PER peptides dock a critical CK1-dependent phosphoserine into anion binding Site 1, changes in peptide binding along the kinase active site suggest different mechanisms of recognition used to bind and inhibit the kinase.

3.4 Discussion

The CK1 kinase family is defined by several highly conserved anion binding sites located around the substrate binding cleft that regulate kinase dynamics, substrate specificity, and temperature compensation of circadian

rhythms [20, 31, 35]. It has long been proposed these anion binding sites mediate the recruitment of phosphorylated substrates to prime activity on the CK1 consensus motif pSxxS and/or bind the autophosphorylated tail of the kinase to inhibit its activity [32, 51]. Here, we show that CK1-dependent phosphorylation of key regulatory sites on its substrate PER near the kinase anchoring domain leads to feedback inhibition of the kinase through these conserved anion binding sites. Anchoring interactions can significantly enhance the kinetics of kinase activity on low to moderate affinity substrates nearby [52], as was recently demonstrated for CK1 and its activity on low affinity, non-consensus phosphorylation sites on PER and FRQ [53]. Inhibition of CK1 activity by phospho-PER is conserved in both mammals and *Drosophila* through anion binding Site 1, although other details of the PER-inhibited kinase complex differ by species. Notably, the loss of these CK1-dependent phosphosites in *Drosophila* [25], mice [22], and humans [18] shortens circadian period by several hours *in vivo*, demonstrating the functional importance of CK1 feedback inhibition on the molecular clock.

NMR spectroscopy allowed us to probe the kinetics and mechanism of the progressive, sequential phosphorylation of the FASP region in human PER proteins by CK1. The sequential nature of kinase activity here suggests that targeting the initial, rate-limiting priming step at the FASP region could be a powerful way to influence circadian rhythms. In fact, CK1 activity is influenced by other post-translational modifications on or around the FASP priming site,

such as O-GlcNAcylation [54, 55] and acetylation [56], demonstrating how this region is poised to integrate different metabolic signaling inputs for control over the clock. Our data suggest that CK1 inhibition by the human PER2 pFASP region depends on similar spacing between successive phospho-serines on the FASP and the distance between anion coordination sites in the substrate binding region of CK1. Although the structures of inhibited CK1 illustrate a common binding mode for the first three phosphorylation sites of the FASP region, deletion of downstream phosphorylation sites in the U2OS *Per1* and *Per2* indel cell lines demonstrates that they also contribute to kinase inhibition and period control as suggested by our molecular dynamics simulations.

The CK1-dependent site in the *Drosophila* PER-Short domain (pS589) bound to the kinase at Site 1, similar to the priming serine of the human pFASP (pS662), although a change in the conformation of the kinase activation loop created a new peptide-binding channel that led the dPER peptide down toward the bottom of the kinase. We could not visualize density for the peptide after residue 595 in our structure, but substitution of dPER residues G593 or P597 also phenocopies the *per^S* mutation (S589N) [25, 48], suggesting that they also contribute to binding and feedback regulation of the kinase. Furthermore, we observed that phosphorylation of S596, either alone or in combination with S589, enhanced inhibition of CK1 by the PER-Short domain peptide *in vitro*, indicating that additional interactions between the C-terminal half of the PER-Short domain and CK1 may have been occluded by crystal packing.

Despite a high degree of similarity between the kinases, expressing mammalian CK1 variants in *Drosophila* does not always recapitulate their effects on circadian period [21, 33, 57-59]. This could be due to differences in substrate identity or accessibility given changes in the molecular architecture of mammalian and *Drosophila* clocks [60]. However, the differences we observed in the mechanism of CK1 feedback inhibition by human and *Drosophila* PER may contribute to these functional differences as well. In addition to this, allosteric links between anion binding Site 1 and Site 2 in human CK1 profoundly influence the structural dynamics of the activation loop [35] and it is not yet known if the DBT kinase domain exhibits similar dynamics.

Molecular mechanisms that regulate the stable association between PER-CK1, PER stability, and repressive activity appear to be broadly conserved across eukaryotes. Notably, the CK1 binding motifs are conserved in PER homologs from mammals [11, 12], *Drosophila* [45, 47] and *C. elegans* [61], and there is functional conservation with the two helical motifs (FCD1/2) that constitute the CK1 interaction domain in *Neurospora* FRQ [62, 63]. CK1 mediates the repressive activity of PER in the mammalian clock, where cryptochromes facilitate the recruitment of PER1/2-CK1 to the transcription factor CLOCK:BMAL1 in the nucleus, leading to its phosphorylation and displacement from DNA early in the repressive phase [6, 64]. Similar mechanisms of displacement-type repression are also found in *Drosophila* [60] and *Neurospora* (He et al, 2006) circadian clocks. These mechanisms

generally depend on CK1 activity and the strength of kinase anchoring [6, 62], although DBT catalytic activity may not be required for displacement-type repression in *Drosophila* [65]. Our data suggest a model whereby phosphorylation of key regulatory sites in PER close to the CK1BD results in feedback inhibition of CK1, thereby directly regulating the ability of CK1 to phosphorylate PER and possibly other substrates within the circadian clock.

It is not yet clear where in the cell and when in the ~24-hr cycle of the molecular clock that regulation of CK1 activity by the PER pFASP/Per-Short domain occurs. In mammals, PER1/2 form stable complexes with CRY1/2 and CK1 in the cytoplasm [3], although PER proteins remain largely hypophosphorylated until after nuclear entry [4, 66]. PER phosphorylation is counterbalanced by phosphatases in mammals [67-69] and *Drosophila* [70], so further work will be necessary to determine how kinase and phosphatase activity are integrated with other post-translational modifications to regulate FASP/PER-Short phosphorylation and influence feedback regulation of CK1 activity.

3.5 Materials and Methods

Further information and requests for resources and reagents should be directed to and will be fulfilled by the lead contact, Carrie L. Partch (cpartch@ucsc.edu)

Materials availability

- Plasmids generated in this study are available upon request.
- U2OS reporter cell lines generated in this study are available upon request.

Data and code availability

- Data and code generated in this study are available upon request.
- NMR chemical shift assignments for the human FASP peptide have been deposited at BMRB and will be publicly available upon publication. The BMRB entry number is listed in the Key Resources Table.
- Crystal structures of human CK1δ in complex with phosphorylated PER peptides have been deposited to the PDB and will be publicly available upon publication. Accession codes are listed in the Key Resources Table.

Experimental model and subject details

Cell lines

- The HEK293T cell line was purchased from ATCC (#CRL-3216).
- The *Drosophila* S2 cell line was purchased from Thermo Fisher Scientific (#R69007).
- The U2OS cell line was purchased from ATCC (#HTB-96).
 - Generation of *Per* KI cell lines is described in detail in Park et al, 2022.

Per mutant clones in *Per^{Luc}* reporter cell lines

Heterozygous KI clones, H10 for *Per1^{Luc}* and LH1 for *Per2^{Luc}*, were used to generate mutations in *Per1* and *Per2*, respectively. These mRuby3-expressing reporter cells were infected with all-in-one CRISPR adenovirus (*Per2*-E17-S662) or transfected with all-in-one pAdTrack-Cas9-DEST plasmids expressing GFP as described previously [71]. sgRNA sequence and selected clones are summarized in the table below. For clonal isolation of mutant cells, GFP-positive cells were sorted by FACS into 96-well plates, and these clones

were further selected based on alterations in period and/or phase in bioluminescence rhythms. In each project, the majority of putative mutant clones showed a similar degree of period lengthening or shortening in bioluminescence screening. The clones used in this study were fully characterized by sequencing and immunoblotting (**Supplemental File 1a.**)

| Genes | Targets | sgRNA Sequences (PAMs) | Selected clones |
|-------------|-------------------|---------------------------|---|
| <i>Per1</i> | Exon 17 (S714) | GGCCAATAAGGCGGAGAGTG(TGG) | <i>Per1^{Luc}</i> 1, 17, 38 |
| <i>Per2</i> | Exon 17 (S662) | GCCGGGCAAGGCAGAGAGTG(TGG) | <i>Per2^{Luc}</i> 17-1, 17-3, 48, 50 |
| <i>Per2</i> | Exon 17 (H678) | AGCAGCACCATCGTCCATGT(GGG) | <i>Per2^{Luc}</i> 10, 25, 36 |

Expression and purification of recombinant proteins

All proteins were expressed from a pET22-based vector in *Escherichia coli* BL21 (DE3) Rosetta2 cells (Sigma Aldrich) based on the Parallel vector series [72]. The wild-type recombinant FASP peptide (residues 645–687) or PAS-Degron peptide (residues 475–505) were cloned from human PER2. All peptides were expressed downstream of an N-terminal TEV-cleavable His-NusA tag (HNXL). Human CK1 δ catalytic domains (CK1 δ Δ C, residues 1–317 for kinase assays and 1-294 for crystallography) were all expressed in BL21

(DE3) Rosetta2 cells (Sigma Aldrich) with a TEV-cleavable His-GST tag. Mutations were made using standard site-directed mutagenesis protocols and validated by sequencing. All proteins and peptides expressed from Parallel vectors have an N-terminal vector artifact (GAMDPEF) remaining after TEV cleavage and the peptides have a tryptophan and polybasic motif (WRKKK) following the vector artifact. Cells were grown in LB media (for natural abundance growths) or M9 minimal media with the appropriate stable isotopes, i.e., $^{15}\text{N}/^{13}\text{C}$, for NMR as done before [17] at 37°C until the O.D.₆₀₀ reached ~0.8; expression was induced with 0.5 mM IPTG, and cultures were grown for approximately 16–20 hr more at 18°C.

For CK1δ kinase domain protein preps, cells were lysed in 50 mM Tris pH 7.5, 300 mM NaCl, 1 mM TCEP, and 5% glycerol using a high-pressure extruder (Avestin) or sonicator on ice (Fisher Scientific). HisGST-CK1δ ΔC fusion proteins were purified using Glutathione Sepharose 4B resin (GE Healthcare) using standard approaches and eluted from the resin using Phosphate Buffered Saline with 25 mM reduced glutathione. His-TEV protease was added to cleave the His-GST tag from CK1δ ΔC at 4°C overnight. Cleaved CK1δ ΔC was further purified away from His-GST and His-TEV using Ni-NTA resin (Qiagen) and subsequent size exclusion chromatography on a HiLoad 16/600 Superdex 75 prep grade column (GE Healthcare) in 50 mM Tris pH 7.5, 200 mM NaCl, 5 mM BME, 1 mM EDTA, and 0.05% Tween 20. Purified CK1δ ΔC proteins used for *in vitro* kinase assays were buffer exchanged into storage

buffer (50 mM Tris pH 7.5, 100 mM NaCl, 1 mM TCEP, 1 mM EDTA, and 10% glycerol) using an Amicon Ultra centrifugal filter (Millipore) and frozen as small aliquots in liquid nitrogen for storage at -80°C.

For PER2 peptide preps, cells were lysed in a buffer containing 50 mM Tris pH 7.5, 500 mM NaCl, 2 mM TCEP, 5% glycerol and 25 mM imidazole using a high-pressure extruder (Avestin) or sonicator on ice (Fisher Scientific). His-NusA-FASP or His-NusA-PAS-Degron fusion proteins were purified using Ni-NTA resin using standard approaches and eluted from the resin using 50 mM Tris pH 7.5, 500 mM NaCl, 2 mM TCEP, 5% glycerol and 250 mM imidazole. His-TEV protease was added to cleave the His-NusA tag from the PER2 peptides at 4°C overnight. The cleavage reaction was subsequently concentrated and desalted into low imidazole lysis buffer using a HiPrep 26/10 Desalting column. Peptides were purified away from His-NusA and His-TEV using Ni-NTA resin with 50 mM Tris pH 7.5, 500 mM NaCl, 2 mM TCEP, 5% glycerol and 25 mM imidazole. Peptides were purified by size exclusion chromatography on a HiLoad 16/600 Superdex 75 prep grade column, using NMR buffer (25 mM MES pH 6.0, 50 mM NaCl, 2 mM TCEP, 10 mM MgCl₂) or 1x kinase buffer (25 mM Tris pH 7.5, 100 mM NaCl, 10 mM MgCl₂, and 2 mM TCEP) for NMR or ADP-Glo kinase assays, respectively.

NMR kinase assays

NMR spectra were collected on a Varian INOVA 600 MHz or a Bruker 800 MHz spectrometer equipped with a ^1H , ^{13}C , ^{15}N triple resonance z-axis pulsed-field-gradient cryoprobe. Spectra were processed using NMRPipe [73] and analyzed using CCPNmr Analysis [74]. Backbone resonance assignments were made using standard BioPack triple resonance experiments (HNCACB, CBCA (CO)NH, HNCO, HN (CA)CO and HSQC) collected using non-uniform sampling on a sample of 0.5 mM ^{13}C , ^{15}N -labeled FASP in NMR buffer with 10% D_2O . Non-uniform sampling reconstructions were performed using software developed and provided by the Wagner lab [73]. NMR kinase reactions were performed at 25°C with 0.2 mM ^{15}N -FASP, 2.5 mM ATP and 1 μM CK1 δ ΔC (WT or K224D). SOFAST HMQC spectra (total data acquisition = 6 min) were collected at the indicated intervals for 3 hr and relative peak volumes were calculated and normalized as described previously [17]. For PER1 FASP peptide kinase assays, samples were prepared as above and incubated for 2 hrs and then quenched with 20 mM EDTA and then HSQC spectra were collected. Data analysis was performed using Prism (GraphPad), with data fit to either a one-phase exponential or linear regression.

Kinetic modeling

Mathematica 11.0 (Wolfram Research) was used to model the 5-step ordered distributive kinetic model for sequential FASP phosphorylation (**Figure**

3.2a-c). Mathematica code is provided in the supplementary information (**Supplementary File 1c**).

ADP-Glo kinase assays (substrate titrations)

Kinase reactions were performed on the indicated recombinant peptides (FASP WT or Alanine mutants) using the ADP-Glo kinase assay kit (Promega) according to manufacturer's instructions. All reactions were performed in 30 μ L volumes using 1x kinase buffer (25 mM Tris pH 7.5, 100 mM NaCl, 10 mM $MgCl_2$, and 2 mM TCEP) supplemented with ATP and substrate peptides. To determine apparent kinetic parameters K_M and V_{max} , duplicate reactions with 100 μ M ATP and 0.2 μ M CK1 δ Δ C kinase were incubated in 1x kinase buffer at room temperature for 1 hr with the indicated amount of substrate peptide (and repeated for $n = 3$ independent assays). 5 μ L aliquots were taken and quenched with ADP-Glo reagent after the 1 hr incubation, and Luminescence measurements were taken at room temperature with a SYNERGY2 microplate reader (BioTek) in 384-well microplates. Linearity of the 1 hr reaction rate was determined by performing larger reactions (50 μ L) with CK1 δ Δ C and quenching at discrete time points (data not shown). Data analysis was performed using Excel (Microsoft) or Prism (GraphPad).

ADP-Glo kinase assays (peptide inhibition)

Kinase reactions were performed on the recombinant PAS-Degron peptide (**Supplementary Figure 3.2b**) using the ADP-Glo kinase assay kit (Promega) according to manufacturer's instructions. Synthetic peptide inhibitors were solubilized in 1x kinase buffer (25mM Tris pH 7.5, 100 mM NaCl, 10 mM MgCl₂, and 2 mM TCEP) at a concentration of 10 mM. All kinase reactions were performed in 30 μ L reactions supplemented with ATP, PAS-Degron substrate, and synthetic peptide inhibitors. Duplicate reactions (repeated for n = 3 independent assays) with 100 μ M ATP, 0.2 μ M CK1 δ Δ C kinase, and 100 μ M PAS-Degron substrate were incubated in 1x kinase buffer at room temperature for 1 hr in the presence of increasing amounts of synthetic peptide inhibitors (phosphorylated FASP or dPER peptides) as indicated. 5 μ L aliquots were quenched with ADP-Glo reagent after the 1 hr incubation, and luminescence measurements were taken at room temperature with a SYNERGY2 microplate reader (BioTek) in 384-well microplates. Data analysis was performed using Excel (Microsoft) or Prism (GraphPad).

Full-length PER2 kinase assay (peptide inhibition)

HEK293 cells transfected with Myc-PER2 plasmid were lysed in cell lysis buffer (50 mM Tris-HCl pH 8.0, 150 mM NaCl, 1% Nonidet P-40, and 0.5% deoxycholic acid containing Complete protease inhibitors (Roche) and PhosStop phosphatase inhibitors (Roche)). 300 μ g of the protein lysate was

added with 3 μ g of anti-Myc antibody (9E10) and allowed to rotate at 4°C for 1 hr, which was followed by addition of Protein A/G magnetic beads (Thermo Scientific) and rotation at 4°C for 1hr. Then the beads were collected and washed 3x with lysis buffer. Beads were then collected and treated with FastAP alkaline phosphatase (Thermo Scientific) for 30 min at 37°C and washed 3x with lysis buffer and 2x with kinase assay buffer (25 mM Tris pH 7.5, 5 mM beta glycerophosphate, 2 mM DTT and 0.1 mM sodium orthovanadate). CK1 δ Δ C (200 ng) was incubated with either 1 mM of non-phospho (NP) FASP peptide RKKK(mouse PER2 residue 642)TEVSAHLSSLTLPGKAESVVSLTSQ [17] or the human PER2 4pFASP peptide GKAEpSVApSLTpSQcPSYA for 15 min at 25°C. The beads were split into three samples with kinase assay buffer containing 10 mM of magnesium chloride and 200 μ M of ATP. The first portion was left untreated while the second and third were incubated with CK1 δ - Δ C (200 ng) that had been pre-incubated with NP FASP or 4pFASP peptide, respectively, and incubated for 60 min at 25°C. The beads were collected by centrifugation and protein was eluted by adding protein loading dye and analyzed by SDS-PAGE gel for Western blotting with anti-mouse PER2 pSer 659 antibody as previously described [17].

Real-time PER2::LUC half-life measurement

1 μ g of the indicated human PER2::LUC expression plasmids (under a PGK promoter) were transiently transfected alone or with 100 ng myc-CK1 ϵ

(under a CMV promoter) in 35 mm dishes of HEK293T cells in MOPS-buffered high glucose media supplemented with D-luciferin (8.3g/L DMEM, 0.35 mg/mL sodium bicarbonate, 5 mg/mL glucose, 0.02 M MOPS, 100 U/mL penicillin, 100 µg/mL streptomycin, and 100 mM D-luciferin). Dishes were sealed with 40 mm cover glasses and vacuum grease (Sigma Aldrich), and then placed in a LumiCycle 32 (Actimetrics) at 37°C. 24 hrs post transfection, 40 µg/mL cycloheximide (Sigma) was added per 35 mm dish and luminescence recording was initiated. Luminescence data were used to calculate PER2::LUC half-life in Prism (GraphPad) using one-phase decay algorithm as described previously [13], beginning from the point of cycloheximide addition to the plateau at minimum luciferase activity (n ≥ 4).

Co-immunoprecipitation assays

Human myc-PER2, FLAG-CK1δ and FLAG-β-TrCP expression plasmids (1.5 µg, 1.5 µg WT or 0.75 µg K38A, and 3 µg of plasmid DNA, respectively) were co-transfected in 60 mm dishes of HEK293T cells in DMEM supplemented with 1% penicillin/streptomycin and 10% HyClone FetalClone II FBS (Fisher Science). The proteasome was inhibited 16 hrs prior to harvest with 10 µM MG132 (Sigma Aldrich) and cells were harvested 72 hrs post transfection. Cells were lysed in 350 µL mammalian cell lysis buffer (20 mM Tris pH 7.5, 150 mM NaCl, 1mM TCEP, 1% NP-40) supplemented with EDTA-free protease inhibitors (Pierce) and phosphatase inhibitors (1 mM NaF, 1 mM

β -glycerophosphate and 1 mM Na_3VO_4). 30 μL input samples were prepared with 2x SDS sample buffer, and the remaining lysate was incubated with 30 μL of anti-Myc agarose slurry (cat. #sc-40 AC, Santa Cruz Biotechnology) and tumbled overnight at 4°C. Bound samples were washed 3x with 400 μL of IP wash buffer (20 mM Tris pH 7.5, 150 mM NaCl) and 6x SDS sample buffer. All samples were briefly boiled at 95°C and resolved by 7.5% polyacrylamide-SDS gel electrophoresis (PAGE) and transferred to nitrocellulose membrane via Trans-Blot Turbo transfer system (Bio-Rad). Membranes were incubated in TBST blocking buffer (20 mM Tris pH 7.5, 150 mM NaCl, 0.1% TWEEN 20 and 5% (weight/vol, w/v) Marvel dried skimmed milk) for 1 hr and then incubated with antibody (1:2000 α -Myc HRP (cat. #sc-40 HRP), Santa Cruz Biotechnology) or 1/1000 α -OctA HRP (cat. #sc-166355 HRP, Santa Cruz Biotechnology)) in blocking buffer at 4°C overnight. Membranes were washed the next day 3x with TBST and chemiluminescence detection was performed using Immobilon reagent (Millipore) and imaged with ChemiDoc (Bio-Rad). Representative blot shown (n = 3).

Crystallization and structure determination

All peptides were solubilized in a solution of 0.15 M Succinic Acid pH 5.5 and 20% (w/v) PEG 3350 and soaked overnight into crystals of human CK1 δ (1-294) that were crystallized using the hanging drop vapor diffusion method as follows: the 4pFASP peptide was added to CK1 δ crystals that were

crystallized in 0.13 M Succinic Acid pH 5.5 and 27% (w/v) PEG 3350; the 3pFASP peptide was added to CK1 δ crystals that were crystallized in 0.1 M Succinic Acid pH 5.5 and 15% (w/v) PEG 3350; the 2pFASP peptide was added to CK1 δ crystals that were crystallized in 0.15 M Succinic Acid pH 5.5 and 22% (w/v) PEG 3350; and the pS589 peptide was added to CK1 δ crystals that were crystallized in 0.16 M Succinic Acid pH 5.5 and 23% PEG (w/v) 3350. The crystals were looped and briefly soaked in a drop of cryo-preservation solution (80% peptide solution, 20% glycerol) and then flash-cooled in liquid nitrogen for X-ray diffraction data collection. Data sets were collected at the 23-ID-D beamline at the Advanced Photon Source (APS) at the Argonne National Laboratory. Data were indexed, integrated and merged using the CCP4 software suite [75]. Structures were determined by molecular replacement with Phaser MR [76] using the apo structure of wild-type CK1 δ Δ C (PDB: 6PXO). Model building was performed with Coot [77] and structure refinement was performed with PHENIX [78]. All structural models and alignments were generated using PyMOL Molecular Graphics System 2.0 (Schrödinger). X-ray crystallography data collection and refinement statistics are provided in **Table 3.1**.

pLogogram analysis

The Comparative Site Search function of PhosphoSitePlus (v6.6.0.4) [79] was used to obtain a list of known CK1 δ substrates (**Supplementary File**

1b). The substrates were all limited to 15 residues in length with the center residue being the site of phosphorylation. The Sequence Logo Analysis tool from PhosphoSitePlus was used on the resulting dataset to generate a pLogogram indicating the relative frequency of amino acid types in positions flanking the site of phosphorylation.

Molecular dynamics

Molecular modeling: To build the molecular model of 5pFASP-CK1, we started from the 3pFASP x-ray structure and then added E661 and residues 669 to 675 with Maestro (Schrodinger Release 2020-3) in a linear conformation. To avoid artificial interactions arising from the short size of the peptide, we capped the N- and C-terminal residues with acetyl (ACE) and N-methyl amine (NME) groups, respectively. Hydrogens were added with PrepWizard module, and a restrained minimization was to remove potential clashes between the modeled FASP peptide and the enzyme.

System preparation: CK1-5pFASP complex was solvated in a pre-equilibrated TIP3P [80] water box with at least 15 Å between the protein and the box boundaries. The net charge of the system was neutralized with a Na⁺ ion. Parameters for protein residues, capping groups, and Na⁺ were obtained from ff14SB forcefield [81].

Equilibration: Minimization and equilibration were performed with AMBER16 [82] using the following protocol: (i) 2000 steps of energy

minimization with $500 \text{ kcal mol}^{-1} \text{ \AA}^{-1}$ position restraints on all protein atoms; (ii) 5000 steps of energy minimization with $500 \text{ kcal mol}^{-1} \text{ \AA}^{-1}$ position restraints on all CK1 atoms and on the backbone atoms of FASP; (iii) 5000 steps of energy minimization with $500 \text{ kcal mol}^{-1} \text{ \AA}^{-1}$ position restraints on all backbone atoms; (iv) 5000 steps of energy minimization with $500 \text{ kcal mol}^{-1} \text{ \AA}^{-1}$ position restraints on CK1 backbone atoms; (v) 5000 steps of energy minimization without any position restraints; (vi) 50 ps of NVT simulations, with gradual heating of the system to a final temperature of 300 K and $10 \text{ kcal mol}^{-1} \text{ \AA}^{-1}$ position restraints on protein atoms; (vii) 1 ns of NPT simulation with $100 \text{ kcal mol}^{-1} \text{ \AA}^{-1}$ position restraints on protein atoms; and (viii) 1 ns of NPT simulation to equilibrate the density (or final volume of the simulation box).

Simulations: Gaussian accelerated MD simulations (GaMD) were performed in the NVT regime, with a time step of 2 fs. The PME method was used to calculate electrostatic interactions with periodic boundary conditions [83]. To accelerate sampling of the conformational space, we used boost parameters as described in [44]. All systems had a threshold energy $V = V_{\text{max}}$ and were subjected to a dual boost acceleration of both dihedral and total potential energies. To optimize the acceleration parameters, we first ran 2 ns of conventional MD simulation (without boost potentials) during which V_{min} , V_{max} , V_{avg} , and σ_{avg} were recorded and used to calculate boost potentials as previously detailed [44]. These potentials were employed to start 50 ns of preparatory GaMD simulations, during which the boost statistics and boost

potentials were updated until the maximum acceleration was achieved. The maximum acceleration was constrained by setting the upper limit of the standard deviation of the total boost potential to be ≤ 6 kcal/mol. Starting from the same equilibrated structure, we launched 10 independent GaMD simulations with different initial velocities. Each simulation ran for 100 ns, totalizing 1 μ s of sampling time.

Bioluminescence recording of *Per^{Luc}* reporter cell lines

Cells were plated into 24-well plates or 35 mm dishes to be approximately 90% confluent 24 hours prior to the start of the experiment. Immediately before the start of the experiment, cells were given a two-hour serum shock with 50% horse serum in DMEM or 10 μ M forskolin (Sigma Aldrich) in DMEM (Fig S5), washed with phosphate-buffered saline (PBS) and fresh DMEM supplemented with 1% FBS, 7.5 mM sodium bicarbonate, 10 mM HEPES, 25 U/mL penicillin, 25 μ g/mL streptomycin, and 0.1 mM luciferin. The plates were sealed with cellophane tape and the dishes with a 40 mm cover glass and vacuum grease before placing them into a Lumicycle 32 or 96 (Actimetrics). For all bioluminescence experiments, the results were reproduced in at least two independent experiments. Real-time levels, period, and phase of the bioluminescence rhythms were evaluated using the Lumicycle software (Actimetrics). Student's t-test was used to compare data from WT and mutant cells.

Circadian sampling and drug treatments in *Per^{Luc}* reporter cell lines

To measure PER rhythms in WT and mutant cells, cells were seeded in 60 mm dishes to be 90% confluent 24 hours prior to the experiment. These cells were treated with 50% horse serum in DMEM for 2 hrs and harvested at the indicated times. For cycloheximide (CHX) treatment, 8 µg/mL CHX (Sigma Aldrich) was added to cells and cells were collected at specified times after the treatment. For CHX washout experiments, cells were treated with CHX for 8 hrs followed by the normal DMEM, and cells were harvested at the indicated times after the CHX treatment.

Immunoblotting of *Per^{Luc}* reporter cell lines

Cells were harvested from 60 mm dishes and flash-frozen on dry ice. Protein extraction and immunoblotting were performed as previously described [10]. Briefly, cells were homogenized at 4°C in 70 µL extraction buffer (EB) (0.4 M NaCl, 20 mM HEPES pH 7.5, 1 mM EDTA, 5 mM NaF, 1 mM dithiothreitol, 0.3% Triton X-100, 5% glycerol, 0.25 mM phenylmethylsulfonyl fluoride (PMSF), 10 mg/mL aprotinin, 5 mg/mL leupeptin, 1 mg/mL pepstatin A). Homogenates were cleared by centrifugation for 12 min at 12,000 g at 4°C. Supernatants were mixed with 2x SDS sample buffer and boiled. Proteins were separated by electrophoresis through SDS polyacrylamide gels and then transferred to nitrocellulose membranes. Membranes were blocked with 5% (w/v) non-fat dry milk in TBS-0.05% Tween-20 (TBST), incubated with primary

antibodies (GP62 for PER1 and GP49 for PER2 [71]) overnight followed by incubation with secondary antibodies for 1 h. The blots were developed using the WestFemto enhanced chemiluminescence substrate (Thermo Fisher Scientific).

***Drosophila* S2 cell experiments**

The plasmids pMT-*dbt*-V5, pAc-3XFLAG-His-*dper*/Tev100-6Xc-myc [24], pAc-*dper* WT (aa1-1224)-V5, pAc-*dper* S596A (aa1-1224)-V5 [23], pAc-*dper* WT (aa560-1034)-V5 [84] were previously described. pAc-*dper* S596A (aa560-1034)-V5 was generated via PCR mutagenesis using pAc-*dper* WT (aa560-1034)-V5 as a template as described in [23] and the QuikChange II site-directed mutagenesis kit (Agilent). *Drosophila* S2 cells and *Schneider's Drosophila* medium were obtained from Life Technologies (Thermo Fisher Scientific). S2 cells were seeded at 1×10^6 cells/mL in a 6-well plate and transfected using Effectene (Qiagen). S2 cells were co-transfected with 0.2 μ g of pMT-*dbt*-V5, 0.8 μ g of pAc-3X-FLAG-His-*dper*/Tev100-6Xc-myc, and varying amounts of *dper*-V5 plasmids as indicated. Expression of *dbt* was induced with 500 μ M CuSO₄ 36 hours after transfection. Cells were harvested at the indicated time points after kinase induction and extracted with 100-150 μ L EB2 (20 mM Hepes pH 7.5, 100 mM KCl, 5% glycerol, 5 mM EDTA, 1 mM DTT, 0.1% Triton X-100, 25 mM NaF, 0.5 mM PMSF). 1 μ L of AcTEV protease (Thermo Fisher Scientific) was added to protein extracts and incubated 16

hours at 4°C. Following TEV cleavage, protein concentration was measured using Pierce Coomassie Plus Assay Reagents (Thermo Fisher Scientific). 2X SDS sample buffer was added and the mixture boiled at 95°C for 5 minutes. Equal amounts of proteins were resolved by 16% polyacrylamide-SDS gel electrophoresis (PAGE) and transferred to nitrocellulose membrane (Bio-Rad) using a Semi-Dry Transfer Cell (Bio-Rad). Membranes were incubated in 5% Blocking Buffer (Bio-Rad) for 40 minutes at room temperature, and then incubated with anti-FLAG (cat. # F1804, Millipore Sigma) at 1:7000 for 16-20 hours at room temperature. Blots were washed with 1X TBST for 1 hour, incubated with anti-mouse IgG HRP (cat. #12-349, Millipore Sigma) at 1:2000 for 1 hour. After washing, chemiluminescence detection was performed using Clarity ECL reagent in combination with the ChemiDoc imager (Bio-Rad). ImageJ Version 2.0.0-rc-67/1.52d (NIH) was used to quantify hypophosphorylated PER and nonspecific signals (indicated by asterisks). PER signal was normalized to nonspecific signal and the data were scaled with normalized PER signal at 0 hr to a value of 1. Two-way ANOVA with Sidak multiple comparisons test was performed using Prism (GraphPad).

Quantification and statistical analyses

All statistical analyses were done using Prism (Graphpad). P-values were calculated using Student's t-test, one-way ANOVA with Tukey's multiple comparisons test, or two-way ANOVA with Sidak multiple comparisons test as

indicated in different figures. In all figures, * indicates $p < 0.05$, ** $p < 0.01$, *** $p < 0.001$, **** $p < 0.0001$; ns, not significant.

Supplemental File Titles and Legends

Supplementary Table 3.1. Sequencing details for mutant *PER^{Luc}* U2OS cell lines.

Supplementary Table 3.2. PhosphositePlus kinase substrate data set used for pLogogram analysis.

Supplementary Table 3.3. Kinetic modeling of ordered distributive mechanism using Mathematica.

References

1. Takahashi, J.S., *Transcriptional architecture of the mammalian circadian clock*. Nat Rev Genet, 2017. **18**(3): p. 164-179.
2. Koike, N., et al., *Transcriptional architecture and chromatin landscape of the core circadian clock in mammals*. Science, 2012. **338**(6105): p. 349-54.
3. Aryal, R.P., et al., *Macromolecular Assemblies of the Mammalian Circadian Clock*. Mol Cell, 2017. **67**(5): p. 770-782 e6.
4. Lee, C., et al., *Posttranslational mechanisms regulate the mammalian circadian clock*. Cell, 2001. **107**(7): p. 855-67.
5. Michael, A.K., et al., *Formation of a repressive complex in the mammalian circadian clock is mediated by the secondary pocket of CRY1*. Proc Natl Acad Sci U S A, 2017. **114**(7): p. 1560-1565.

6. Cao, X., et al., *Molecular mechanism of the repressive phase of the mammalian circadian clock*. Proc Natl Acad Sci U S A, 2021. **118**(2).
7. Lee, Y., et al., *Stoichiometric relationship among clock proteins determines robustness of circadian rhythms*. J Biol Chem, 2011. **286**(9): p. 7033-42.
8. Chen, R., et al., *Rhythmic PER abundance defines a critical nodal point for negative feedback within the circadian clock mechanism*. Mol Cell, 2009. **36**(3): p. 417-30.
9. Crosby, P. and C.L. Partch, *New insights into non-transcriptional regulation of mammalian core clock proteins*. J Cell Sci, 2020. **133**(18).
10. D'Alessandro, M., et al., *A tunable artificial circadian clock in clock-defective mice*. Nat Commun, 2015. **6**: p. 8587.
11. Eide, E.J., et al., *Control of mammalian circadian rhythm by CKepsilon-regulated proteasome-mediated PER2 degradation*. Mol Cell Biol, 2005. **25**(7): p. 2795-807.
12. Lee, C., D.R. Weaver, and S.M. Reppert, *Direct association between mouse PERIOD and CKepsilon is critical for a functioning circadian clock*. Mol Cell Biol, 2004. **24**(2): p. 584-94.
13. Zhou, M., et al., *A Period2 Phosphoswitch Regulates and Temperature Compensates Circadian Period*. Mol Cell, 2015. **60**(1): p. 77-88.
14. Masuda, S., et al., *Mutation of a PER2 phosphodegron perturbs the circadian phosphoswitch*. Proc Natl Acad Sci U S A, 2020. **117**(20): p. 10888-10896.
15. Ohsaki, K., et al., *The role of {beta}-TrCP1 and {beta}-TrCP2 in circadian rhythm generation by mediating degradation of clock protein PER2*. J Biochem, 2008. **144**(5): p. 609-18.
16. Vanselow, K., et al., *Differential effects of PER2 phosphorylation: molecular basis for the human familial advanced sleep phase syndrome (FASPS)*. Genes Dev, 2006. **20**(19): p. 2660-72.

17. Narasimamurthy, R., et al., *CK1delta/epsilon protein kinase primes the PER2 circadian phosphoswitch*. Proc Natl Acad Sci U S A, 2018. **115**(23): p. 5986-5991.
18. Toh, K.L., et al., *An hPer2 phosphorylation site mutation in familial advanced sleep phase syndrome*. Science, 2001. **291**(5506): p. 1040-3.
19. Jones, C.R., et al., *Genetic basis of human circadian rhythm disorders*. Exp Neurol, 2013. **243**: p. 28-33.
20. Lowrey, P.L., et al., *Positional syntenic cloning and functional characterization of the mammalian circadian mutation tau*. Science, 2000. **288**(5465): p. 483-92.
21. Xu, Y., et al., *Functional consequences of a CK1delta mutation causing familial advanced sleep phase syndrome*. Nature, 2005. **434**(7033): p. 640-4.
22. Xu, Y., et al., *Modeling of a human circadian mutation yields insights into clock regulation by PER2*. Cell, 2007. **128**(1): p. 59-70.
23. Chiu, J.C., H.W. Ko, and I. Edery, *NEMO/NLK phosphorylates PERIOD to initiate a time-delay phosphorylation circuit that sets circadian clock speed*. Cell, 2011. **145**(3): p. 357-70.
24. Chiu, J.C., et al., *The phospho-occupancy of an atypical SLIMB-binding site on PERIOD that is phosphorylated by DOUBLETIME controls the pace of the clock*. Genes Dev, 2008. **22**(13): p. 1758-72.
25. Konopka, R.J. and S. Benzer, *Clock mutants of Drosophila melanogaster*. Proc Natl Acad Sci U S A, 1971. **68**(9): p. 2112-6.
26. Top, D., et al., *CK1/Doubletime activity delays transcription activation in the circadian clock*. Elife, 2018. **7**.
27. Park, J.L., K; Kim, H; Shin, H; Lee, C, *Endogenous circadian reporter cell lines as an efficient platform for studying circadian mechanisms*. Co-submitted with this manuscript, 2022.

28. Smith, M.J., et al., *Real-time NMR monitoring of biological activities in complex physiological environments*. *Curr Opin Struct Biol*, 2015. **32**: p. 39-47.
29. Flotow, H., et al., *Phosphate groups as substrate determinants for casein kinase I action*. *J Biol Chem*, 1990. **265**(24): p. 14264-9.
30. Cordier, F., et al., *Ordered phosphorylation events in two independent cascades of the PTEN C-tail revealed by NMR*. *J Am Chem Soc*, 2012. **134**(50): p. 20533-43.
31. Shinohara, Y., et al., *Temperature-Sensitive Substrate and Product Binding Underlie Temperature-Compensated Phosphorylation in the Clock*. *Mol Cell*, 2017. **67**(5): p. 783-798 e20.
32. Longenecker, K.L., P.J. Roach, and T.D. Hurley, *Three-dimensional structure of mammalian casein kinase I: molecular basis for phosphate recognition*. *J Mol Biol*, 1996. **257**(3): p. 618-31.
33. Venkatesan, A., et al., *The Circadian tau Mutation in Casein Kinase 1 Is Part of a Larger Domain That Can Be Mutated to Shorten Circadian Period*. *Int J Mol Sci*, 2019. **20**(4).
34. Zeringo, N.A. and J.J. Bellizzi, 3rd, *A PER2-derived mechanism-based bisubstrate analog for casein kinase 1epsilon*. *Chem Biol Drug Des*, 2014. **84**(6): p. 697-703.
35. Philpott, J.M., et al., *Casein kinase 1 dynamics underlie substrate selectivity and the PER2 circadian phosphoswitch*. *Elife*, 2020. **9**.
36. Flotow, H. and P.J. Roach, *Role of acidic residues as substrate determinants for casein kinase I*. *J Biol Chem*, 1991. **266**(6): p. 3724-7.
37. Marin, O., et al., *A noncanonical sequence phosphorylated by casein kinase 1 in beta-catenin may play a role in casein kinase 1 targeting of important signaling proteins*. *Proc Natl Acad Sci U S A*, 2003. **100**(18): p. 10193-200.

38. Isojima, Y., et al., *CKIepsilon/delta-dependent phosphorylation is a temperature-insensitive, period-determining process in the mammalian circadian clock*. Proc Natl Acad Sci U S A, 2009. **106**(37): p. 15744-9.
39. Wu, G., et al., *Structure of a beta-TrCP1-Skp1-beta-catenin complex: destruction motif binding and lysine specificity of the SCF(beta-TrCP1) ubiquitin ligase*. Mol Cell, 2003. **11**(6): p. 1445-56.
40. Reischl, S., et al., *Beta-TrCP1-mediated degradation of PERIOD2 is essential for circadian dynamics*. J Biol Rhythms, 2007. **22**(5): p. 375-86.
41. Cullati, S.N., et al., *Kinase domain autophosphorylation rewires the activity and substrate specificity of CK1 enzymes*. Mol Cell, 2022.
42. Nolen, B., S. Taylor, and G. Ghosh, *Regulation of protein kinases; controlling activity through activation segment conformation*. Mol Cell, 2004. **15**(5): p. 661-75.
43. Gallego, M., et al., *An opposite role for tau in circadian rhythms revealed by mathematical modeling*. Proc Natl Acad Sci U S A, 2006. **103**(28): p. 10618-23.
44. Miao, Y., V.A. Feher, and J.A. McCammon, *Gaussian Accelerated Molecular Dynamics: Unconstrained Enhanced Sampling and Free Energy Calculation*. J Chem Theory Comput, 2015. **11**(8): p. 3584-3595.
45. Kim, E.Y., et al., *A DOUBLETIME kinase binding domain on the Drosophila PERIOD protein is essential for its hyperphosphorylation, transcriptional repression, and circadian clock function*. Molecular and Cellular Biology, 2007. **27**(13): p. 5014-5028.
46. Kivimae, S., L. Saez, and M.W. Young, *Activating PER repressor through a DBT-directed phosphorylation switch*. PLoS Biol, 2008. **6**(7): p. e183.
47. Nawathean, P., D. Stoleru, and M. Rosbash, *A small conserved domain of Drosophila PERIOD is important for circadian phosphorylation,*

- nuclear localization, and transcriptional repressor activity.* Mol Cell Biol, 2007. **27**(13): p. 5002-13.
48. Baylies, M.K., et al., *New short period mutations of the Drosophila clock gene per.* Neuron, 1992. **9**(3): p. 575-81.
 49. Rothenfluh, A., M. Abodeely, and M.W. Young, *Short-period mutations of per affect a double-time-dependent step in the Drosophila circadian clock.* Curr Biol, 2000. **10**(21): p. 1399-402.
 50. Rutila, J.E., et al., *The analysis of new short-period circadian rhythm mutants suggests features of D. melanogaster period gene function.* J Neurogenet, 1992. **8**(2): p. 101-13.
 51. Graves, P.R. and P.J. Roach, *Role of COOH-terminal phosphorylation in the regulation of casein kinase I delta.* J Biol Chem, 1995. **270**(37): p. 21689-94.
 52. Dyla, M., et al., *The optimal docking strength for reversibly tethered kinases.* Proc Natl Acad Sci U S A, 2022. **119**(25): p. e2203098119.
 53. Marzoll, D., et al., *Casein kinase 1 and disordered clock proteins form functionally equivalent, phospho-based circadian modules in fungi and mammals.* Proc Natl Acad Sci U S A, 2022. **119**(9).
 54. Durgan, D.J., et al., *O-GlcNAcylation, novel post-translational modification linking myocardial metabolism and cardiomyocyte circadian clock.* J Biol Chem, 2011. **286**(52): p. 44606-19.
 55. Kaasik, K., et al., *Glucose sensor O-GlcNAcylation coordinates with phosphorylation to regulate circadian clock.* Cell Metab, 2013. **17**(2): p. 291-302.
 56. Levine, D.C., et al., *NAD(+) Controls Circadian Reprogramming through PER2 Nuclear Translocation to Counter Aging.* Mol Cell, 2020. **78**(5): p. 835-849 e7.

57. Fan, J.Y., et al., *Drosophila and vertebrate casein kinase Idelta exhibits evolutionary conservation of circadian function*. Genetics, 2009. **181**(1): p. 139-52.
58. Xing, L., et al., *Correlated evolution between CK1delta Protein and the Serine-rich Motif Contributes to Regulating the Mammalian Circadian Clock*. J Biol Chem, 2017. **292**(1): p. 161-171.
59. Sekine, T., et al., *Casein kinase I epsilon does not rescue double-time function in Drosophila despite evolutionarily conserved roles in the circadian clock*. J Biol Rhythms, 2008. **23**(1): p. 3-15.
60. Patke, A., M.W. Young, and S. Axelrod, *Molecular mechanisms and physiological importance of circadian rhythms*. Nat Rev Mol Cell Biol, 2020. **21**(2): p. 67-84.
61. Jeon, M., et al., *Similarity of the C. elegans developmental timing protein LIN-42 to circadian rhythm proteins*. Science, 1999. **286**(5442): p. 1141-6.
62. Liu, X., et al., *FRQ-CK1 interaction determines the period of circadian rhythms in Neurospora*. Nat Commun, 2019. **10**(1): p. 4352.
63. He, Q., et al., *CKI and CKII mediate the FREQUENCY-dependent phosphorylation of the WHITE COLLAR complex to close the Neurospora circadian negative feedback loop*. Genes Dev, 2006. **20**(18): p. 2552-65.
64. Chiou, Y.Y., et al., *Mammalian Period represses and de-represses transcription by displacing CLOCK-BMAL1 from promoters in a Cryptochrome-dependent manner*. Proc Natl Acad Sci U S A, 2016. **113**(41): p. E6072-E6079.
65. Yu, W., et al., *DOUBLETIME plays a noncatalytic role to mediate CLOCK phosphorylation and repress CLOCK-dependent transcription within the Drosophila circadian clock*. Mol Cell Biol, 2009. **29**(6): p. 1452-8.

66. Beesley, S., et al., *Wake-sleep cycles are severely disrupted by diseases affecting cytoplasmic homeostasis*. Proc Natl Acad Sci U S A, 2020. **117**(45): p. 28402-28411.
67. Gallego, M., H. Kang, and D.M. Virshup, *Protein phosphatase 1 regulates the stability of the circadian protein PER2*. Biochemical Journal, 2006. **399**: p. 169-175.
68. Lee, H.M., et al., *The period of the circadian oscillator is primarily determined by the balance between casein kinase 1 and protein phosphatase 1*. Proceedings of the National Academy of Sciences of the United States of America, 2011. **108**(39): p. 16451-16456.
69. Schmutz, I., et al., *Protein Phosphatase 1 (PP1) Is a Post-Translational Regulator of the Mammalian Circadian Clock*. Plos One, 2011. **6**(6).
70. Sathyanarayanan, S., et al., *Posttranslational regulation of Drosophila PERIOD protein by protein phosphatase 2A*. Cell, 2004. **116**(4): p. 603-15.
71. Jin, Y.H., et al., *Streamlined procedure for gene knockouts using all-in-one adenoviral CRISPR-Cas9*. Sci Rep, 2019. **9**(1): p. 277.
72. Sheffield, P., S. Garrard, and Z. Derewenda, *Overcoming expression and purification problems of RhoGDI using a family of "parallel" expression vectors*. Protein Expr Purif, 1999. **15**(1): p. 34-9.
73. Delaglio, F., et al., *NMRPipe: a multidimensional spectral processing system based on UNIX pipes*. J Biomol NMR, 1995. **6**(3): p. 277-93.
74. Vranken, W.F., et al., *The CCPN data model for NMR spectroscopy: development of a software pipeline*. Proteins, 2005. **59**(4): p. 687-96.
75. Winn, M.D., et al., *Overview of the CCP4 suite and current developments*. Acta Crystallogr D Biol Crystallogr, 2011. **67**(Pt 4): p. 235-42.
76. McCoy, A.J., et al., *Phaser crystallographic software*. J Appl Crystallogr, 2007. **40**(Pt 4): p. 658-674.

77. Emsley, P., et al., *Features and development of Coot*. Acta Crystallogr D Biol Crystallogr, 2010. **66**(Pt 4): p. 486-501.
78. Adams, P.D., et al., *The Phenix software for automated determination of macromolecular structures*. Methods, 2011. **55**(1): p. 94-106.
79. Hornbeck, P.V., Zhang, B., Murray, B., Kornhauser, J.M., Latham, V., Skrzypek, E., *PhosphoSitePlus, 2014: mutations, PTMs and recalibrations*. Nucleic Acids Res., 2015. **43**:D512-20.
80. Jorgensen, W.L., et al., *Comparison of Simple Potential Functions for Simulating Liquid Water*. Journal of Chemical Physics, 1983. **79**(2): p. 926-935.
81. Maier, J.A., et al., *ff14SB: Improving the Accuracy of Protein Side Chain and Backbone Parameters from ff99SB*. Journal of Chemical Theory and Computation, 2015. **11**(8): p. 3696-3713.
82. Case, D.A., Betz, R.M., Cerutti, D.S., Cheatham III, D.E., Darden, T.A., Duke, R.E., Giese, T.J., Gohlke, H., Goetz, A.W., Homeyer, N., et al., *AMBER 16*. 2016: (University of California, San Francisco).
83. Darden, T., D. York, and L. Pedersen, *Particle Mesh Ewald - an N.Log(N) Method for Ewald Sums in Large Systems*. Journal of Chemical Physics, 1993. **98**(12): p. 10089-10092.
84. Ko, H.W., et al., *A hierarchical phosphorylation cascade that regulates the timing of PERIOD nuclear entry reveals novel roles for proline-directed kinases and GSK-3beta/SGG in circadian clocks*. J Neurosci, 2010. **30**(38): p. 12664-75.

Chapter 4

Future Directions

4.1 Dissecting the molecular level details of CK1 dynamics and substrate selectivity

4.1.2 Summary

In this section, I summarize the progress I have made on a project related to the molecular determinants of CK1 activity on the FASP priming site and the allosteric regulation of CK1 identified via our molecular dynamics (MD) collaboration with Clarisse Ricci. These MD simulations shed light on CK1 recognition of an unprimed FASP peptide and the biochemical experiments I performed are in agreement with the MD model. The allosteric activation loop switch identified in Chapter 2 is further analyzed to uncover the network of residues that allosterically communicate information from anion binding Site 1 and the activation loop, providing a mechanism to reshape the free energy landscape of the activation loop conformation in the CK1 *tau* mutation. I then highlight preliminary biochemical experiments that I performed to disrupt the activation loop switch, with results that were in agreement with MD.

4.1.3 Molecular dynamics and biochemistry support a model for priming of the FASP region

Priming of the PER2 FASP region represents a crucial rate-limiting step in the regulation of circadian timing [1]. Activity at this initial site within the FASP serine cluster essentially gates the sequential phosphorylation of downstream serines that leads to the stabilization of PER2 [1]. Moreover, as discussed in Chapter 3, I showed that the phosphorylated FASP feedback inhibits CK1 activity and likely influences kinase activity on other clock components given the stable anchoring of PER and CK1 throughout the circadian cycle. To further extend our understanding of the critical FASP priming step, our collaborator Clarisse Ricci performed preliminary Gaussian accelerated molecular dynamics simulations (GaMD) starting from a modeled structure of a complex with CK1 and a p63 PAD peptide [2] (**Figure 4.1a**). Applying a distance cutoff between the phospho-accepting serine within the substrate and the ultimate phosphate of ATP allowed for the filtering of “productively bound” states that represent catalytically prone conformations. Upon clustering analysis of the resulting conformations, clusters representing binding modes with FASP in an extended conformation displayed lower atomic fluctuations accumulated by residue (RMSF), suggesting that these binding modes are more stable and realistic (**Figure 4.1b**). Analysis of the representative cluster 4 revealed consistent interactions that were observed within the productive states. In this binding mode, the lysine at position -3 forms a salt bridge with the β phosphate

of ATP, often assisted by residue D132 of CK1 located just downstream of the catalytic HRD motif (**Figure 4.1c**). The -1 Glu forms salt bridges with R178 or K224 for a significant amount of time over the course of the MD simulations (**Figure 4.1d**). C-terminal to the priming serine, the +1 valine residue fits into a small hydrophobic pocket created between Y225 and L173 of the activation loop (**Figure 4.1e**), nearly identical to +1 branched chain residue observed in the binding of pFASP [3] and phosphorylated PAD structures [2] (see chapter 3). This small +1 hydrophobic pocket is therefore a likely determinant of substrate specificity, precluding substrates with bulkier residues in this position from binding within the substrate cleft. The interaction with the small +1 hydrophobic residue and Y225 also suggests a stabilizing mechanism for locking the activation loop in the downward conformation.

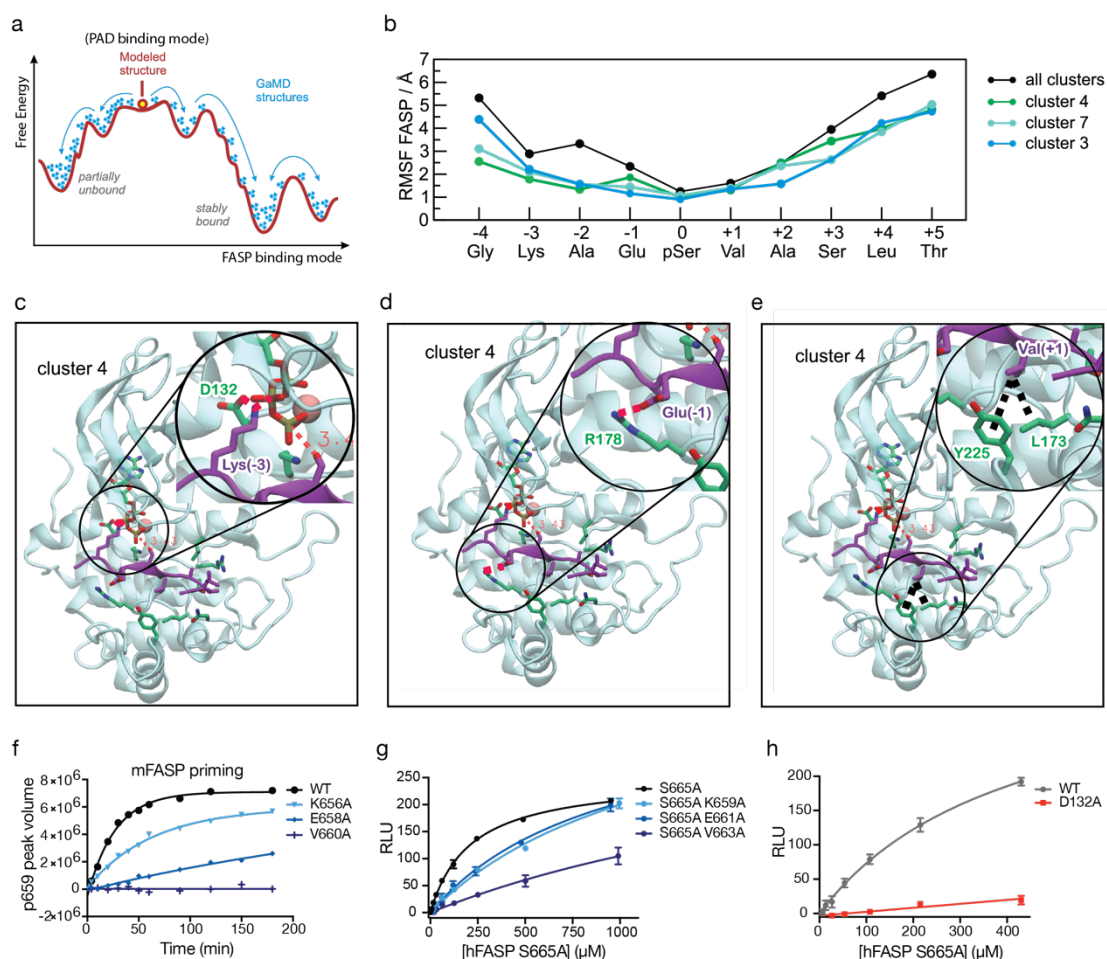


Figure 4.1. Biochemistry and molecular dynamics of modeled CK1:FASP complex suggest priming mechanism

a. Schematic representation of molecular dynamics experiment. CK1:PAD crystal structure was used as starting point, with residues in PAD mutated to corresponding FASP residues. **b.** Atomic fluctuations accumulated by residues (RMSF) down to -4 and up to +5 of the priming serine in FASP. **c,d,e.** CK1:FASP conformations extracted from GaMD simulations highlighting key interactions between the kinase and FASP substrate. **f.** NMR kinase assay monitoring priming activity as the accumulation of peak volume corresponding to pS659 of mFASP (spectra not shown). **g.** Substrate titration of hFASP mutants in priming only (S665A) background (see Figure 3.1). RLU (Relative Luminescence Units). Data are mean and SD of $n = 2$ replicates. **h.** Titration of hFASP S665A (priming-only) substrate comparing CK1 WT and D132A, data are mean and SD of $n = 2$ replicates.

To confirm the importance of these residues for substrate selective mechanism of FASP priming, we used the NMR kinase assay [1, 3, 4] with alanine mutants at these positions to monitor CK1 priming activity. Using the same mouse FASP peptide from chapter 2 [4], we observed lower priming activity for these mutants as compared to the WT substrate (**Figure 4.1f**), with the +1 valine showing the most dramatic loss in activity. To get a better sense of the effect of these mutations in the context of the extended human FASP peptide [3], we performed substrate titrations using FASP mutants that also contained the S665A mutation that halts kinase activity after the priming site [3]. In this context the mutants also showed decreased priming activity, with the +1 valine also having the most dramatic effect (**Figure 4.1g**). Alternatively, the CK1 D132A mutation also decreased kinase activity on a FASP S665A substrate (**Figure 4.1h**); however, it is possible that this result is partly due to effects on nucleotide binding, since D132 makes contacts with the β phosphate of ATP in the MD structure (**Figure 4.1c**). Taken together, these results support a possible binding mode for FASP priming and help to explain the importance of the +1 residue for substrate selectivity. Moreover, our lab has shown that K659 is acetylated by CBP (data not shown) and it is known that other PTMs such as O-GlcNAcylation occur at the priming and downstream serines [5, 6]. These PTMs provide a likely mechanism for integrating metabolic cues with the circadian clock, as they are positioned to affect the rate-limiting step of FASP phosphorylation which has far reaching consequences on circadian timing.

The free energy landscape of the activation loop is governed by an allosteric network

As previously described in Chapter 2, the conformation of the CK1 activation loop is controlled by allosteric coupling between anion binding Sites 1 and 2, located on either side of the substrate binding cleft [4]. The CK1 *tau* mutation disrupts anion binding at Site 1, leading to altered dynamics within the activation loop switch to remodel the substrate binding cleft [4]. Here we extend this analysis to describe the differences in the free energy landscape between WT and *tau* activation loop conformations. Our collaborator Clarisse Ricci performed Adaptive Biasing Force (ABF) simulations of CK1 to characterize the conformational landscape of the activation loop, using the RMSD values of residues 151 to 185 with respect to the 'loop down' and 'loop up' conformations obtained from crystal structures. The resulting two-dimensional free energy landscapes further suggest the *tau* mutation stabilizes the loop up conformation (**Figure 4.2a**). The loop down conformation is the most stable for WT, whereas the conformational landscape is significantly altered by the *tau* mutation to bias the conformational equilibrium toward the loop up conformation (**Figure 4.2a**).

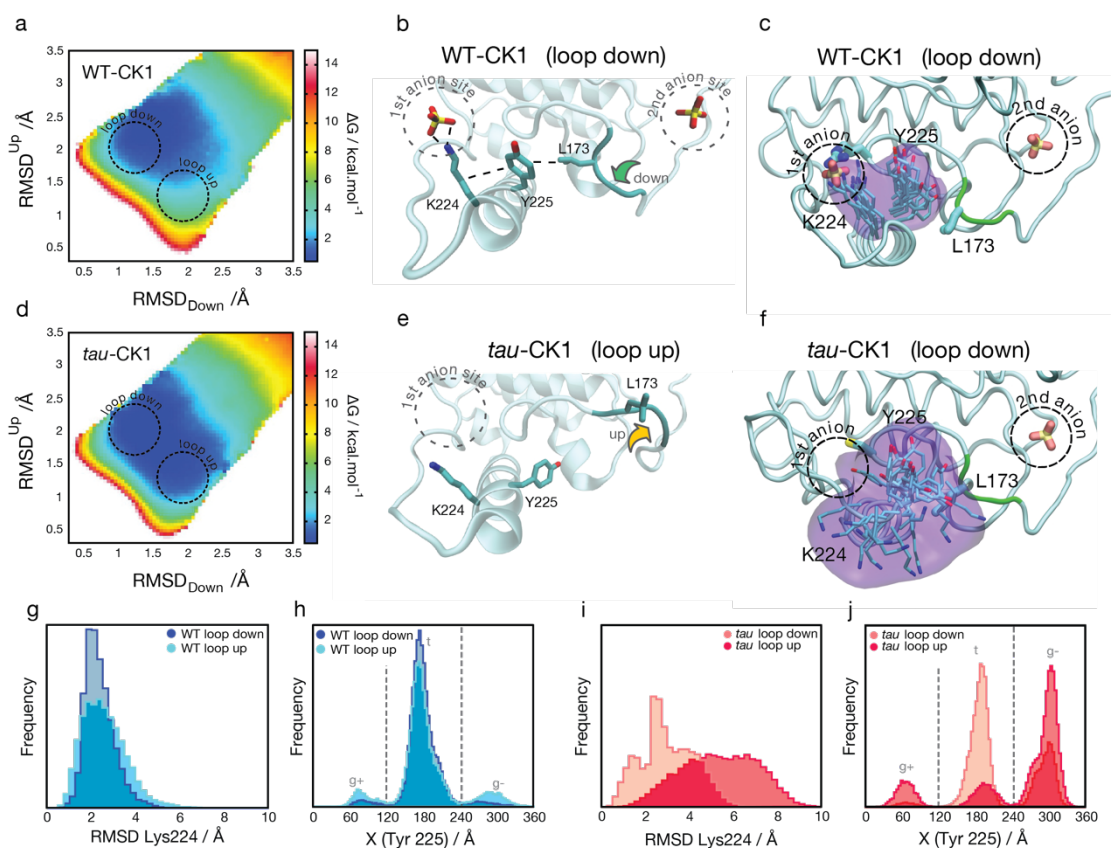


Figure 4.2. The *tau* mutation allosterically reshapes the free energy landscape of the CK1 substrate binding region

a. Two-dimensional free energy landscape of CK1 WT activation loop. **b.** Extracted frame from MD simulation of CK1 WT depicting key interactions between anion, K224, Y225 and L173, coupling anion binding Site 1 to the activation loop. **c.** Overlay of representative K224 and Y225 conformations observed in CK1 WT simulations showing restricted mobility and strong coupling between Y225 and L173. **d.** Two-dimensional free energy landscape of CK1 *tau* activation loop, showing low energy ‘loop up’ conformation. **e.** Extracted frame from MD simulation of CK1 *tau*. **f.** Overlay of K224 and Y225 conformations observed in *tau* simulations. K224 frequently adopts solvent exposed orientations increasing the mobility of Y225 and decreasing the coupling between Y225 and L173. **g,i.** RMSD distribution of K224 in CK1 WT and *tau* simulations comparing loop conformations. **h,j.** Distribution of *gouche+* (*g+*), *trans* (*t*), and *gouche-* (*g-*) rotamers for Y225 in CK1 WT and *tau* simulations.

We then examined the RMSD of residues connecting Site 1, the activation loop, and Site 2 to gain a deeper insight into how the *tau* mutation can allosterically control the equilibrium dynamics of the activation loop. By extracting conformations of CK1 WT and *tau* from the MD simulations, we observed that Y225 forms interactions with L173 of the activation loop when it is in the downward conformation, and further, Y225 can also interact with the sidechain of its neighbor, K224. These interactions could transfer information from Site 1, from K224 through Y225 to the activation loop (**Figure 4.2b**).

In CK1 WT, when Site 1 is occupied by an anion, K224 is locked into a conformation that allows Y225 to remain in a position that is strongly coupled to L173, locking the activation loop in the downward conformation (**Figure 4.2c**). A transition from the downward conformation to the upward conformation would likely demand a concerted rearrangement of the bulky sidechain of Y225, which is less flexible when K224 is locked into position by coordination of an anion in Site 1. By contrast, the *tau* mutation (R178C [7]) remodels the free energy landscape, resulting in a low energy conformation of the 'loop up' conformation (**Figure 4.2d**). The *tau* mutation creates a more hydrophobic environment in Site 1, imparting significantly more mobility freedom for K224. Consequently, Y225 also displays higher mobility and loses coupling with L173 and the ability to lock the activation loop in the downward conformation (**Figure 4.2d-e**). By monitoring the RMSD of K224 and the 1st X dihedral angle of Y225, we found that the conformational flexibility gained by K224 as a result of the

tau mutation led to an altered distribution of conformations available for Y225, with the most stable conformation in WT now being the most unstable in *tau* (**Figure 4.2g-j**). These results provide strong evidence for how the *tau* mutation reshapes the free energy landscape of the CK1 activation loop to significantly remodel the substrate binding cleft. As suggested by other eukaryotic kinases such as PKA, communication is mainly driven by entropy-driven allostery, where rather than large conformational rearrangements or folding/unfolding of domains, communication is achieved by changes in the dynamic properties of residues [8]. By further developing our understanding of the allosteric networks present in CK1 we can gain deeper insight into the substrate selectivity mechanisms that regulate kinase activity at the PER2 FASP and Degron regions.

Targeting the allosteric network interactions disrupts kinase activity on the Degron

As elaborated on in the previous section, CK1 dynamics and substrate selectivity are allosterically regulated. In Chapter 2, we showed that the L173A mutation significantly reduced CK1 activity on both FASP and Degron substrates, leading to a global decrease in kinase activity but leading to a similar half-life for PER2 by maintaining a FASP/Degron efficiency ratio similar to CK1 WT [4]. Loss of kinase activity is likely due to disruption of the allosteric network as discussed above. To further examine the effect of mutations on

residues within this network, we performed Y225A and H185A mutations based on the interactions observed between these residues in the crystal structures (**Figure 4.3a-b**). Like L173A, the Y225A and H185A mutations reduced CK1 activity on the Degron, suggesting that the coupling interactions between these residues is important for CK1 activity on the Degron (**Figure 4.3c**). Future studies that integrate structure, molecular dynamics and mutational analysis will help to provide a deeper understanding of how CK1 alleles with altered circadian phenotypes influence kinase activity and influence circadian timing.

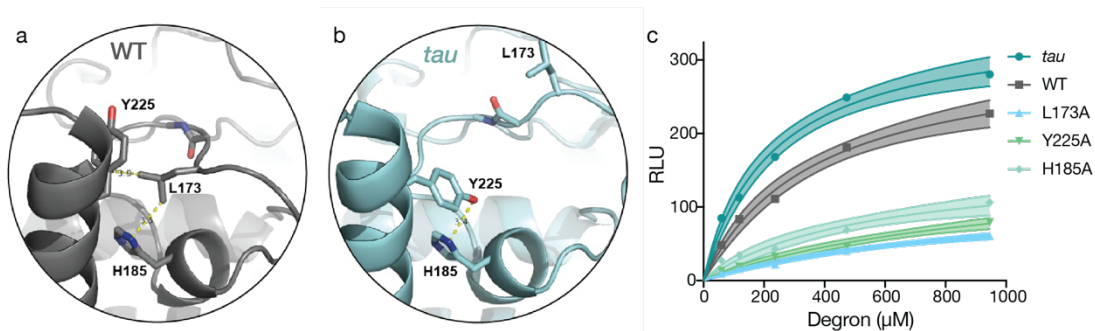


Figure 4.3. Mutation of interacting residues identified within allosteric network disrupt kinase activity on Degron peptide

a. Zoom of CK1 WT crystal structure showing interactions between Y225 and L173, and L173 and H185. **B.** Zoom of CK1 *tau* crystal structure showing interaction between Y225 and H185. **C.** Substrate titration of Degron peptide comparing kinase activity between CK1 mutants. L173A, Y225A and H185A similarly reduce kinase activity on the Degron. Data are mean and SD of $n = 2$ replicates.

4.2 Molecular determinants of the CK1 activity and β -TrCP recruitment at the PER2 degron

4.2.1 Summary

In this section, I focus on the degradation arm of the PER2 phosphoswitch model. I provide a discussion of the molecular features of the PER2 PAS-degron and suggest future experiments to elucidate the mechanism of β -TrCP recruitment. I conduct preliminary experiments to confirm that the β -TrCP recognition motif in hPER2 functions similarly to that of mPER2, and that the gain of function by CK1 tau for the mPER2 Degron is recapitulated in the context of hPER2 substrates, with the predominant gain of function shown to be at residues other than the two serines of the β -TrCP recognition motif. I further examine the site-specific phosphorylation of the Degron by CK1 and, as a proof of principle, show that kinase activity within the Degron is observable in the context of the tandem PAS domains. I also discuss future directions to uncover whether CK1 activity in the Degron follows an ordered mechanism and suggest that preliminary results support a model where the gain of function for S478 by CK1 *tau*, as observed by phosphospecific antibody, could be templated by phosphorylation of alternate residues within the Degron.

4.2.2 Molecular features of the β -TrCP recognition motif in the context of the PER2 PAS-Degron

As discussed throughout the preceding chapters, the phosphodegron located immediately downstream of the tandem PAS-domains in hPER2 shares a conserved recognition motif (DSG Φ XS) with other known β -TrCP substrates [9], such as β -Catenin (**Figure 4.4a**). Although the hPER2 sequence does not possess the invariant Asp residue which precedes the first phosphorylation site, it has been suggested that the serine in this position may be phosphorylated to generate a motif that more closely matches the consensus motif [10]. When the substrate becomes doubly phosphorylated at the indicated residues within the motif, it becomes competent for binding and directing the ubiquitination activity of the fully assembled E3 ligase (**Figure 4.4b**), SCF ^{β -TrCP¹}, on nearby lysine residues [9-11]. The interdomain distance of approximately 50+ Å between the face of the β -TrCP and the E2 active Cystine has been shown to optimally increase the effective concentration of lysine residues between 9-13 residues downstream of the β -TrCP recognition motif [9]. A crystal structure of β -TrCP and a doubly phosphorylated B-catenin peptide reveal a binding mode where the intramolecular distance between the two phosphorylated serine residues of the substrate is approximately 13.4 Å (**Figure 4.4c**), and the entire motif binds to the pocket formed on the face of the WD40 repeat domain of β -TrCP [9]. The Gly residue after the N-terminal

pSer residue extends downward into the cavity at the center of the WD40 repeat structure and is likely a determinant of substrate specificity due to its smaller size, as other residues in this position may be sterically occluded.

The PER2 PAS domains facilitate homo/heterodimerization of PER molecules [12, 13]. The crystal structure of the tandem mPER2 domains [12] (3GDI) reveal a dimeric structure of the PAS domains where the intrinsically disordered Degron regions of each monomer are poised to protrude from the same face of the dimer. A homology model of an AlphaFold2 hPER2 structure containing residues from PAS-A to the end of the Degron motif was used to visualize the proximity of the two motifs from each of the monomers. Interestingly, the intermolecular distance between the first Ser residues (S480) of each hPER2 molecule has an approximate distance (12.4 Å) that is remarkably similar to the intramolecular distance between the two Ser residues within the linear recognition motif (**Figure 4.4c-d**). While there is some evidence that dimerization of PER2 alters protein stability [12, 14], and that a mutation within the interdomain linker alters the flexibility of the PAS-B / Ja linker to influence β -TrCP binding, PER2 stability and circadian rhythms in mice [15], it is not well understood whether dimerization influences the recruitment of β -TrCP. There are known instances of structurally formed consensus recognition motifs, where residues are brought together in a spatial conformation that is similar to the linear recognition motif [16]. Given the localization of the two Degron motifs in the PAS-Deg dimer (**Figure 4.4d**), it

would be interesting to examine whether a structurally formed recognition motif contributes to β -TrCP recruitment in the context of PER2 dimerization.

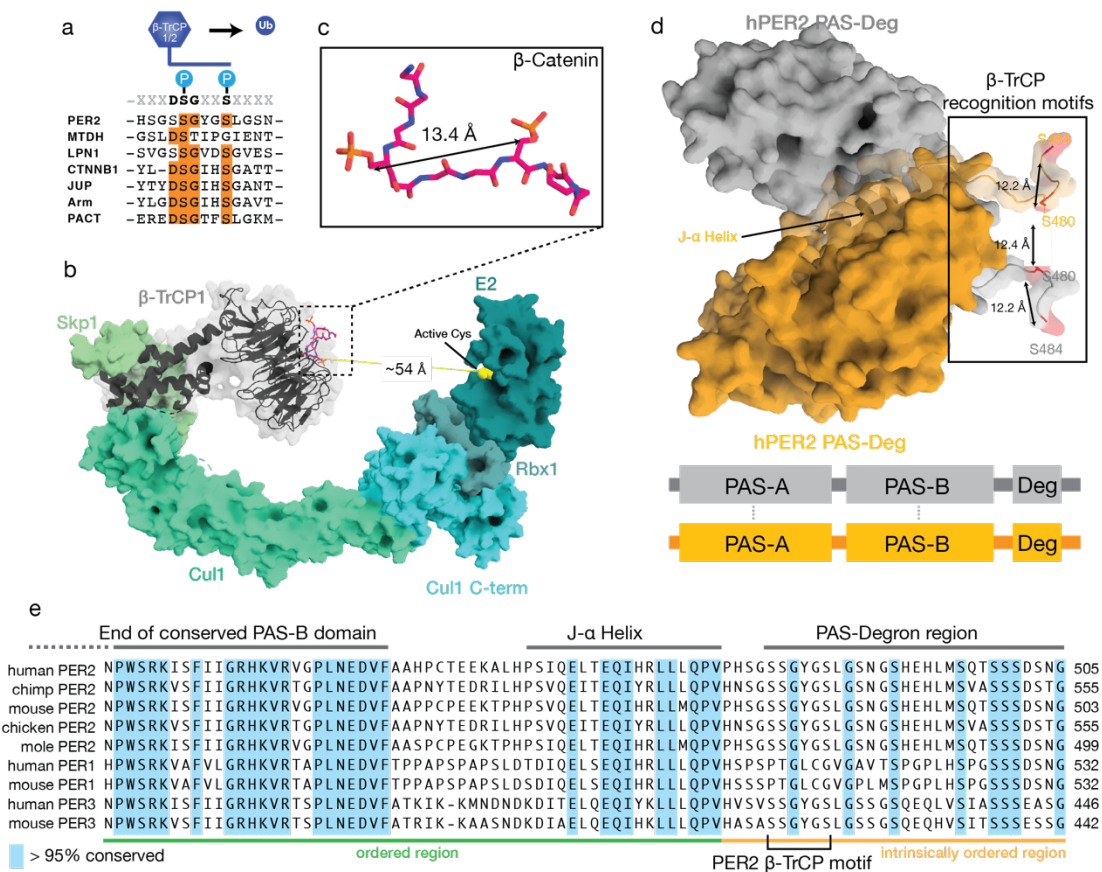


Figure 4.4. The hPER2 β-TrCP recognition motif has unique molecular features

a. Multiple sequence alignment showing conservation of hPER2 β-TrCP recognition motif with other known β-TrCP substrates. **b.** Model of SCF^{β-TrCP1} complex with phosphorylated β-catenin peptide bound. Model was constructed based on procedure outlined in Wu et al., 2003. **c.** Zoom of β-catenin peptide showing distance between phosphorylated Ser residues. **d.** Domain architecture and homology model of hPER2 PAS-Degron homodimer. Model was constructed using an AlphaFold2 model of hPER2 PAS-Deg monomer aligned to crystal structure of the mPER2 PAS-domain dimer (3GD1). The β-TrCP recognition motif extends from the J-α helix of each monomer and protrudes from the dimer interface in close proximity. **e.** Multiple sequence alignment of mammalian PERIOD proteins, highlighting key structural and conserved features.

A key feature of the PAS domain architecture is a C-terminal structure motif known as the J α helix (**Figure 4.4d**). The J α helix is important for signaling by LOV domains [17], where binding between the J α helix and its adjacent, structured PAS domain is regulated by conformational changes as a response to light [17]. It is also worth noting that the hPER J α helix contains a sequence that contains a functionally important nuclear export signal (NES) sequence [12, 18] (**Figure 4.4e**) that directs cytoplasmic accumulation when fused to a heterologous protein [18]. This sequence is hidden in the crystal structure by forming contacts with the PAS-B domain. Moreover, there is a lysine residue located within the interdomain linker between PAS-B and the J α helix (**Figure 4.4e**) that could be a potential site for ubiquitination, as it is located nearly the ideal distance from the β -TrCP recognition motif [9]. These molecular details raise questions of whether the dynamics between the J α helix and the PAS domains regulate CK1 activity at the Degron, ubiquitination activity near the Degron, recruitment of β -TrCP, the nuclear export of hPER2 and/or some combination of all of these.

4.2.3 Phosphorylation of S480 is a key determinant of β -TrCP recruitment

While mutation of S478 of mPER2 increases PER stability, disrupts β -TrCP recruitment and lengthens circadian period [11, 19], the equivalent residue in hPER2, S480, has not yet been studied. Preliminary experiments suggest that mutation S480A in hPER2 disrupts β -TrCP binding and stabilizes

hPER2 (**Figure 4.5a-c**). Perhaps interestingly, while the CK1 *tau* mutation increases the recruitment of β -TrCP as expected, hPER2 S480A also shows enhanced β -TrCP recruitment in the context of CK1 *tau* (**Figure 4.5b**). While this result will require further exploring, this could be consistent with a gain of function for CK1 *tau* at a site other than S480, such as S484 or another serine residue located nearby, or even at an auxiliary region such as the N-terminal Degron that is conserved with hPER1 [10].

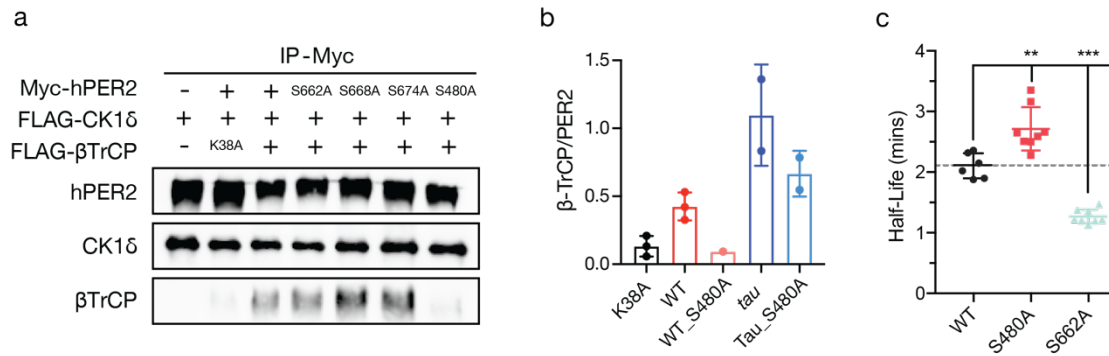


Figure 4.5. Phosphorylation of S480 is a key determinant of β -TrCP recruitment to PER2

a. Western blot of representative co-immunoprecipitation experiment showing CK1-mediated recruitment of β -TrCP. Mutations within the FASP region enhance Degron activity and β -TrCP recruitment (see Chapter 3.3). The S480A mutation disrupts β -TrCP recruitment. **b.** Quantification of co-immunoprecipitation experiments as in panel a. S480A disrupts β -TrCP recruitment in both CK1 WT and *tau* conditions. **c.** Quantification of real time hPER2-LUC half-lives (see Chapters 2.3.13 and 3.3.3). Mutation of the human FASP priming site (S662A) decreased PER2 stability, whereas S480A increased PER2 stability.

4.2.4 Determining the phosphorylation profile of a minimal hPER2 Degron substrate

In Chapter 2, we show that CK1 *tau* has a gain of function on the Degron and a substrate preference for the Degron over the FASP region when both are added *in trans*, using peptides corresponding to mouse PER2 [4]. These results extend to hPER2 substrates (**Figure 4.6a-c**). While *tau* does exhibit enhanced activity at the hPER2 Degron, and specifically at S478 of mPER2 by phosphospecific antibody [4, 20], it is not known how much of the gain of function observed *in vitro* is distributed within the β -TrCP recognition motif. Future experiments examining the influence of residues flanking the consensus Degron motif on β -TrCP binding could shed light on these questions.

As mentioned in the previous section, although studies have shown that the β -TrCP recognition motif with the Degron region regulates β -TrCP binding, PER2 stability, and circadian period, it is not clear how CK1 activity is directed within the Degron region and to what extent the *tau* mutations alters the distribution of kinase activity within. It is worth noting that the β -TrCP recognition motif within the PER2 PAS-Degron is not conserved with PER1 [10] (**Figure 4.4e**), and that both PER1 and PER2 contain an N-terminal Degron [10], and possibly as-yet-unknown Degrons that contribute to PER turnover given the modest period effect observed in the transgenic mouse with the S478A mutation [19].

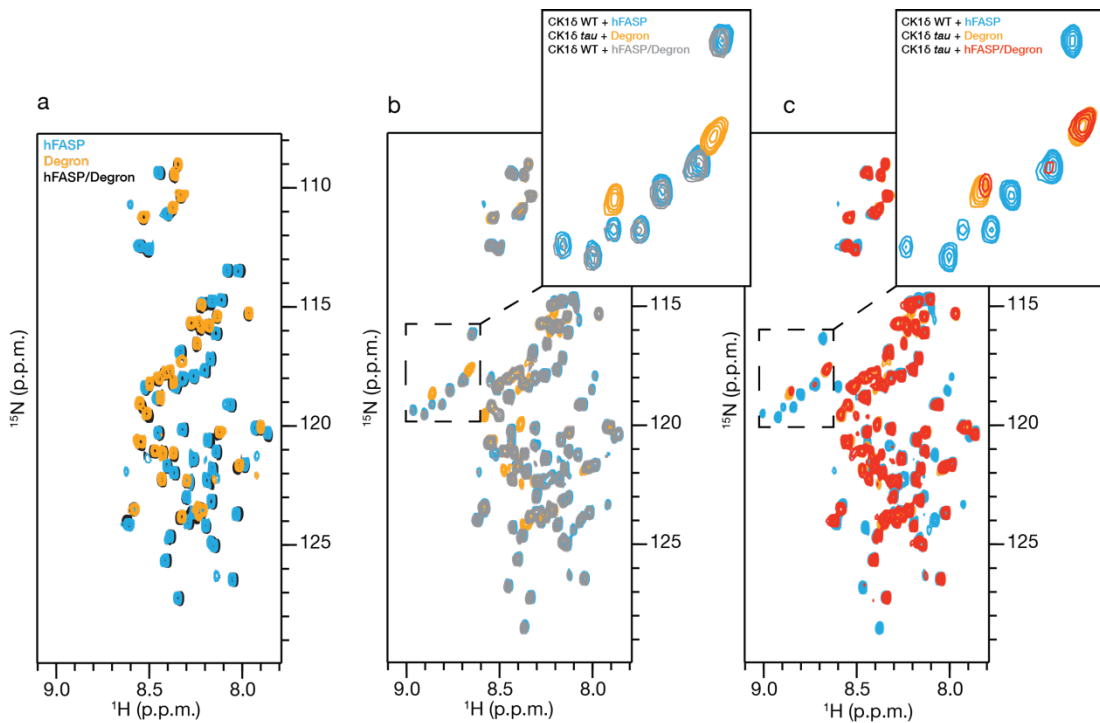


Figure 4.6. The altered mPER2 substrate selectivity of CK1 *tau* is recapitulated with hPER2 substrates

a. Overlay of ^1H , ^{15}N -HSQC spectra of hPER2 Degron, FASP, and Degron + FASP together. Peaks corresponding to each substrate show minimal overlap. **b.** Overlay of spectra corresponding to 3-hour timepoint of NMR kinase assay. When FASP and Degron are added together in *trans* and incubated with CK1 WT, all observable activity corresponds to phosphorylation of the FASP peptide. **c.** When FASP and Degron are added together in *trans* and incubated with CK1 *tau*, nearly all observable activity corresponds to phosphorylation of the Degron peptide.

There are a total of 11 serine residues located within the Degron peptide (**Figure 4.7a**), with serine residues downstream of the β -TrCP motif sharing a higher level of conservation (**Figure 4.4e**). To try to disambiguate CK1 activity within the hPER2 Degron, the $^1\text{H}, ^{15}\text{N}$ -HSQC spectrum of the minimal Degron peptide used in all the *in vitro* experiments throughout this dissertation was assigned (**Figure 4.7a**). Given that CK1 WT shows little to no activity within our standard NMR kinase assay conditions [1, 3, 4], an examination of the emerging phosphorylation profile over the course of 24 hours was performed using CK1 *tau* (**Figure 4.7b**). As can be seen from the resulting time-course, CK1 phosphorylates two distinct residues within the first 3 hours of the reaction, with little to no activity observed for any other residues. This specific activity persists for roughly the first 8 hours. However, at 24 hours the phosphorylation profile clearly shows the appearance of more than 11 peaks (**Figure 4.7b**). This result immediately raises a number of questions. First and foremost, it is unknown whether kinase activity in the Degron is non-specific or whether it follows an ordered mechanism. Moreover, the reaction appears to have not gone to completion since peaks remain for the unmodified serines within the spectrum. Due to the proximity of serine residues within the peptide, it is likely that the phosphorylation profile is reporting on multiple phosphorylation states within a heterogeneous population or an ordered mechanism. Future studies will need to uncover whether initial activity of the first two phosphorylation

events observed within the beginning reaction window template activity at other sites within the Degron.

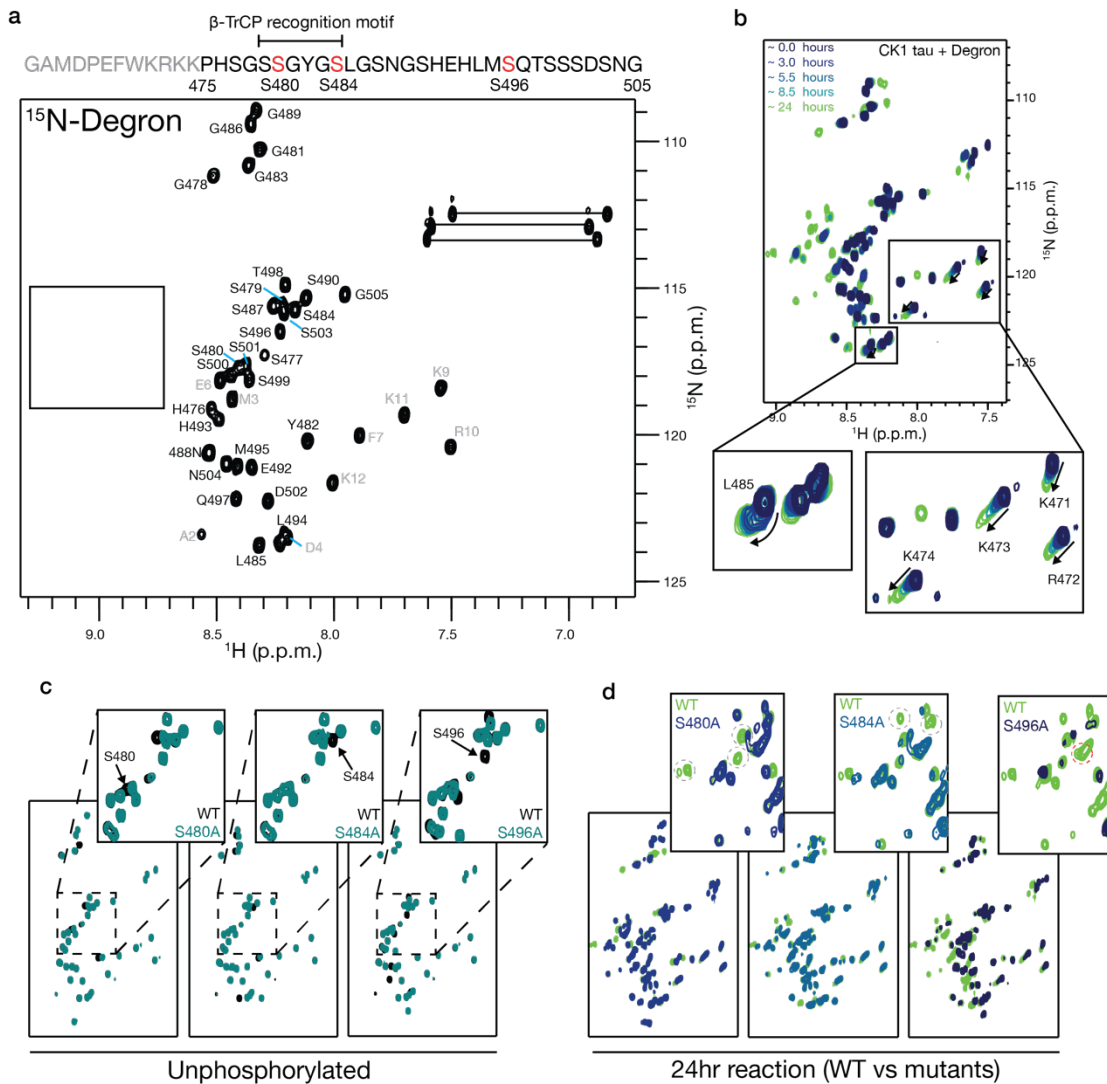


Figure 4.7. NMR spectra of the emerging phosphorylation profile of the minimal Degron peptide

a. Sequence and ^1H , ^{15}N -HSQC spectra of hPER2 Degron with residue assignments. Boxed region in spectrum indicates region where phosphoserines appear. **b.** Overlay of spectra corresponding to timepoints of identical kinase reactions with CK1 *tau*, quenched with EDTA. Boxed regions highlight peaks that display significant shifts and/or peak broadening as a function of reaction time. **c.** Overlay of S480A, S484A, and S496A Degron mutants with the WT peptide. The indicated loss of peaks in the spectrum confirm the peak assignments as in panel a. **d.** Overlay of spectra corresponding to a 24 hour reaction with CK1 *tau*, comparing Degron mutants with the WT peptide. Dashed gray circles represent potential phosphopeaks for pS480 and pS484, dashed red circle represents pS496 based on loss of peak

in with the S496A mutation in addition to triple resonance-based assignment of the phosphopeak to pS496 in a Degron peptide incubated with CK1 *tau* for 5 hours.

Given the functional importance of the β -TrCP recognition motif within the Degron, serine to alanine mutations were introduced at the two serine residues (S480A and S484A), further confirming the assignment of these residues by the standard backbone walking strategy (**Figure 4.7c**). Upon performing an NMR kinase reaction, the same two phosphoserine peaks were observed within the first 3 hours of the reaction, demonstrating that they are not the two serine residues within the β -TrCP motif (**Figure 4.7d**). This result could be consistent with a gain of function at alternate residues that ultimately enhance activity within the β -TrCP recognition motif, as observed by western blotting with a phosphospecific antibody [4, 20]. To assign the two phosphopeaks that emerge within the initial window of the reaction, I collected triple resonance spectra on a peptide that was incubated with CK1 *tau* for approximately 5 hours and found one of the phosphopeaks to correspond to S496, with the other likely corresponding to S503, but I have not yet conducted experiments with S503A to validate this assignment. Interestingly, the S496A mutation significantly reduces the amount of phosphopeaks compared to the WT Degron after 24 hours (**Figure 4.7d**), consistent with the model that kinase activity at this site may act as a template for further activity within the Degron.

4.2.4 Phosphorylation of the hPER2 Degron in the context of the PAS domains

Disambiguating the NMR spectrum of the minimal Degron peptide would seem to be a tractable exercise, as the emerging peaks are well dispersed over the course of the kinase reaction (**Figure 4.7b**). However, a troubling feature of the phosphorylated Degron spectrum is a peak shift and broadening of non-native lysine residues at the N-terminus of the peptide (**Figure 4.7b**). These residues were added to the substrate to create a polybasic motif to bind PVDF/nitrocellulose membrane for hot-ATP assays. These changes seem to report on the extent of phosphorylation within the peptide over the course of the reaction, perhaps due to interactions between this charged patch and the phosphorylated residues within the peptide, suggesting a potential pitfall for using similar substrates. Considering these complications, we decided to perform kinase reactions on a larger native substrate that includes the tandem PAS domains through the Degron (**Figure 4.4d, Figure 4.8a**). The qualities of NMR relaxation have been leveraged previously to study PTMs and protein interactions on flexible regions of proteins in the context of larger, structured domains [21, 22]. The PAS-Degron substrate is ~40 kDa (**Figure 4.8a**) and forms a ~80 kDa dimer in solution [12]. As suggested by the AlphaFold2/homology structure of the hPER2 PAS-Degron dimer, the Degron region extends as a disordered segment, away from the PAS-dimer core (**Figure 4.8a**). Owing to the size of the dimer structure, residues within the

structured domain undergo faster spin-spin relaxation, resulting in a broadened linewidth and weaker NMR signal (**Figure 4.8a**). This is advantageous because it allows for observing the more flexible Degron region in the context of the native dimer structure without the spectrum becoming crowded. An overlay of the ^1H , ^{15}N -HSQC spectrum of the PAS-Degron and minimal Degron peptide shows a nearly identical overlap (**Figure 4.8b**), with residues present in the minimal peptide spectrum corresponding to the non-native cloning artifact that is not present in the PAS-Degron (**Figure 4.7a**).

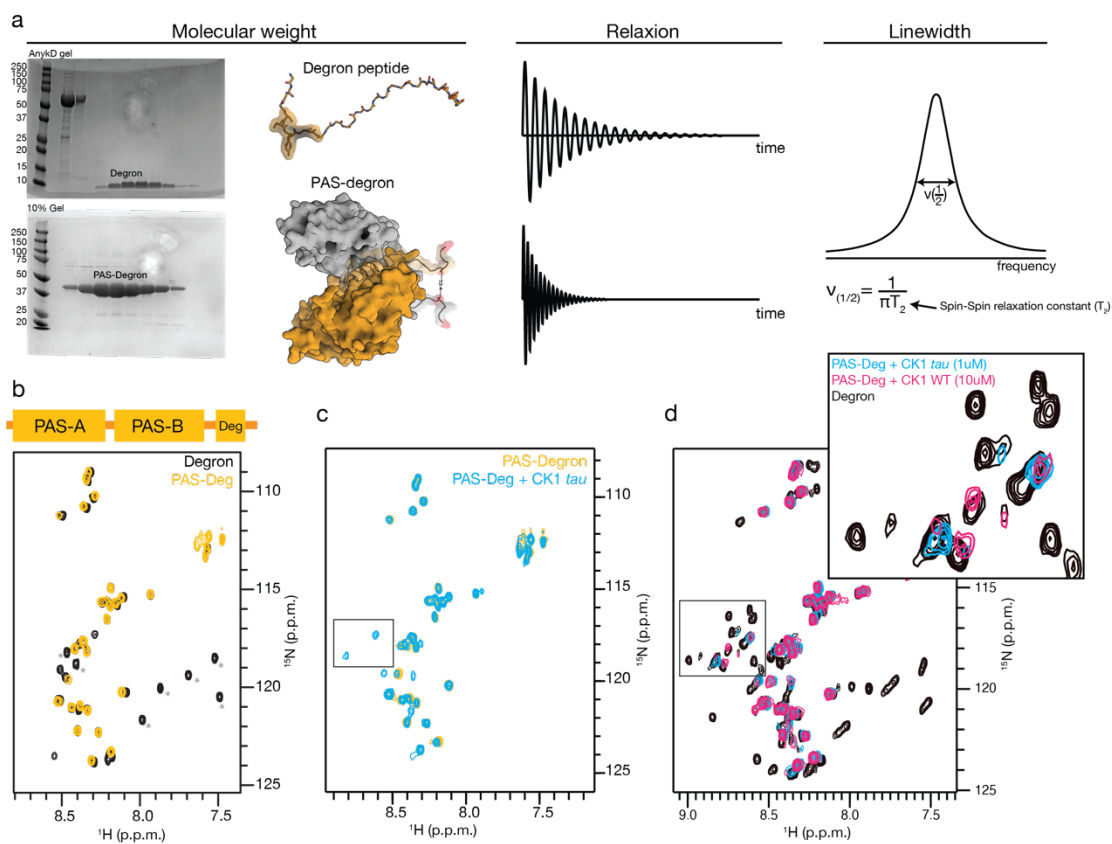


Figure 4.8. NMR kinase assay can monitor site-specific Degron activity in the context of the tandem PAS domains

a. SDS-PAGE gels of Superdex 75 prep size exclusion chromatography fractions size of purified isotopically labeled Degron and PAS-Degron substrates and their corresponding structures. β -TrCP recognition motif is shown as part of transparent surface. The flexible Degron experiences a longer relaxation time than the PAS-dimer core, leading to a narrow linewidth and stronger signal. **b.** Domain map of PAS-Degron and overlay of ^1H , ^{15}N -HSQC spectra of PAS-Degron and minimal Degron peptide. Asterisk indicates non-native residues present at the N-terminus of the minimal Degron peptide (see Figure 4.7a) that are not present in the PAS-Degron. **c.** Overlay of unphosphorylated PAS-Degron spectrum and PAS-Degron after 3-hour reaction with CK1 *tau*. **d.** Overlay of spectra corresponding to PAS-Degron incubated with CK1 *tau* (blue), PAS-Degron incubated with a 10-fold increase of CK1 WT (pink) as compared to CK1 *tau*, and the minimal Degron peptide incubated with CK1 *tau* for 24 hours. The first two phosphopeaks that emerge in the PAS-Degron overlay exactly with the first two phosphopeaks that emerge in the minimal Degron peptide.

To examine kinase activity within the PAS-Degron, NMR kinase assays were performed with the same conditions used for the minimal Degron peptide [4], i.e., using CK1 *tau* and equimolar concentrations of Degron or PAS-Degron substrate. It should be noted however that these reactions cannot be used to compare kinetics between the two types of substrates, since the PAS-Degron forms a dimer in solution. That is, a 2:1 molar ratio of Degron peptide to PAS-Degron should be used to account for the dimeric state of the latter, because for each CK1:PAS-Degron encounter complex, there will be twice as many possible phosphorylation sites as compared to a CK1:Degron encounter complex [2]. Upon performing the NMR kinase assay, the PAS-Degron shows a nearly identical phosphorylation profile after 3 hours, with two distinct peaks emerging (**Figure 4.8c**). Due to the extremely poor activity within the Degron by CK1 WT, a similar reaction was performed with 10-fold more CK1 WT than *tau* to be able to observe phosphorylation activity (**Figure 4.8d**). Interestingly, after 90 minutes of incubation with CK1 WT, the emerging phosphorylation profile of the PAS-Degron shows differences from the emerging profile with CK1 *tau* (**Figure 4.8d**). As discussed in this section and Chapter 2, CK1 WT and *tau* display different substrate specificities, so this result is perhaps not unexpected. Future studies that characterize the difference in substrate specificity at the PER2 PAS-Degron between CK1 WT and *tau* would help to elucidate the overall multisite mechanism within this region and shed light on

how this differential activity ultimately affects the recruitment of β -TrCP, PER2 stability, and circadian timing. That is, we must first decipher the phospho-code at the Degron that maximally recruits β -TrCP, and then examine how the relative activities of CK1 mutants within this region compare to this phospho-code.

4.3 Targeting CK1 to modulate kinase activity on PER2 substrates

Throughout this dissertation, specifically in Chapter 2 and the beginning of Chapter 4, I discussed the importance of protein dynamics. In solution, proteins are not just the low energy snapshots we observe in crystal structures, but are rather dynamic and represent a conformational landscape that can have vast consequences on protein function [23]. As we discovered in CK1, a dynamic allosteric network between conserved anion binding sites controls the conformation of the activation loop segment and significantly remodels the substrate binding region [4]. These local dynamics also lead to corresponding changes in the overall global dynamics of the kinase. As we showed in Chapter 2, these changes in protein dynamics lead to functional consequences, such as altered substrate specificity, and thus regulate the balance of kinase activity on targets within the molecular clock. Moreover, in Chapter 3 we discussed how CK1 is targeted by feedback inhibition via product binding at conserved anion binding sites within the substrate binding cleft, and highlighted the

incompatibility of activation loop conformations with certain peptide binding modes [3].

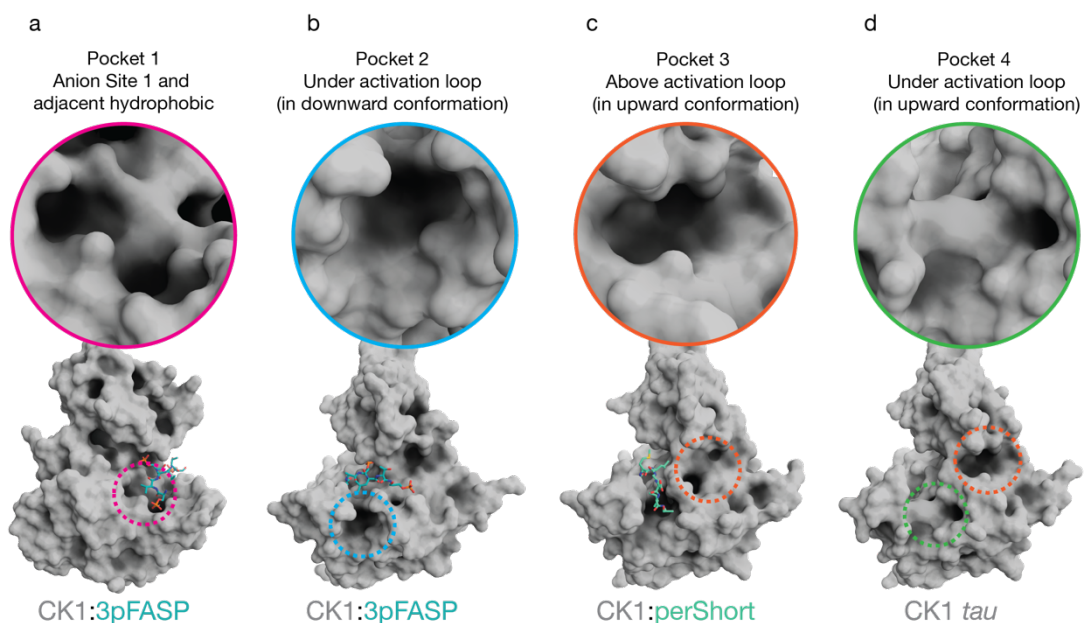


Figure 4.9. CK1 contains targetable pockets that are positioned to effect substrate selectivity

a. Zoom of pocket containing anion binding Site 1 and a smaller adjacent pocket that accommodates small, branched chain residues observed in crystal structures in complex with peptides. **b.** Zoom of larger pocket observed underneath the activation loop when locked in the downward conformation by coordination of pFASP at anion binding Site 2. **c.** Zoom of representative pocket observed above the activation loop/under the N-terminal lobe in apo structure and CK1 bound to the phosphorylated dPER-Short peptide. **d.** Zoom of pocket/groove observed below the activation loop when it is in the upward conformation.

Given the importance of substrate selectivity for PER2 turnover, the rate limiting priming of FASP and the generation of the inhibitory pFASP, and the effect that these outcomes potentially have on PER2 activity as a transcriptional repressor, there exists a great opportunity to therapeutically target CK1 to modulate these biochemical mechanisms. Examination of the crystal structures that have been solved during this dissertation shows that there are several small pockets that could be candidates for targeting with small molecules (**Figure 4.9a-d**). For example, targeting of the anion binding Site 1 and the adjacent pocket that accommodates the small, branched chain residue in 3pFASP could potentially regulate FASP priming and pFASP binding (**Figure 4.9a**). This anion binding site facilitates the anchoring interaction involved in the CK1 consensus recognition mechanism [4, 24, 25], therefore targeting of this site could regulate substrate specificity. In structures of CK1 in complex with pFASP peptides, the activation loop segment is locked in the downward conformation by the coordination of a phosphoserine at anion binding Site 2. In this conformation, a pocket forms underneath the activation loop (**Figure 4.9b**) that could be another potential target to bias the activation loop toward this conformation, with a small molecule essentially acting as a molecular glue to hold the activation loop down. Alternatively, targeting of this pocket could disrupt the type of binding mode observed in the complex with the phosphorylated dPER-Short peptide from dPER (**Figure 4.9c**). Further, in the upward conformation of the activation loop two pockets are formed, one above

and one below the activation loop (**Figure 4.9c-d**). Targeting of these two pockets could modulate the dynamics of the activation loop switch to affect substrate selectivity or the binding of phosphorylated regulatory sequences such as pFASP or the phosphorylated dPER-Short regions. The ability to tune circadian rhythms via targeting of CK1 at these sites rather than target the ATP binding site could lead to new CK1 specific inhibitors/modulators and novel therapeutic avenue.

4.4 Materials and Methods

All materials and methods in this chapter are outlined in the published materials and methods sections of Chapters 2 and 3.

References

1. Narasimamurthy, R., et al., *CK1delta/epsilon protein kinase primes the PER2 circadian phosphoswitch*. Proc Natl Acad Sci U S A, 2018. **115**(23): p. 5986-5991.
2. Gebel, J., et al., *p63 uses a switch-like mechanism to set the threshold for induction of apoptosis*. Nat Chem Biol, 2020. **16**(10): p. 1078-1086.
3. Philpott, J.M., et al., *PERIOD phosphorylation leads to feedback inhibition of CK1 activity to control circadian period*. bioRxiv, 2022: p. 2022.06.24.497549.
4. Philpott, J.M., et al., *Casein kinase 1 dynamics underlie substrate selectivity and the PER2 circadian phosphoswitch*. Elife, 2020. **9**.

5. Durgan, D.J., et al., *O-GlcNAcylation, novel post-translational modification linking myocardial metabolism and cardiomyocyte circadian clock*. J Biol Chem, 2011. **286**(52): p. 44606-19.
6. Kaasik, K., et al., *Glucose sensor O-GlcNAcylation coordinates with phosphorylation to regulate circadian clock*. Cell Metab, 2013. **17**(2): p. 291-302.
7. Lowrey, P.L., et al., *Positional syntenic cloning and functional characterization of the mammalian circadian mutation tau*. Science, 2000. **288**(5465): p. 483-92.
8. Kornev, A.P. and S.S. Taylor, *Dynamics-Driven Allostery in Protein Kinases*. Trends Biochem Sci, 2015. **40**(11): p. 628-647.
9. Wu, G., et al., *Structure of a beta-TrCP1-Skp1-beta-catenin complex: destruction motif binding and lysine specificity of the SCF(beta-TrCP1) ubiquitin ligase*. Mol Cell, 2003. **11**(6): p. 1445-56.
10. Eide, E.J., et al., *Control of mammalian circadian rhythm by CKlepsilon-regulated proteasome-mediated PER2 degradation*. Mol Cell Biol, 2005. **25**(7): p. 2795-807.
11. Ohsaki, K., et al., *The role of {beta}-TrCP1 and {beta}-TrCP2 in circadian rhythm generation by mediating degradation of clock protein PER2*. J Biochem, 2008. **144**(5): p. 609-18.
12. Hennig, S., et al., *Structural and functional analyses of PAS domain interactions of the clock proteins Drosophila PERIOD and mouse PERIOD2*. PLoS Biol, 2009. **7**(4): p. e94.
13. Kucera, N., et al., *Unwinding the differences of the mammalian PERIOD clock proteins from crystal structure to cellular function*. Proc Natl Acad Sci U S A, 2012. **109**(9): p. 3311-6.
14. Beesley, S., et al., *Wake-sleep cycles are severely disrupted by diseases affecting cytoplasmic homeostasis*. Proc Natl Acad Sci U S A, 2020. **117**(45): p. 28402-28411.

15. Militi, S., et al., *Early doors (Edo) mutant mouse reveals the importance of period 2 (PER2) PAS domain structure for circadian pacemaking*. Proc Natl Acad Sci U S A, 2016. **113**(10): p. 2756-61.
16. de Oliveira, P.S., et al., *Revisiting protein kinase-substrate interactions: Toward therapeutic development*. Sci Signal, 2016. **9**(420): p. re3.
17. Moglich, A., R.A. Ayers, and K. Moffat, *Structure and signaling mechanism of Per-ARNT-Sim domains*. Structure, 2009. **17**(10): p. 1282-94.
18. Vielhaber, E.L., et al., *Nuclear export of mammalian PERIOD proteins*. J Biol Chem, 2001. **276**(49): p. 45921-7.
19. Masuda, S., et al., *Mutation of a PER2 phosphodegron perturbs the circadian phosphoswitch*. Proc Natl Acad Sci U S A, 2020. **117**(20): p. 10888-10896.
20. Zhou, M., et al., *A Period2 Phosphoswitch Regulates and Temperature Compensates Circadian Period*. Mol Cell, 2015. **60**(1): p. 77-88.
21. Morrison, E.A., et al., *The conformation of the histone H3 tail inhibits association of the BPTF PHD finger with the nucleosome*. Elife, 2018. **7**.
22. Morrison, E.A., et al., *Nucleosome composition regulates the histone H3 tail conformational ensemble and accessibility*. Nucleic Acids Res, 2021. **49**(8): p. 4750-4767.
23. Henzler-Wildman, K. and D. Kern, *Dynamic personalities of proteins*. Nature, 2007. **450**(7172): p. 964-72.
24. Zeringo, N.A. and J.J. Bellizzi, 3rd, *A PER2-derived mechanism-based bisubstrate analog for casein kinase 1epsilon*. Chem Biol Drug Des, 2014. **84**(6): p. 697-703.
25. Flotow, H., et al., *Phosphate groups as substrate determinants for casein kinase I action*. J Biol Chem, 1990. **265**(24): p. 14264-9.

Chapter 5

Conclusions

5.1 The core molecular clock is highly interconnected

In Chapter 1, we discussed how each of the negative feedback elements of the circadian clock are highly regulated at both protein and genetic levels. The CRY/PER/CK1 repressive complex regulates the transcriptional activity of CLOCK:BMAL1 and circadian timing, and each of the proteins that make up the repressive complex have homologues and isoforms with variable function and that are differentially regulated by PTMs and other protein-protein interactions.

Two common features of the negative elements of the core clock discussed in Chapter 1 are post-translational modifications and autoregulation. The level of interconnectivity between the functions of these negative elements is such that perturbation of any one element is likely to affect the function the other. In this chapter, we highlighted how CRY1 repression is autoregulated by its C-terminal tail, how structural differences between CRY1 and CRY2 give rise to differential activities, and how PER2 may regulate CRY isoform activity by modulating their interaction with CLOCK. We discuss the critical roles of PER2 as the stoichiometrically limiting factor regulating circadian timing, and how an elaborate network of PTMs on PER2 regulate its abundance. We

further highlight how CK1 sits at the center of the clock by regulating PER2 abundance, and how CK1 activity on PER2 is highly regulated by allostery and autoinhibition from its C-terminal tail.

5.2 Protein dynamics are key determinants of protein function and circadian timing

Protein dynamics are crucial aspects that govern how a protein will function. While intrinsically disordered regions are highly flexible and dynamic, structured domains can also undergo dramatic conformational rearrangements and movements. Interdomain interactions, conformational rearrangements and coordinated movements along the free energy landscape of a protein require that proteins be thought of as dynamic and 'breathing' in solution or in the context of the cellular milieu.

In Chapter 1, we discussed how the critical interaction between the HI-loop of CLOCK PAS-B and the secondary pocket of the CRY PHR is regulated by dynamics of the serine loop adjacent to the secondary pocket, ultimately controlling the size and flexibility of the pocket and the affinity for CRY binding to CLOCK. We also highlighted how the intrinsically disordered PER2 CBD binds to the CRY PHR to add another layer of functional regulation to the CRY:CLOCK interaction by remodeling the structure of the serine loop. We also discussed how the dynamic equilibrium of CRY tail binding to the PHR regulates the CRY:CLOCK interaction.

In Chapter 1 and 2, we elucidate a dynamic allosteric switch in CK1 that controls the conformation of the activation loop, and we show how this allosteric activation loop switch controls substrate selectivity by remodeling the substrate binding cleft. We show how the CK1 *tau* mutation, that leads to a roughly 4-hour shortening of circadian period, inverts substrate selectivity within the PER2 phosphoswitch compared to CK1 WT and changes the global dynamics of the kinase. In Chapter 4, we leverage molecular dynamics simulations to create a model for how CK1 recognizes and primes the PER2 FASP region, providing a deeper understanding of this rate-limiting step in the regulation of circadian timing. We further analyze how the allosteric network connecting the anion anchoring site of CK1 (Site 1) and the activation loop remodels the free energy landscape of CK1 with the *tau* mutation. Taken together, we propose that CK1 dynamics are fundamental to circadian timing by controlling substrate selectivity on PER2.

5.3 CK1 feedback regulation is a hallmark of the mammalian circadian clock

CK1 is an ancient clock component that is highly conserved in organisms with circadian rhythms, from humans to green algae (**Figure 2.6.1**). In Chapter 1, we discuss how CK1 is autoregulated by its C-terminal tail. Unlike other Ser/Thr kinases, CK1 is constitutively active but auto-phosphorylates its tail to become inactive, and CK1 δ isoforms differentially regulate substrate

selectivity on the PER2 FASP region to regulate circadian period. In Chapter 3, we show how the phosphorylated FASP region feedback inhibits CK1 activity at the PER2 degron to stabilize PER2, and we show that the extent of FASP phosphorylation correlates with the potency of pFASP inhibition, the state of PER2 hyperphosphorylation and its stability. In addition to showing this mechanism is conserved in PER1, we also show that this mechanism of feedback inhibition is conserved between the mammalian and *Drosophila* circadian systems, where phosphorylation of the perShort domain of dPER similarly attenuates kinase activity at an N-terminal Degron in dPER. In the Chapter 3 discussion, we also suggest that pFASP product inhibition could act as a mechanism to regulate PER2 activity as a transcriptional repressor since PER2 facilitates CK1-mediated displacement of CLOCK from DNA. The stable interaction between CK1 and the PER2 CKBD positions pFASP to feedback inhibit CK1 activity on substrate targets such as CLOCK. While it has been recently shown that the stable interaction between CK1 and PER1/2 is required for CLOCK hyperphosphorylation and displacement from DNA, the effect of CK1 phosphorylation on CLOCK as a function of mutations within the FASP region has yet to be explored.

5.4 Molecular level details of PER2 turnover are critical for understanding circadian period

Throughout this dissertation, most of the focus has been on understanding how CK1 activity on PER2 is regulated towards the FASP region, and how the phosphorylated FASP region in turn regulates circadian period. Understanding the function of the FASP region is very important because mutations in this region lead to both shorten and lengthen circadian period, suggesting that regulation of the FASP region is positioned relatively high within the hierarchy of timekeeping mechanisms within the clock. In Chapters 1-3 we discussed how the phosphorylated FASP region stabilizes PER2, but a complete understanding of PER2 stability requires the study of how PER2 turnover is regulated by phosphodegrons.

In Chapter 4, I have gathered my unpublished data and provided a discussion to describe the state of various projects as they relate to FASP priming, CK1 substrate selectivity, and the molecular determinants of PER2 turnover. PER2 stability is regulated at least in part by CK1 activity at a Degron region located C-terminal to the tandem PAS domains, leading to recruitment of β -TrCP and proteasomal degradation. In this chapter, I discuss the results of preliminary experiments probing the multisite phosphorylation within the Degron by CK1 and show that CK1 activity on in this region can be monitored with site specific resolution in the context of the tandem PAS-domains and dimerization. While the phosphorylation of the serines within the β -TrCP

recognition motif is important for β -TrCP binding and PER2 stability, I show that CK1 *tau* leads to a gain of function at other residues within the Degron region, raising the question of whether CK1 activity follows an ordered mechanism within the Degron region and what phosphorylation landscape within the Degron leads to maximal recruitment of β -TrCP.

Chapter 4 is closes with a discussion of the potential to target CK1 as a therapeutic strategy. The crystal structures solved throughout this dissertation shed light on key interactions between CK1 and PER and conformations of the kinase that influence its function. These results provide a novel opportunity to rationally target CK1 with the goal of modulating its activity within the core molecular clock.

5.5 CK1 and PER2 form a critical regulatory nexus within the core molecular clock

Our understanding of the molecular mechanisms of circadian timing are increasingly relying upon elucidation of how intrinsically disordered regions regulate protein function. The disordered C-terminal tails of CRY and CK1 both regulate the functional activity of their respective N-terminal structured domains, and intrinsically disordered domains within PER regulate protein interactions and accumulate PTMs that ultimately influence PER activity as a transcriptional repressor. The largely intrinsically disordered nature of PER is

fundamentally important to its function as a labile scaffold to assemble larger repressive complexes.

A survey of the functional domains within PER2 highlight the importance of PER2 abundance in clock function. PER2 PAS domains dimerize, facilitating the nucleation of PER proteins and their binding partners. The CK1BD, embedded within the central disordered region of PER2, facilitates the stable interaction between CK1 and PER2 throughout most of their circadian cycle. This stable interaction is required for CK1 mediated phosphorylation of CLOCK and its displacement from DNA, as well as PER2 turnover. CK1 is recruited to the CK1BD via two ordered domains that flank the disordered FASP region. This stable CK1:PER2 complex suggests that the effective concentration of FASP/pFASP is likely increased by being held near the kinase throughout the PER2 circadian cycle. The FASP region acts as a critical regulatory region for circadian period through feedback inhibition of CK1. Taken together, these features of the core molecular clock suggest that the interactions between PER and CK1 are central to circadian timekeeping.

As discussed throughout these chapters, PER2 is highly regulated by PTMs. A critical missing piece to our understanding of how CK1 and PER2 interactions contribute to circadian timekeeping is when and where CK1 activity on PER2 occurs, and how this activity integrates with other PTMs on PER2 such as acetylation. Future studies will need to address the post-translational state of PER2 throughout its circadian cycle in the cytoplasm and nucleus and

integrate these findings with the molecular mechanisms discussed throughout this dissertation.